Earth ArXiv

Dear Reader,

Thank you for your interest in this paper. This manuscript is a non-peer reviewed preprint submitted to EarthArXiv. Please note that once this manuscript has undergone peer review, subsequent versions may have slightly different content. If accepted, the final version of this manuscript will be available via the `Peer-reviewed publication DOI' link.

If the content of this preprint has informed your thinking on your own research, we ask that you consider citing our work using the following citation format (or similar), depending on journal rules for citing non-peer reviewed preprints:

Chen, C. Y., McGee, D., Woods, A., Pérez, L., Hatfield, R. G., Edwards, R. L., Cheng, H., Valero-Garcés, B. L., Lehmann, S. B., Stoner, J. S., Schwalb, A., Tal, I., Seltzer, G. O., Tapia, P. M., Abbott, M.A., Rodbell, D. T. (2019). U–Th dating of lake sediments: Lessons from the 700 kyr sediment record of Lake Junín, Peru. https://doi.org/10.31223/osf.io/c765k

For more information on EarthArXiv, visit the following sites:
- FAQs: https://eartharxiv.github.io/faq.html
- EOS article: https://eos.org/science-updates/earth-science-is-ready-for-preprints

In the spirit of open science, we welcome you to contact the lead author, **Christine Y. Chen** (cychen.geo[at]gmail[dot]com) with any feedback to help improve the manuscript.

Happy reading!

Sincerely,
Christine Y. Chen and co-authors

U-Th dating of lake sediments: Lessons from the 700 kyr sediment record of Lake Junín, Peru

Christine Y. Chen[a,b,*], David McGee[b], Arielle Woods[c], Liseth Pérez[d], Robert G. Hatfield[e], R. Lawrence Edwards[f], Hai Cheng[f,g], Blas L. Valero-Garcés[h,i], Sophie B. Lehmann[c], Joseph S. Stoner[e], Antje Schwalb[d], Irit Tal[b], Geoffrey O. Seltzer[j,**], Pedro Miguel Tapia[k], Mark B. Abbott[c], Donald T. Rodbell[l]

[a]*Massachusetts Institute of Technology-Woods Hole Oceanographic Institution Joint Program in Oceanography, Cambridge, MA, 02139, USA*
[b]*Department of Earth, Atmospheric and Planetary Sciences, Massachusetts Institute of Technology, Cambridge, MA, 02139, USA*
[c]*Department of Geology and Environmental Science, University of Pittsburgh, Pittsburgh, PA, 15260, USA*
[d]*Institut für Geosysteme und Bioindikation, Technische Universität Braunschweig, Langer Kamp 19c, 38106, Braunschweig, Germany*
[e]*College of Earth, Ocean, and Atmospheric Science, Oregon State University, Corvallis, OR, 97330, USA*
[f]*Department of Earth and Environmental Sciences, University of Minnesota Twin Cities, Minneapolis, MN, 55455, USA*
[g]*Institute of Global Environmental Change, Xi'an Jiaotong University, Xi'an, 710054, Shaanxi, China*
[h]*Pyrenean Institute of Ecology, CSIC, Avda Montañana 1005, 50059, Zaragoza, Spain*
[i]*Laboratorio Internacional en Cambio Global, CSIC-PUC-UFRJ, Avda Montañana 1005, 50059, Zaragoza, Spain*
[j]*Department of Earth Sciences, Syracuse University, Syracuse, NY, 13244, USA*
[k]*Instituto Nacional de Investigación en Glaciares y Ecosistemas de Montañas, Huaraz, Ancash, Peru*
[l]*Department of Geology, Union College, Schenectady, NY, 12308, USA*

Abstract

Deep sediment cores from long-lived lake basins are fundamental records of paleoenvironmental history, but the power of these reconstructions has often been limited by poor age control. Uranium-thorium (U-Th) dating has the potential to fill a gap in current geochronological tools available for such sediment archives. We present our systematic approach to U-Th date carbonate-rich sediments from the ∼100-m-long drill core from Lake Junín, Peru. The results form the foundation of an age-depth model spanning ∼700 kyrs. High uranium concentrations (0.3–4 ppm) of these sediments allow us to date smaller quantities of material, giving us the opportunity to improve sample selection by avoiding detrital contamination, the greatest limiting factor to the success of previous U-Th dating efforts in other lake basins. The dates from 174 analyses on 55 bulk carbonate samples revealed significant scatter that could not be resolved with traditional isochrons, suggesting that at least some of the sediments have not remained closed systems. To understand the source of noise in the geochronological data, we first apply threshold criteria that screen samples by their U/Th ratio, reproducibility, and $\delta^{234}U_{initial}$ value. We then compare these results with facies types, trace element concentrations, carbonate and total organic carbon content, color reflectance, mineralogy, and ostracode shell color to investigate the causes of open system behavior. We find that the greatest impediment to U-Th dating of these sediments is not detrital contamination, but

---

*Corresponding author. Email address: cychen.geo@gmail.com (C. Y. Chen).
**Deceased.

rather post-depositional remobilization of uranium. After examining U-Th data in these contexts, we identify samples that have likely experienced the least amount of alteration, and use dates from those samples as constraints for the age-depth model. Our work has several lessons for future attempts to U-Th date lake sediments, namely that geologic context is equally important as the accuracy and precision of analytical measurements when determining the age of sample materials. In addition, we caution that significant geologic scatter may remain undetected if not for labor intensive tests of reproducibility achieved through replication. As a result of this work, the deep sediment core from Lake Junín is the only continuous record in the tropical Andes spanning multiple glacial cycles that is constrained entirely by independent radiometric dates. As such, this record is uniquely poised to offer new insights on past climate and environmental changes in the tropical Andes, complementing and testing the long but tuned sediment records from Sabana de Bogotá to the north ($\sim$5°S; Groot et al., 2011) and Lake Titicaca to the south ($\sim$16°S; Fritz et al., 2004, 2007).

1. Introduction

Since the founding of the International Continental Drilling Program (ICDP) in 1996 (Colman, 1996), scientific teams have recovered dozens of deep lake sediment cores from nearly every continent in the world. Due to their continuity, resolution, and wide geographic distribution, these sediment records have provided important long-term perspectives on Earth's terrestrial environmental history. As the spatial and temporal coverage of such records expand, the next step is to combine these records with complementary studies from marine and ice cores to address longstanding questions about the linkages and causal relationships among terrestrial, marine, and atmospheric phenomena. Here, the challenge lies in comparing the timing, rate, and duration of past land surface and ecosystem changes to those of past events identified elsewhere in the oceans, atmosphere, and other continental regions. Thus, the extent to which tests for leads and lags in the climate system are useful is limited not by the quality of environmental proxy interpretation, but rather by the quality of the temporal constraints.

While ice and marine cores are often amenable to layer counting or anchoring to globally synchronous reference timescales (*e.g.*, oxygen isotope "chronostratigraphy" in marine sediments, methane gas concentrations in ice cores), determining a reliable age-depth model for long lacustrine sediment sequences is generally more problematic. Because lake basins occupy a broad range of environments, each drilling location often contains a site-specific accumulation of terrigenous and biogenic sediment as well as a unique post-depositional alteration history influenced by non-climatic processes like tectonics and volcanism. Thus, aligning such records to external reference timescales (colloquially known as "tuning") requires a thorough investigation of how global climate events and more proximal geologic processes affect local paleoenvironmental proxy variability. Proving such relationships convincingly can be a formidable undertaking, but in the absence of other data, tuning is often the only means available to establish time constraints. As a result, such records are limited in their ability to address climatic questions that are dependent on the relative timing of events (*e.g.*, Prokopenko et al., 2006; Nowaczyk et al., 2013; Stockhecke et al., 2014; Francke et al., 2016).

Therefore, when possible, absolute chronological data from radiometric and paleomagnetic dat-

ing techniques are highly desirable and generally serve as first-order constraints on age-depth models of sediment cores. The success and utility of such methods is dependent on factors such as the availability and quality of datable materials, the time range of the method, and the adherence to assumptions underpinning each technique within a given sediment sequence. When these factors align, the resulting independent chronologies allow for compelling investigations of forcing relationships (*e.g.*, the radiocarbon- and tephra-based chronologies of Laguna Potrok Aike in Patagonia [Kliem et al., 2013] and Lake Petén Itzá in Guatemala [Kutterolf et al., 2016]). However, problems commonly arise when suitable dating materials are absent or the true age of the sediments is outside the applicable temporal range of a method: for instance, datable tephras are rare in most environments and the radiocarbon method is generally limited to the last 50 ka.

Currently, there exists a gap in comprehensively tested high-precision geochronological tools in the time interval between 50 and 780 ka, beyond the limit of radiocarbon dating and up to the most recent geomagnetic reversal (Brunhes–Matuyama), after which paleomagnetic reversal stratigraphy can be applied. Here, methods like uranium-thorium (U-Th), cosmogenic exposure, and optically stimulated luminescence (OSL) dating have potential (*e.g.*, Roberts et al., 2018). However, these systems have mostly been underexplored in their broad application to lake sediments or have not been refined since improvements in instrumentation have opened new doors for sample selectivity. Ideally, data from multiple complementary chronological tools with different operating assumptions can be used to cross-validate one another (*e.g.*, Colman et al., 2006; Shanahan et al., 2013), and in the process, reveal information about the nature of uncertainties and biases specific to each technique.

To this end, we present our efforts to U-Th date the carbonate-rich sediments from the deep drill core extracted in 2015 from Lake Junín, Peru. Our strategy for sample selection, tests for internal consistency that leverage stratigraphic coevality constraints, and use of other corresponding sedimentological, geochemical, and paleoecological data to inform our interpretations of the U-Th data can serve as a framework for future attempts to apply U-Th dating techniques to long cores. Our results also indicate that future work to establish or refine U-Th-based lake sediment chronologies must include deliberate tests that probe for possible open system behavior or excess "geologic scatter"—unresolved errors that can affect the accuracy and precision of dates due to unknown geologic complexities not accounted for in typical uncertainty calculations and corrections (Ludwig and Paces, 2002). Without a methodical exploration of U-Th data in context of other geologic information, age-depth models that contain single, standalone U-Th analyses that, at face value, seem like valid ages, may in fact hide the existence of geologic scatter and therefore be inaccurate.

The organization of this paper is as follows: We first provide a basic overview of the principles behind U-Th dating and review previous efforts to apply U-Th geochronology to lake sediments (Section 2). After describing the relevant background of Lake Junín (Section 2.3) and our methods for core sampling, U-Th geochemistry, and isotopic measurement (Section 3), we then present the results of 174 U-Th analyses from 55 unique samples (Section 4). Of these, only 72 analyses from 18 samples are used in the final chronology for the core. We explain our screening procedure for evaluating the validity of each U-Th date (Section 5), and then interpret our analyses alongside other sedimentological, geochemical, and paleoecological data to show that uranium remobilization, not detrital contamination, is the most likely cause for discrepancies in our data (Section 6). We then simulate the impact of detrital contamination and uranium remobilization on the isotopic evolution of our samples to further support this conclusion (Section 7). Using the U-Th age constraints that pass our criteria and radiocarbon dates from Woods et al. (2019), we then describe the construction

of the age-depth model for the Lake Junín sediment record (Section 8). We end with a discussion on the uncertainties in U-Th age estimates learned from this study and propose considerations for future U-Th dating of lake sediments (Section 9).

Because terminology is important, hereafter, we distinguish between the terms *date* and *age*, adopting the convention followed by other geochronologists (*e.g.*, Schoene et al., 2013; Dutton et al., 2017): a date is a number calculated from a decay equation and isotopic measurements, whereas an age is an interpretation of a date in the context of other information and represents a geologically meaningful time.

2. Background

Thus far, the application of U-Th dating in continental paleoclimate archives has been most visible and transformative in unrecrystallized corals and dense carbonate precipitates like cave stalagmites and groundwater vein calcites (*e.g.*, Winograd et al., 1992; Cheng et al., 2000; Wang et al., 2001). In comparison, U-Th dating of lake sediments has historically been less straightforward. To place the challenges of our work in this context, in this section, we briefly describe the basic principles of U-Th dating, the geologic processes in lake sediments that can compromise the underlying assumptions of this dating system, and the strategies used by other studies to overcome or account for these issues.

2.1. Basic principles of U-Th dating

There are several "uranium-series disequilibrium" dating methods that make use of the decay chains of various actinide nuclides (*e.g.*, ^{238}U, ^{235}U; see Bourdon et al., 2003). Unlike other notable radiometric chronometers such as uranium-lead or potassium-argon, which compare the concentrations of a parent nuclide to that of its stable daughter product, uranium-series disequilibrium dating schemes instead compare the activity—the number of disintegrations per unit time per unit mass of a material—of a parent nuclide to those of their series of unstable daughter products. These methods estimate time by measuring the degree to which different daughter isotopes along a decay chain are out of *secular equilibrium*, a steady state in which the activity of both the parent and daughter nuclides are equal (*i.e.*, the number of daughter nuclides forming is equal to the number of daughter nuclides decaying). Because the half-lives of the parent isotopes are much longer than that of all intermediate daughter products in these decay chains, a material containing the parent isotope that has remained unperturbed for several million years will have reached secular equilibrium (*i.e.*, the activity ratio of the parent nuclide to its daughter product will be equal to 1).

Disturbances to this equilibrium caused by various natural geochemical processes form the basis of uranium-series disequilibrium dating. For example, because of differences in the solubility of uranium and thorium complexes in natural waters of near-surface and surface environments, the highly soluble parent uranium is separated from its effectively insoluble daughter product thorium in a marine or lacustrine carbonate deposit. Once this separation occurs, the system will follow the laws of radioactivity, restoring equilibrium between the parent and daughter nuclides at a rate determined by their respective decay constants. Thus, the timing of carbonate formation is determined by measuring the extent to which daughter product growth has restored the system to secular equilibrium (*i.e.*, the extent to which the activity ratio of the parent nuclide and its daughter product has returned to unity). Using measurements of relevant activity ratios, a date can then be calculated from decay equations and constants.

Of the many uranium-series dating techniques available, in this paper, we use the more widely

4

applied ^{230}Th-^{234}U-^{238}U disequilibrium dating method, for which "U-Th dating" commonly serves as shorthand (Fig. 1). U-Th dating has been most widely applied in carbonate minerals: not only are they nearly ubiquitous in most continental waters, but they also contain relatively higher amounts of uranium and are less prone to post-depositional alteration than other lacustrine precipitates, like halite. As previously mentioned, the conditions that increase the solubility and mobility of uranium tend also to decrease the solubility and mobility of thorium. In oxic environments, uranium generally assumes its highest oxidation state (U^{6+}) in the form of the highly soluble uranyl ion (UO_2^{2+}) which easily forms stable complexes with carbonate ions (CO_3^{2-}), further enhancing its solubility. UO_2^{2+} is then adsorbed onto or structurally incorporated into carbonate mineral host phases (Langmuir, 1978; Reeder et al., 2000, 2001; Kelly et al., 2003, 2006). In contrast, thorium is generally very insoluble and immobile in most aqueous environments where pH > 3, with some exceptions (Chabaux et al., 2003). The solubility of both uranium and thorium increase significantly when forming complexes with organic ligands like humic and fulvic acids (Langmuir and Herman, 1980; Halbach et al., 1980; Murphy et al., 1999; Lenhart et al., 2000). Thus, in most conditions, except for those that are highly reducing or organic-rich, fluids are enriched in uranium and depleted in thorium, and this extreme fractionation is preserved when calcium carbonate forms from such waters.

Two equations take advantage of this behavior to form the backbone of U-Th dating. The first is the ^{230}Th age equation:

$$\left[\frac{^{230}\text{Th}}{^{238}\text{U}}\right] - 1 = -e^{-\lambda_{230}t} + \left(\left[\frac{^{234}\text{U}}{^{238}\text{U}}\right] - 1\right)\left(\frac{\lambda_{230}}{\lambda_{230} - \lambda_{234}}\right)\left(1 - e^{-(\lambda_{230} - \lambda_{234})t}\right) \tag{1}$$

where square brackets around ratios indicate activity ratios; λ symbols are decay constants; and t is the date (Bateman, 1910; Broecker, 1963; see Edwards, 1988 and Ivanovich and Harmon, 1992 for derivation). The ^{234}U/^{238}U activity is more commonly expressed using delta (δ) notation, representing the deviation in parts per thousand (permil; ‰) of ^{234}U/^{238}U from secular equilibrium: δ^{234}U $= ([^{234}$U/^{238}U$]-1) \times 1000$. From this equation, it is clear that measuring three key isotopes—^{238}U, ^{234}U, and ^{230}Th—allows us to uniquely solve for t (Fig. 1A).

The term in Eq. 1 involving δ^{234}U exists to account for the enrichment of ^{234}U over ^{238}U commonly observed in natural waters (Thurber, 1962). This disequilibrium is caused by the preferential leaching of ^{234}U during water-rock interactions due to its displacement inside the crystal lattice of the host mineral by the alpha recoil of its parent ^{234}Th (Kigoshi, 1971; Kronfeld, 1974; Fleischer, 1982; Chabaux et al., 2008). After solving for t using Eq. 1, we can use a second equation to determine the starting value of δ^{234}U at the time of fractionation (δ^{234}U$_{\text{initial}}$):

$$\delta^{234}\text{U}_{\text{m}} = \left(\delta^{234}\text{U}_{\text{initial}}\right)e^{-\lambda_{234}t} \tag{2}$$

where the subscript m represents the present measured value. Thus, these two equations allow us to solve for two unknowns with the measurement of two isotopic ratios.

Fig. 1B shows the expected isotopic evolution of ^{230}Th/^{238}U activity and δ^{234}U$_{\text{initial}}$ over time, provided the system remains closed. Fig. 1C shows the graphical solution to Eqs. 1 and 2: straight, sub-vertical lines represent solutions to the ^{230}Th age equation and curved lines emanating from the y-axis are solutions to the δ^{234}U equation. From this figure, two observations about this dating system can be made: (1) for a given analytical error, as the true age of the sample increases, so too does the error in the age estimate due to the increasing closeness of the age isolines; and (2) although both ^{230}Th/^{238}U and ^{234}U/^{238}U have not yet returned to their secular equilibrium values
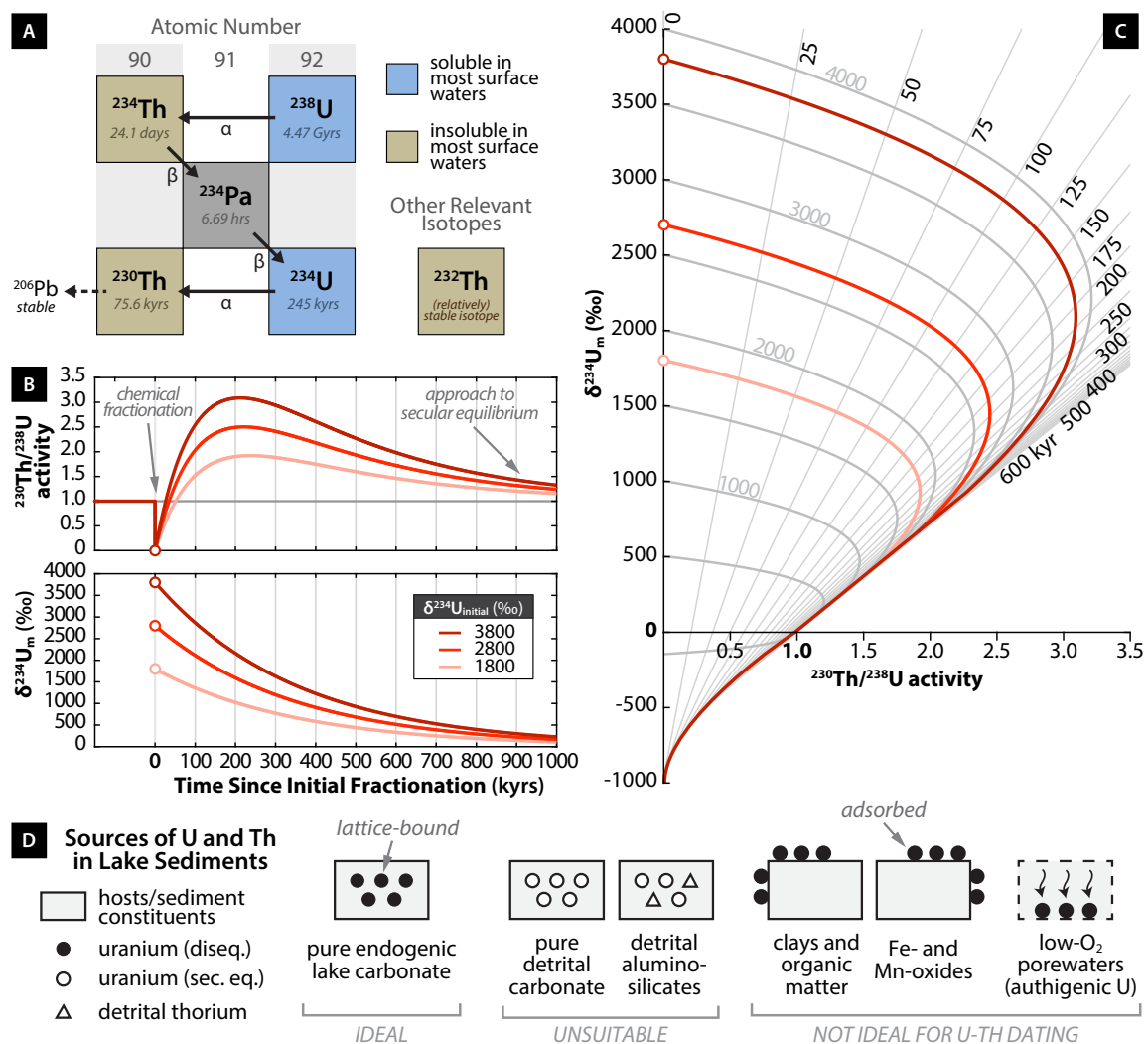
Figure 1: The basic principles of U-Th dating. [**A**] Schematic of the portion of the ^{238}U decay chain that is relevant for U-Th dating. The half-lives and type of particle emitted during radioactive decay (an α or β particle) of each isotope are shown. Ultimately, the decay chain ends with the stable ^{206}Pb. [**B**] and [**C**] Panels illustrating the evolution of ^{230}Th/^{238}U activity and measured δ^{234}U (δ^{234}U$_m$)—the two ratios used for the calculation of U-Th dates—after initial fractionation. The three thick red-shaded lines represent different pathways towards secular equilibrium based on the value of δ^{234}U$_{initial}$ (see legend in bottom of Panel B). Values shown are within the range of values observed in the Lake Junín sediments, but are otherwise arbitrary and selected purely for demonstration. Panel C plots the same curves in Panel B but in ^{230}Th/^{238}U activity-δ^{234}U$_m$ space to show the graphical solution to the age equations. Hollow circles mark the initial isotopic composition of the sample. Straight gray lines represent solutions to the ^{230}Th age equation (Eq. 1, lines labeled in kyrs with black text) and curved gray contours represent solutions to the δ^{234}U equation (Eq. 2, some curves labeled with their δ^{234}U$_{initial}$ in gray). The plot of data in ^{230}Th/^{238}U activity-δ^{234}U$_m$ space originates from Edwards (1988). [**D**] Schematic of uranium and thorium sources in lake sediments. Black circles represent uranium in ^{230}Th/^{238}U disequilibrium whereas white circles represent uranium in secular equilibrium. To simplify, the detrital carbonate and aluminosilicate constituents represent bedrock-derived material of old age (>2 Ma). The placement of circles and triangles within or around boxes represents how uranium and thorium are associated with each host: bound within the crystal lattice or adsorbed to the substrate surface. The box furthest to the right represents the low-oxygen porewater uranium sink, where uranium changes from a soluble to insoluble valence state and accumulates authigenically.

6

even after 1 Myrs, the age isolines eventually are so closely spaced that current analytical abilities cannot distinguish between a sample of a finite age and a sample of infinite age. This characteristic and current mass spectrometry techniques dictate the practical limit of U-Th dating at $\sim$700 kyrs (Stirling et al., 2000; Edwards et al., 2003; Cheng et al., 2016; Fig. 1A).

2.2. Previous work on U-Th dating of lake sediments

With all radiometric chronometers, a date is only interpretable as a meaningful age if the system meets the following criteria for *closed-system behavior*: (1) all decay products were absent at the time of formation, or can be corrected for if present; and (2) there was no gain or loss of any radionuclides after formation other than by radioactive decay. For U-Th dating of lake sediments, the most common obstacle is the lack of material that fulfill these criteria. Even carbonate-rich sediments remain difficult to date, as the carbonates often contain non-ideal constituents or have experienced post-depositional alteration due to various weathering, transport, and mixing processes common in lake basins (Fig. 1D).

Despite the challenge, geochronologists have devised ways to circumvent these issues. Table 1 is a list of lake sediment studies in which U-Th dating was applied, each with varying degrees of success. We distinguish between studies working with evaporites and carbonates, as these are the two most common materials used. Success has been limited primarily by the incorporation of detrital materials that introduce initial ^{230}Th, which increases uncertainties and, if not fully corrected for, potential inaccuracies. Detrital contamination is usually even more problematic for non-carbonate evaporites like gypsum or halite because these materials typically have very low amounts of uranium derived from precipitating waters. The most common detrital materials found in carbonates and evaporites are clay minerals (aluminosilicates and bulk limestone; Fig. 1D). Attempts to chemically separate detritus from bulk sediment have been made, but selective acid leaches meant to isolate endogenic material from the detrital component were found to also differentially fractionate the uranium and thorium isotopes in unpredictable ways (Bischoff and Fitzpatrick, 1991; Luo and Ku, 1991), making sequential acid leaching techniques for age determination ineffective in all but the most controlled experimental cases (Ku and Liang, 1984; Schwarcz and Latham, 1989).

Thus, most U-Th dating applications of lake sediments have applied corrections for detrital contamination by processing a series of coeval samples through total sample dissolution and then using "isochron" techniques. Here, the long-lived isotope ^{232}Th (Fig. 1A) acts as a tracer of contamination: assuming that the endogenic material contains no ^{232}Th or initial ^{230}Th, any ^{232}Th detected is attributed to the detrital component, and the accompanying amount of detrital ^{230}Th is assumed to occur at a particular proportion relative to ^{232}Th – an initial ^{230}Th/^{232}Th ratio.

For this reason, a sample with a higher measured ^{230}Th/^{232}Th or ^{238}U/^{232}Th ratio (more ^{238}U leads to more abundant ^{230}Th) is considered more "clean," while a sample with a lower measured ^{230}Th/^{232}Th or ^{238}U/^{232}Th ratio is considered "dirty" (colloquial terms used in the literature; *e.g.*, Schwarcz and Latham, 1989; Przybylowicz et al., 1991; Stein and Goldstein, 2006). By plotting the isotope ratios of several analyzed portions of a single sample with varying amounts of detritus, an isochron line fit through those analyses can pinpoint the isotope ratios of the endogenic material, and thus provide a date. This approach is considered more rigorous than leaching methods, but is only applicable when there is a single, homogenized source of detritus with a consistent ^{230}Th/^{232}Th ratio forming one end member of the sample mixtures. Most studies listed in Table 1 apply this isochron method, but the process is labor intensive because at least three analyses are required for a date, and many more for one that is statistically rigorous (Powell et al., 2002).

In some cases where the measured ^{230}Th/^{232}Th ratio of sample material is sufficiently high,

7

Table 1: A list of sites and the associated studies which used U-Th dating to develop an age model for a lacustrine sediment sequence. Also indicated are other types of age constraints used for age model construction, separated into two categories: *absolute constraints* and *other tie points*. In these columns, '1' indicates that the chronological tool played a primary, first-order role in the age model, whereas '2' indicates that the tool played a second-order role, used only after application of first-order data. If no number appears beneath a column, this indicates that the chronological tool was not used to construct the age model at the site. The list of chronological tools in the table header reflects the tools used amongst the selected sites and is not meant to be a comprehensive of all possible tools.

Site	Country	Duration	References	ABSOLUTE CONSTRAINTS [14C]	U-Th[a] carb.	evap.	other	OSL[b]	OTHER TIE POINTS pmag.[c]	tephra[d]	strata[e]	tuning[f]
Lake Junín	Peru	~700 ka	this study	1								
Lake Igelsjön	Sweden	12 ka	Israelson et al. (1997)	1	1							
Babicora Basin	Mexico	65 ka	Metcalfe et al. (2002)	1			1[g]					
Salar de Atacama	Chile	106 ka	Bobst et al. (2001); Lowenstein et al. (2003)			1						
Lake Balikun	China	150 ka	Ma et al. (2004)		1				2			
Death Valley	USA	200 ka	Li et al. (1996); Ku et al. (1998)			1						
Searles Lake	USA	3 Ma	Peng et al. (1978); Bischoff et al. (1985); Lin et al. (1998)	1	1				1			
Qaidam Basin	China	4 Ma	Luo and Ku (1991); Phillips et al. (1993); Wang et al. (2013) and references therein	1	1				1			
Dead Sea	Israel	230 ka	Kaufman et al. (1992); Haase-Schramm et al. (2004); Stein and Goldstein (2006); Torfstein et al. (2015), references therein	1	1						1	1[h]
Bear Lake	USA	250 ka	Colman et al. (2006)	1	1				1			1[i]
Great Salt Lake	USA	280 ka	Balch et al. (2005)	1	1				1	1		
Lake Titicaca	USA	370 ka	Fritz et al. (2004, 2007)	1	1							1[j]
Lake Bosumtwi	Ghana	450 ka	Shanahan et al. (2013)	1	1			1	1		1	2[k]

[a] Applications of U-Th dating are separated into three categories based on material: carbonates ('carb.'), which includes minerals such as calcite and aragonite, and evaporites ('evap.'), which includes minerals such as halite and gypsum.

[b] 'OSL' refers to optically stimulated luminescence dating.

[c] 'pmag.' refers to the use of paleomagnetic excursions, reversals, and intensity to determine age constraints.

[d] 'tephra' refers to records that match tephras from the sediment sequence to well-dated tephras from other sites.

[e] 'strata' refers to matching stratigraphic units in the core to equivalent units in other well-dated records.

[f] 'tuning' refers to the alignment of proxy data to specific anchor points in the standardized timescales of external records ("wiggle matching").

[g] Diatom silica.

[h] The drill core from the Dead Sea Deep Drilling Project was also tuned to the LR04 benthic stack (Lisiecki and Raymo, 2005) and Soreq Cave (Bar-Matthews et al., 2003).

[i] For the deeper part of the core, lithologic units were tied to the Devils Hole oxygen isotope record (Winograd et al., 1992).

[j] Peaks in calcium carbonate content were tied to the Vostok CO_2 record (Petit et al., 1999).

[k] As a test of the age model, the dust record from Lake Bosumtwi was tied to that of EPICA Dome C (Lambert et al., 2008).

single-sample dates are possible by applying an initial ^{230}Th/^{232}Th correction that generously accounts for the full range of possible detrital ^{230}Th/^{232}Th ratios. The ^{230}Th age equation modified to correct for initial ^{230}Th is as follows:

$$\left\{ \left[\frac{^{230}\text{Th}}{^{238}\text{U}} \right] - \left[\frac{^{232}\text{Th}}{^{238}\text{U}} \right] \left[\frac{^{230}\text{Th}}{^{232}\text{Th}} \right]_i \left(e^{-\lambda_{230}t} \right) \right\} - 1 =$$
$$- e^{-\lambda_{230}t} + \left(\left[\frac{^{234}\text{U}}{^{238}\text{U}} \right] - 1 \right) \left(\frac{\lambda_{230}}{\lambda_{230} - \lambda_{234}} \right) \left(1 - e^{-(\lambda_{230} - \lambda_{234})t} \right) \quad (3)$$

where i refers to the initial value at the time of fractionation (Edwards et al., 1987). For impure carbonates, this detrital correction is usually the largest contributor to the uncertainty of the final date, having greatest effect on samples with low uranium or low ^{230}Th/^{232}Th ratios. The impact of this correction decreases with the age of the sample: with time, radiogenic ^{230}Th builds up and any initial ^{230}Th decays away, making the proportion of radiogenic ^{230}Th to initial ^{230}Th more favorable. Single-sample dating has thus far only been successful in more recent studies where carbonates with high uranium concentrations (>3 ppm) are available and inductively-coupled plasma mass spectrometers allow for smaller amounts of material to be processed, making it easier to avoid detritus when sampling (*e.g.*, Balch et al., 2005; Fritz et al., 2007; see Table 1).

Thus, the presence of initial ^{230}Th in sample materials has viable workarounds. However, less directly addressed is the issue of possible post-depositional gain or loss of uranium. In addition to clays, other sediment constituents like organic matter and Fe-Mn hydroxides serve as sources of uranium separate from endogenic materials; here, uranium is adsorbed to the mineral and solid surfaces of these impurities (Ames et al., 1983a,b,c; Porcelli et al., 1997; Ku et al., 1998; Schmeide et al., 2000; Chappaz et al., 2010; Fig. 8D). In theory, utilizing these other uranium sources for dating can be satisfactory if the uranium has remained immobile since their initial incorporation, as they are initially without ^{230}Th and would accumulate radiogenic ^{230}Th with time. Indeed, uranium associated with organic matter and clays enclosed in evaporites has been beneficial to the dateability of such low-uranium deposits (*e.g.*, Ku et al., 1998). However, adsorbed uranium is far more susceptible to post-depositional remobilization than uranium bound within the crystal lattice of carbonates (Alam and Cheng, 2014). Furthermore, organic matter and clays can also adsorb additional uranium introduced to the materials via fluid flow, for instance when low-oxygen pore-waters render uranium insoluble and cause it to accumulate authigenically (Fig. 1D; Yliruokanen, 1980; Bone et al., 2017).

Due to this capacity for organic matter to uptake uranium, there have been some attempts to date peats in highly organic-rich sediments that exhibit high uranium concentrations of 1–100 ppm (Van Der Wijk et al., 1986; Rowe et al., 1997; Geyh and Mu, 2005; Frechen et al., 2007), but open system behavior is commonly evidenced by age reversals or anomalous uranium isotope values in these materials. The sediment sequence at Lake Junín is interspersed with thick peat and organic-rich mud layers throughout its length, signaling that the lake has likely experienced considerable changes in lake level and redox conditions. In the following section, we provide further details about these sediments.

2.3. Background on the lake sediments from Lake Junín

Lake Junín (11.0°S, 76.2°W, 4100 m a.s.l.; Fig. 2) was targeted as a site for deep drilling because of its potential to yield the first continuous, absolutely dated record in the tropical Andes
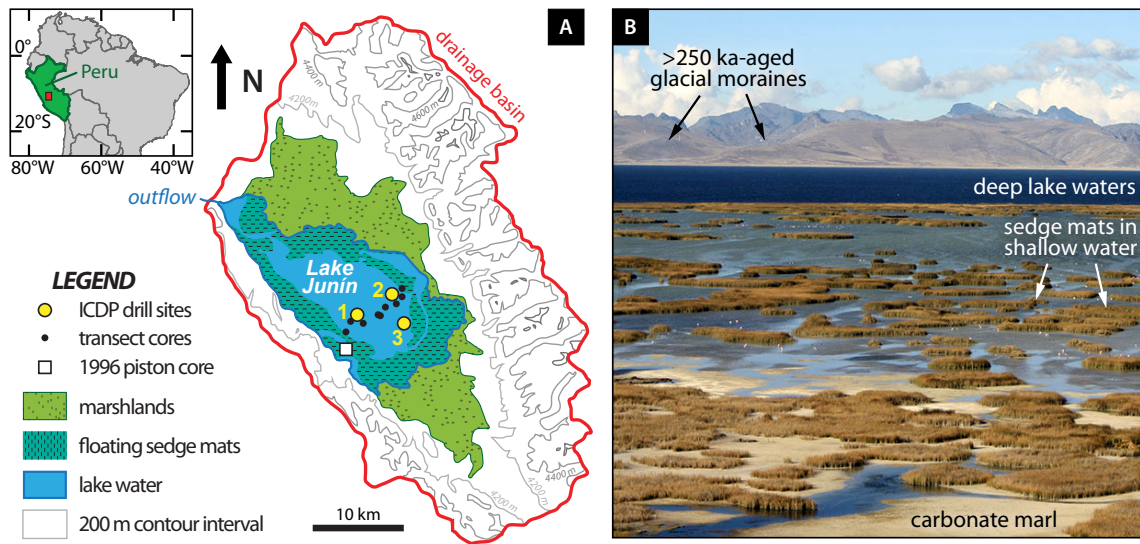
9

Figure 2: [**A**] Map of Lake Junín and its drainage basin, and the location of the three ICDP drill sites (yellow circles), the nine Livingstone core locations taken along a transect across the lake (black circles), and the 1996 piston core (white square; Seltzer et al., 2000). The composite splice for Lake Junín is composed of cores from Site 1 and two transect cores from the center of the basin (Hatfield et al., 2019). [**B**] More recently deposited carbonate silt found among the sedge mats fringing the lake margins. The carbonate silt is subaerially exposed during the dry season (June-July-August) when lake levels drop ∼1–2 m. For scale, small white specks in the shallow water are Chilean flamingos (∼1 m). Photograph taken by Charles Casey from the western shore, facing approximately northwest across the lake.

that spanned multiple glacial-interglacial cycles. Located on the high plateau between the eastern and western cordilleras of the central Peruvian Andes, this relatively shallow (<15 m) lake is the largest water body located entirely within Peru, occupying an area of ∼300 km^2 fringed by marshlands and dense sedge mats (Wright, 1983). Bedrock consists primarily of Paleozoic-Mesozoic marine carbonates, with some exposure of pre-Cambrian crystalline silicate rocks along the eastern cordillera (Cobbing et al., 1981). The lake owes its origin to >250-ka-aged coalescing glacial outwash fans that dam the northern and southern ends of the lake, respectively (Hansen et al., 1984). Moraine mapping and cosmogenic exposure ages from boulders on moraine crests indicate that the lake was not overridden by glaciers or ice at any time in the last 1 million years (Smith et al., 2005a, 2005b), making it one of the few studied lakes in the Andes that predates the maximum extent of glaciation.

Previously extracted short (∼20–25 m) cores spanning the last ∼50 kyrs revealed that the lake sediments consist of alternating packages of fine-grained glaciogenic silt and endogenic carbonate silt deposited at a high rate (0.2–1.0 mm yr^{-1}; Hansen et al., 1984; Seltzer et al., 2000). The carbonate silts are interpreted to have formed similar to the way such silts form in present day, in which springs and streams supersaturated in calcite enter the fringing wetlands along the western side of the lake and precipitate carbonate on rooted macrophytes (Flusche et al., 2005; Rodbell et al., 2012). Based on the modern carbonate production processes observed, it was hypothesized that a longer core would contain more carbonate-rich sections, coinciding with warm interglacial and interstadial periods when retreating piedmont glaciers allowed for the formation of marginal
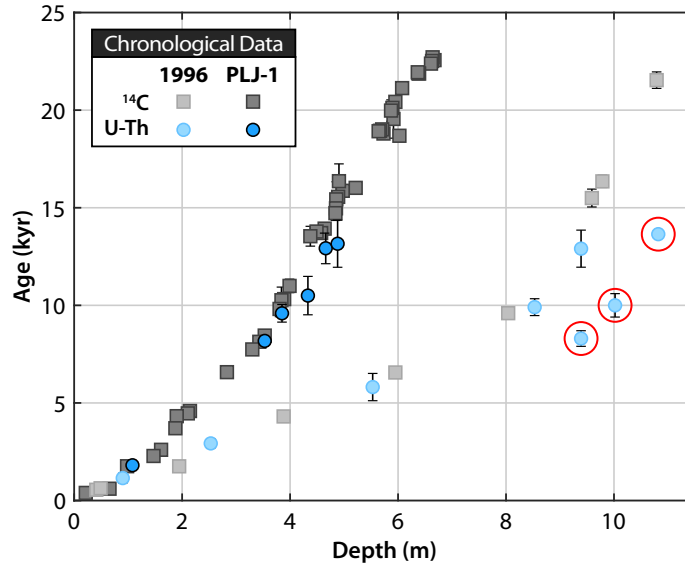
Figure 3: Comparison of radiocarbon (gray squares) and U-Th (blue circles) dates from the 1996 core and the PLJ-1 splice. Radiocarbon data are from Seltzer et al. (2000) for the 1996 core and Woods et al. (2019) for the PLJ-1 splice. Note that most U-Th data shown represent a mean of multiple analyses; see Table A1 for details. Circled in red are outlier U-Th analyses from the 1996 core that contained abundant mollusc shell fragments, and thus may have been affected by post-depositional uptake of uranium, biasing dates to be younger than the true age. Based on the PLJ-1 data, the inferred sedimentation rate (not normalized by dry bulk density) at the lake depocenter over the last 25 kyrs is $\sim$0.3 m kyr^{-1}, which is $\sim$50–60% slower than that of the 1996 core located on the western lake margin (Fig. 2).

wetlands that isolated the basin center from detrital sediment input (Rodbell et al., 2012).

Proving such a temporal link between carbonate deposition, periods of reduced ice cover, and past warm intervals in a longer core would rest on the reliability of the age-depth model. Thus, we conducted a pilot study to determine if U-Th dating could be applied to bulk samples of the carbonate silts. Success would demonstrate than an independent U-Th-based chronology could support a long sediment record from this site, providing motivation for deep drilling. Sample material came from the 1996 piston core taken by G.O. Seltzer and D.T. Rodbell from the shallow western margin of the lake (Fig. 2A). The results from this initial test were encouraging: most of the U-Th analyses attempted on carbonates from the upper 10 m of the core were consistent with the chronology produced by ^{14}C ages (Fig. 3). The three outliers may have been influenced by open system behavior of mollusc shell fragments, which have been previously shown to post-depositionally uptake uranium (Blanchard et al., 1967; Kaufman et al., 1971; McLaren and Rowe, 1996). The preliminary results also revealed that Lake Junín carbonates have high uranium concentrations (0.3–2 ppm) and low detrital content, with ratios of radiogenic ^{230}Th to initial ^{230}Th that are 10 times greater than sediments from Lake Titicaca (Fritz et al., 2007) and the Great Salt Lake (Balch et al., 2005).

Following project approval, the uppermost $\sim$100 m of sediment was drilled and cored in eleven holes across three sites in August 2015. This paper focuses only on sediments recovered from Site 1, the deepest core extracted from the approximate depocenter of the lake. We work primarily from the PLJ-1 splice, which is comprised of core sections from four of the five holes at Site 1 and core sections from two Livingstone transect cores close to the lake depocenter (Fig. 2). More specifics

regarding the coring operation and the subsequent generation of the PLJ-1 splice are described in Hatfield et al. (2019); hereafter, all references to depth in the Lake Junín core refer to the core composite depth below lake floor (CCLF). For complete information on the radiocarbon dates constraining the first ∼50 kyrs of the record, we refer the reader to Woods et al. (2019).

Here we briefly describe the stratigraphy of the PLJ-1 splice; a full description will be detailed in subsequent publications elsewhere. Broadly, the prediction that a long core from Lake Junín would also contain alternating packages of carbonate and glaciogenic sediment was correct: ∼10 m thick packages of cream-colored carbonate silt alternate with ∼10–15 m thick intervals of dark gray, fine-grained carbonate-rich glaciogenic silt throughout the length of the core until ∼85 m, where a thick package of carbonate-rich sand occurs (Fig. 4A). The mean grain size of this bed was incompatible with the drilling tools during core extraction, preventing deeper core recovery. Peat and organic-rich mud layers of ∼1- to 50-cm thickness punctuate both the carbonate and glaciogenic silt intervals and contain abundant microfossils that suggest that the peats represent times of wetland encroachment towards the lake center during lake level lowstands (Woods et al., 2019). Despite this interpretation, there is no stratigraphic evidence of any depositional hiatus or unconformity throughout the core, suggesting that the drill site has been submerged, however shallow in depth, for the duration of the record (Rodbell, Abbott, et al., in prep.).

3. Methods

3.1. Core sampling for U-Th dating

Within the U-Th geochronology community, there is a common expectation that samples with the following characteristics, regardless of substrate type (speleothems, sediments, tufas, *et cetera*), have greater potential for success: light in color (considered an indicator of sample purity), non-porous, homogeneous (either as thin laminae or thicker intervals), and free of shell fragments and other detritus. We took advantage of the opportunity provided by modern mass spectrometry to process smaller amounts of material by making a deliberate effort to limit the amount of detritus included during the initial sampling stage.

Core splitting and sampling took place at the National Lacustrine Core Facility (LacCore) at the University of Minnesota, Twin Cities, in February 2016. After cores were split lengthwise and the centers were extracted with a plastic "U-channel" for paleomagnetic work, sampling for U-Th dating was given first priority on all cores. This order of operations ensured that the most ideal carbonates would be reserved for dating and not be under-utilized for other measurements where less ideal materials would suffice.

Cores were visually assessed for material that fulfilled the criteria described above. Once a carbonate section was identified, we used utility blades, knives from a fruit and vegetable carving set, and tweezers to cut and extract thin wafers of sediment ∼0.2–0.5 cm in thickness (Fig. 5). In sections of core containing finely laminated carbonate sequences, we took care to isolate individual laminae, only sampling the cleanest parts and scraping away undesirable material when necessary. In addition, when possible, we sampled layers that appeared to have more detritus immediately adjacent to these cleaner laminae with the intention of using this material for possible isochron work. We examined smear slides during sampling in order to petrographically verify that samples identified by eye as being relatively detritus-free were as such, and made real-time adjustments in sampling strategy based on results. Fig. 4C shows the depths from which U-Th samples were taken and their relation to stratigraphic units. Sedimentary lithologies were defined following protocols by Schnurrenberger et al. (2003), including smear slide observations.
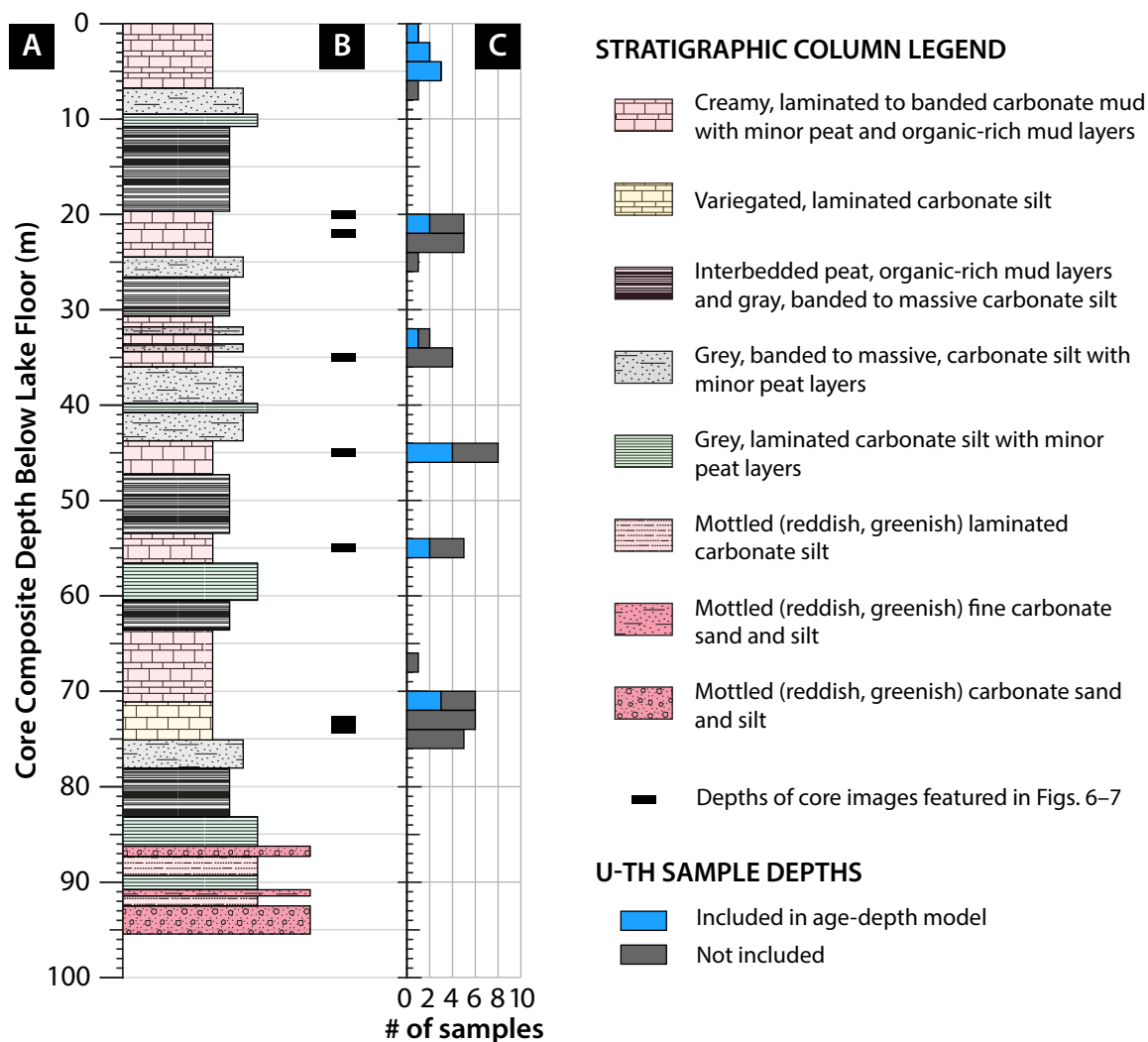
12

Figure 4: [**A**] Stratigraphic column of the PLJ-1 splice, described following the core description scheme proposed by Schnurrenberger et al. (2003). Lithologies in the stratigraphic column legend are listed in ascending order of mean grain size (smaller at the top, larger at the bottom). [**B**] Rectangular bars mark the depths of the cores featured in Figs. 6 and 7. [**C**] Stacked histogram of depths of samples collected for U-Th dating, in which blue represents samples that yielded dates included in the age-depth model and gray represents samples that yielded dates that were not included.

During sampling, we also documented the macro-scale sedimentological characteristics associated with each sample. After observing a variety of carbonate-rich sequences, we divided them into four lithological facies categories:

- **C**ream-colored **m**assive **c**arbonates (**CMC**): cream-colored, massive, medium to thick (∼10–50 cm) bedded carbonate silts found in close association with gray, massive, banded or mottled
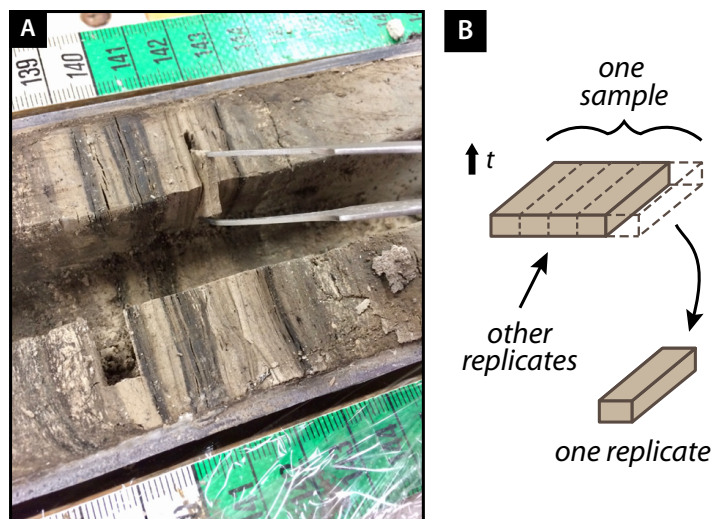
Figure 5: [**A**] The core sampling process for U-Th dating. Surgical straight edges and blades from a fruit carving knife set were used to cut out thin (∼0.2–0.3 cm) wafers of sediment, which were then extracted with tweezers. [**B**] One *sample* consists of a single wafer of sediment extracted as shown in Panel A. Replicate analyses are made on separate sections of the sediment wafer: rather than homogenizing the wafer into a powder and dating the powder multiple times, we date different sections of the sample in order to assess sample reproducibility.

silt, with some thin (∼1–2 cm thick) peat or organic-rich mud layers (Fig. 6)

- **R**ed-**g**reen **a**lternating (**RGA**): red and green laminated sets of carbonate silts that alternate in color every ∼5–20 cm, with some organic-rich peat laminae (Fig. 6)

- **C**ream-colored carbonates with **p**eat beds (**CP1**, **CP2**): Cream-colored, faintly banded carbonate silt interbedded with peat layers, with some associated with thick (∼30–50 cm) overlying peat beds that were laterally continuous across multiple holes at Site 1 (CP1), and others associated with thin (∼3–5 cm), laterally discontinuous peat beds (CP2) (Fig. 7)

Each sample extracted for U-Th dating was subsequently categorized into one of these four facies.

3.2. Sample preparation and chemistry for U-Th dating

After core sampling, sediment wafers were frozen and then placed in a vacuum freeze drier to remove moisture from all material. Most samples retained their original wafer shape after this process. A small portion of each sample was then gently disaggregated for micro-scale sedimentological characterization under a picking microscope. We made qualitative observations on the following: color; hardness of bulk sediment (friable or compacted); and the relative abundance of mollusc shell fragments, ostracode valves, organic fibers (peat fragments, grasses, seed pods), sponge spicules, siliciclastic grains, or other mineral precipitates. For subsequent U-Th analyses, we manually removed mollusc shell pieces from the sample before dissolution, or avoided processing samples containing abundant mollusc shell fragments that could not be reliably removed. Otherwise, all analyses discussed are measurements on bulk samples containing all other aforementioned constituents.
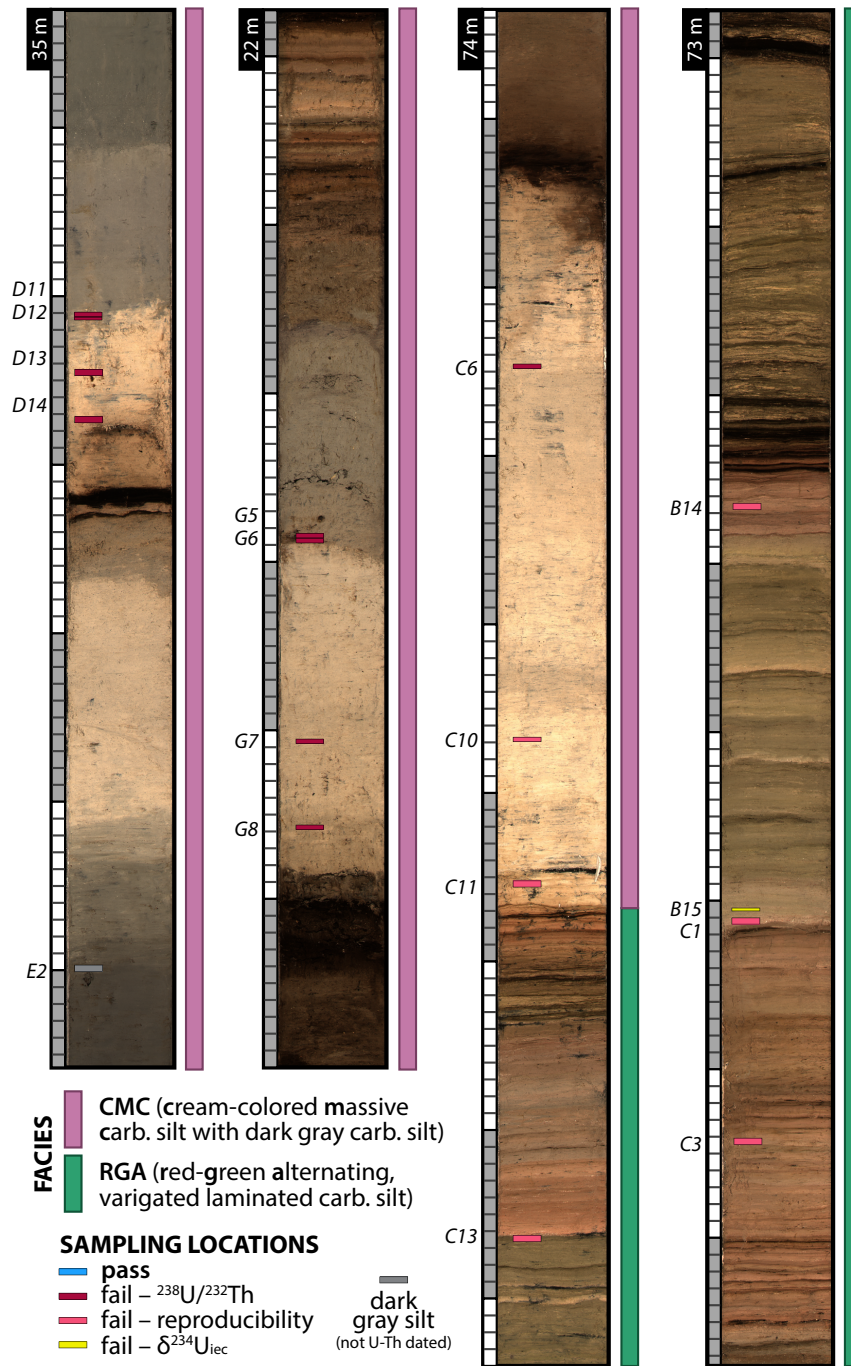
14

Figure 6: Core scanning images and U-Th sample locations of four selected cores that feature the CMC and RGA facies. The approximate corresponding CCLF is noted in the black rectangular box at the top left of each core image. The column of gray and white boxes appended to the left of each core image is a ruler representing alternating blocks of ten centimeters, mimicking the actual ruler used during scanning at LacCore's facilities. Small rectangles plotted on top of the core image represent sample locations and are labeled by sample ID and color-coded by threshold criteria result (see Section 5 and Fig. 8). The columns to the right of each core image represent the facies that is given to a sample collected in that depth interval; for example, for the third core image, samples C6, C10, and C11 are categorized as CMC, while C13 is categorized as RGA. Core scanning images were made using a Geotek MSCL-CIS at the National Lacustrine Core Facility (LacCore).
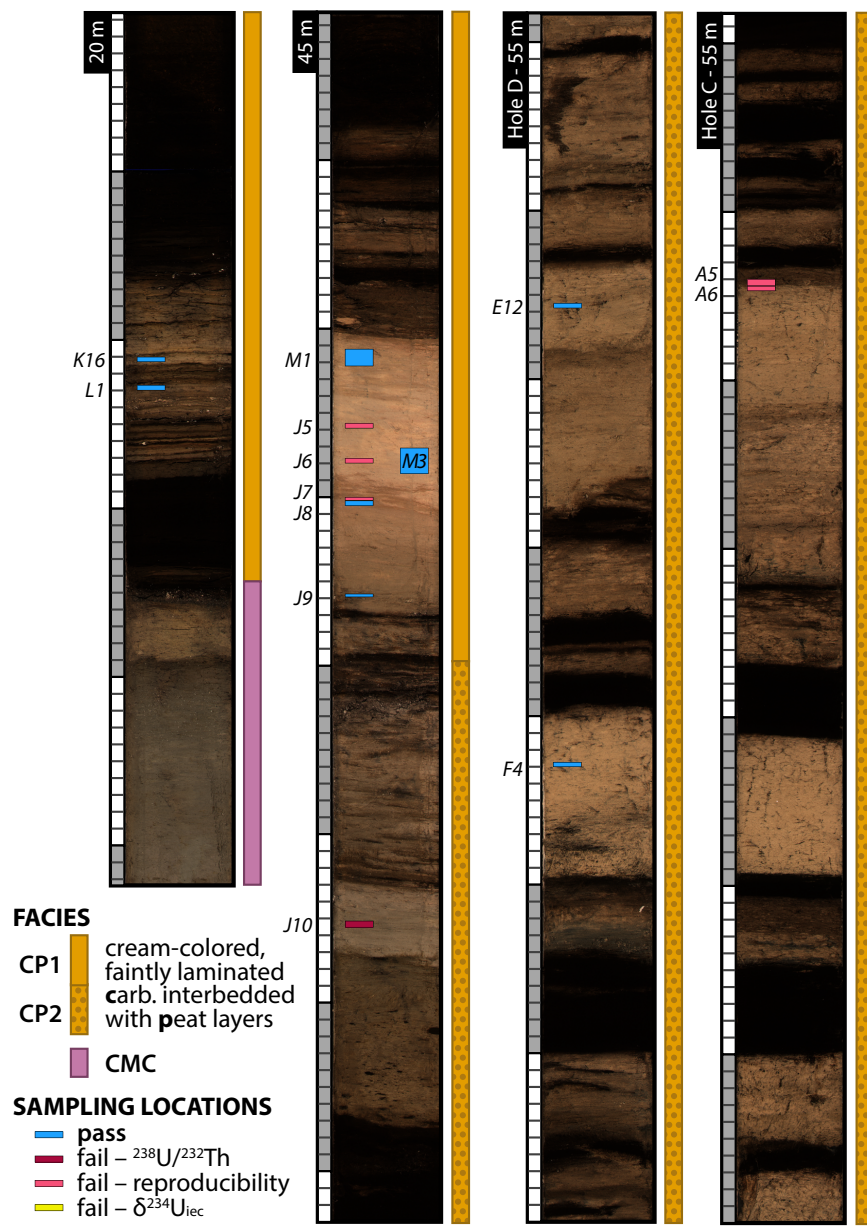
Figure 7: Core scanning images and U-Th sample locations of four cores that feature the CP facies, which is subdivided into CP1 and CP2 to differentiate between samples that are associated with thick (>10 cm) and laterally continuous peat layers (CP1) and those that are not (CP2). Note that the third and fourth images are of cores from the same CCLF but from different holes at Site 1, shown here to demonstrate the lateral discontinuity of some peat and carbonate beds. Holes at Site 1 were spaced approximately ∼20 m apart. Small rectangles plotted on top of the core image represent sample locations and are labeled by sample ID and color-coded by threshold criteria result (see Section 5 and Fig. 8). See caption in Fig. 6 for explanation of other symbology used in the figure.

16

Because U-Th column elusions are time and resource intensive, a small set of samples from different facies were screened for their uranium and thorium concentrations to determine which facies would most likely yield material viable for dating. Powders of $\sim$2 mg were dissolved in dilute HNO_3, and analyses of uranium and thorium concentration were performed on a VG PQ2+ quadrupole ICP-MS and an Agilent 7900 ICP-MS at MIT. Samples with higher U/Th ratios were then identified as materials worth further processing as they are more likely to yield "clean" samples with high $^{230}Th/^{232}Th$ ratios (Section 2.2).

Replicate analyses were then processed through U-Th column elusions in batches of 5 to 15. When possible, we analyzed at least three replicates from each sample horizon. Here, we purposefully apportion different aliquots of the original sediment wafer for each replicate analysis in order to test the reproducibility of dates from stratigraphically coherent material (Fig. 5B). Note that this is an important difference from repeated analyses of a homogenized powder, which would only provide a measure of internal lab errors or the quality of sample homogenization. Our original intention in processing samples this way was not only to test for reproducibility, but also to build isochrons, for which it is necessary to analyze subsamples that span a range of detrital contamination levels.

After sample selection and preparation, sample dissolution was performed in a clean laboratory at MIT. Samples of 5–60 mg were dissolved in HNO_3 and spiked with a ^{229}Th-^{233}U-^{236}U tracer in Teflon beakers cleaned via a boiling-washing procedure with concentrated HNO_3, HCl, and aqua regia. Next, following methods described by Edwards et al. (1987) and Shen et al. (2002), uranium and thorium were co-precipitated with $\sim$4–8 mg of Fe oxyhydroxides and then separated using BioRad AG1-X8 anion exchange resin (100–200 mesh, 0.5 mL column volume). The isotopic compositions of the resulting uranium and thorium fractions were then measured on a Nu Plasma II-ES multi-collector ICP-MS at MIT. We introduced sample solutions through a CETAC Aridus II desolvating nebulizer system coupled to a PFA nebulizer with a 100 µL/min uptake capillary. Each uranium sample analysis was bracketed by a 5 ng/g solution of the CRM-112a standard (New Brunswick Laboratories). Each thorium sample analysis was bracketed by an in-house ^{229}Th-^{230}Th-^{232}Th standard in order to monitor mass bias and variable SEM yield. 2% HNO_3 solution blanks also bracketed each sample and standard analysis to determine the background signal. See Section S1 for details of U-Th measurements on materials from the 1996 core.

3.3. Estimating the initial ^{230}Th correction

As discussed in Section 4, the correction for initial ^{230}Th has a greater impact on impure sample materials, and so it follows that we must carefully consider this correction for the lake sediments at Lake Junín. Ten samples processed from the 1996 core yielded indeterminate ('infinite') dates, in which a unique solution for the ^{230}Th age equation could not be found after iteration. These samples all had ^{232}Th concentrations that were 20–200 times greater than other samples from the 1996 core that yielded calculable dates (2–7 ppm, compared to 0.04–0.1 ppm), forming a statistically distinct population. Similarly, these samples also had $^{238}U/^{232}Th$ ratios that were $\sim$50 times lower than that of other samples (0.3–0.6 ppm). These results suggest that the samples yielding indeterminate ages had high amounts of detrital contamination that contributed a significant amount of initial ^{230}Th at secular equilibrium with ^{238}U, thereby causing apparent infinite dates.

Assuming that the detrital component of the indeterminate samples of the 1996 core is representative of the isotopic composition of detrital material found in all sediments of the PLJ-1 splice, we calculated the average $^{230}Th/^{232}Th$ ratio of the indeterminate samples and used this ratio for the initial ^{230}Th correction in our calculations. This estimate has the effect of counting radiogenic ^{230}Th accumulated in these samples as detrital, but the depths of these samples suggest that their

true age is no older than 30 kyrs and thus we do not expect an appreciable proportion of the ^{230}Th to be radiogenic.

The average ^{230}Th/^{232}Th atomic ratio of the indeterminate samples from the 1996 core is 7.9 $\pm$ 0.9 $\times 10^{-6}$. Our starting assumption is that this ratio is invariant through time, but it is entirely possible—if not expected—that the isotopic composition of detritus is variable due to changes in clastic transport or source regions. To account for these unknowns and other unknown unknowns, we apply an uncertainty of 50% to this average and use an initial ^{230}Th/^{232}Th atomic ratio of 8.0 $\pm$ 4.0 $\times 10^{-6}$ for U-Th data from the PLJ-1 splice.

3.4. Calculating weighted means and uncertainties of samples with replicate analyses

As previously mentioned, we attempted to analyze at least 3–5 replicates for each sample as a test of the reproducibility of unequivocally coeval material. We calculate a date for each individual replicate analysis using Eq. 1 and the initial ^{230}Th/^{232}Th ratio stated above. We then use these dates to calculate an error-weighted mean ($\bar{x}$) and uncertainty ($\sigma_{\bar{x}}$) of all replicate analyses in a sample, in which weights are equal to the inverse of the variance of each date:

$$\bar{x} = \frac{\sum^N x_i/\sigma_i^2}{\sum^N 1/\sigma_i^2}, \quad \sigma_{\bar{x}} = \sqrt{\frac{1}{\sum^N 1/\sigma_i^2}} \qquad (4)$$

where N is the number of replicate analyses in the sample; x_i is the individual date of each replicate; and σ_i^2 is the variance of the individual dates of each replicate.

We then calculate the degree of agreement between replicate analyses to estimate an uncertainty that is appropriate for the observed scatter between dates. To do this, we calculate the Mean Square of Weighted Deviates (MSWD), a measure of the ratio of the observed scatter around the mean to the expected degree of scatter given the analytical uncertainties of each data point (McIntyre et al., 1966; Wendt and Carl, 1991). The value is essentially the chi-squared statistic (goodness of fit) divided by the number of degrees of freedom ($f=N-1$), or the "reduced" chi-squared:

$$\text{MSWD} = \frac{1}{f} \sum^N \frac{(x_i - \bar{x})^2}{\sigma_i^2} \qquad (5)$$

The value of the MSWD tells us if the calculated uncertainties for each date are over- or underestimated based on the observed scatter in data. A value of ~1 indicates that the observed scatter is equal to the predicted scatter; values less than 1 indicate that the observed scatter is less than is predicted by the uncertainties; and values greater than 1 indicate that the observed scatter is more than the predicted scatter. Samples with an MSWD much greater than 1 are considered to have excess "geologic scatter," suggesting possible biases in the calculated dates, perhaps due to a violation of the assumptions underpinning the system (*e.g.*, open system behavior). Thus, for any sample with an MSWD $>$ 1, we expand the uncertainties of the replicate analyses by a factor of $\sqrt{\text{MSWD}}$ and then recalculate the weighted means with these larger uncertainties using Eq. 4. The `IsoplotR` program by Vermeesch (2018) also includes this strategy as one option of treating data with excess geologic scatter (referred to as "overdispersion"). While the presence of excess scatter is non-ideal and raises concerns about the validity and practical use of such dates, the data still represent geologically meaningful information and thus should not necessarily be rejected outright without further consideration (and we will do much considering, starting in Section 5).

Using the MSWD as a black-and-white parameter to evaluate the validity of dates is generally

discouraged, since the highest permissible MSWD is dependent on N ([Wendt and Carl](), [1991]())
and is often subject to interpretation ([Powell et al.](), [2002](); [Ludwig](), [2003]()). Thus, we calculate the
probability of the observed scatter occurring given the uncertainties for each replicate analysis
(a "probability of fit") by computing the chi-square cumulative distribution for $\text{MSWD} \times f$ (the
chi-squared statistic) about f degrees of freedom ([York](), [1968]()).

Some samples only have 1–2 replicates; these were cases in which early replicate analyses yielded
unfavorable results (*i.e.*, low $^{238}U/^{232}Th$ ratios) and were thus not further repeated in the interest
of time and resources. For the remainder of this paper, our discussion of U-Th dates will refer
to the weighted means and uncertainties (MSWD-adjusted) of samples rather than the individual
dates of replicate analyses, unless otherwise noted.

3.5. Other corresponding data

We use other sedimentological, geochemical, paleoecological, and physical data to interpret and
understand our U-Th data. We provide a list of these datasets in Table 2 and their intended use.
More information regarding these methods of measurement can be found in the Supplementary
Materials (Section S2) and other publications currently being prepared elsewhere.

Dataset	Brief Methods	Purpose
Elemental concentrations	sample dissolution, ICP-MS	Determine if there exists any relationship between U-Th data and concentrations of Ca and trace elements Mg, Sr, Al, Ti, P, V, Mn, and Fe. Measurements are made on same sample material used for U-Th dating.
Total inorganic and organic carbon	coulometry	Determine if there exists a relationship between U-Th data and carbon content. Only measurements made within 1 cm of the U-Th sample are paired with U-Th data.
Color reflectance	spectrophotometry on automated core logger	Determine if there exists a relationship between U-Th data and any spectral reflectance wavelength band. Only measurements made within 2.5 mm of the U-Th sample are paired with U-Th data.
Mineralogy	X-ray diffraction	Determine the mineral composition of the carbonate phases, and if there are discernible differences between endogenic and detrital carbonate.
Ostracode assemblages	picking and identification following Pérez et al. (2010) and Karanovic (2012)	Determine if there exists a relationship between U-Th data and ostracode color, taphonomy (number of broken vs. intact valves; adults vs. juveniles), or ecology (benthic vs. swimmer species, ornamentation).

Table 2: Other datasets used in this study for comparison with U-Th data.

4. Results

In total, we generated 174 U-Th dates from 55 bulk samples from the PLJ-1 splice. Uranium
and thorium geochemical data as well as the number of replicates produced for each sample (N

= 3–8) can be found in Table A1. Samples originate from each of the five high (>70%) $CaCO_3$ intervals that occurred every ∼10–15 m in the core (Fig. 4C). All U-Th dates from the uppermost 5 m are broadly consistent with radiocarbon dates from terrestrial macrofossils and charcoal in the same depth interval (Fig. 3; Woods et al., 2019). A sample from ∼6.5 m yielded an indeterminate date and had a $^{230}Th/^{232}Th$ atomic ratio of $7.7 \pm 0.2 \times 10^{-6}$, consistent with our estimate of the detrital $^{230}Th/^{232}Th$ ratio applied in corrections. Sample ^{238}U concentrations are variable and are generally 0.2–4.0 ppm (mean = 1.5±1.2 ppm, 1-σ); ^{232}Th concentrations are also variable, ranging 0.02–2.4 ppm (mean = 0.6±0.5 ppm, 1-σ).

For the deepest part of the core, the oldest U-Th dates suggest that the record is no older than ∼800 ka. This observation is consistent with the absence of evidence of the Brunhes-Matuyama magnetic reversal (aged ∼780 ka) in the paleomagnetic secular variation record (Hatfield et al., in prep.). However, the scatter of dates throughout the entirety of the core is, at first glance, alarming: at ∼20–25 m, the first high-$CaCO_3$ section beyond the interval covered by radiocarbon, U-Th dates already span a range of ∼200 kyrs (Fig. 8). The spread of dates increases with depth, reaching ∼300 kyrs at the bottom of the record. As is, the scatter of data is too great to build any practical age-depth model, even after applying outlier analysis. Furthermore, all attempts to reduce scatter by building isochrons from replicate analyses and adjacent dirty-clean sample pairs failed (high MSWD and low probability-of-fit; Section S3).

Here, we arrive at the main crux of this paper. The scatter of data and the failure to build isochrons is clear evidence that at least some of the dated materials have not remained closed systems or do not otherwise satisfy the operating assumptions of U-Th dating. Despite this noise, is there a way to objectively assess the quality of each U-Th date, and subsequently curate the dataset without biases (avoid "cherry-picking")? In the following sections, we detail our approach to this question. At times, we will refer to specific U-Th samples by their sample name, which consists of an alphabetical letter A–P followed by a number 1–16 (Table A2).

5. Curation of U-Th data using threshold criteria

Noisy U-Th geochronological datasets are nothing new; in attempts to find clarity in uncertain data, a common practice is to apply some screening criteria based on uranium and thorium concentrations. For example, some studies dating corals and carbonate slope sediments have rejected dates that exceed a certain thorium concentration or do not meet a minimum uranium concentration because such dates tend to have larger corrections and errors (Robinson et al., 2002; Henderson et al., 2006; Skrivanek et al., 2018). However, picking the values for these thresholds can be subjective to an extent, especially if there is no clear separation between distinct populations within the data.

As a start towards better understanding the scatter in our data, we consider applying similar thresholds, first by examining the $^{238}U/^{232}Th$ ratio and the probability of fit of all dates for a given sample to a single weighted mean (Fig. 8A and B). $^{238}U/^{232}Th$ ratios ranged between <1 and 30 and probabilities of fit essentially spanned the full domain of possible values, from 0% to 99%. Between 20 and 60 m, we notice that the samples with the oldest dates all have $^{238}U/^{232}Th$ ratios that are <1, including those yielding indeterminate dates (Fig. 8A). One possible explanation for this observation is that these samples have initial ^{230}Th that has not been accounted for with our initial correction, which would bias dates to be older than the true age. The effect of this bias would be greatest in samples with low radiogenic ^{230}Th due to low uranium concentrations. (Note that we later discuss another explanation for these data in Section 7).

Regarding the probability of fit, deciding how low of a probability is acceptable is somewhat
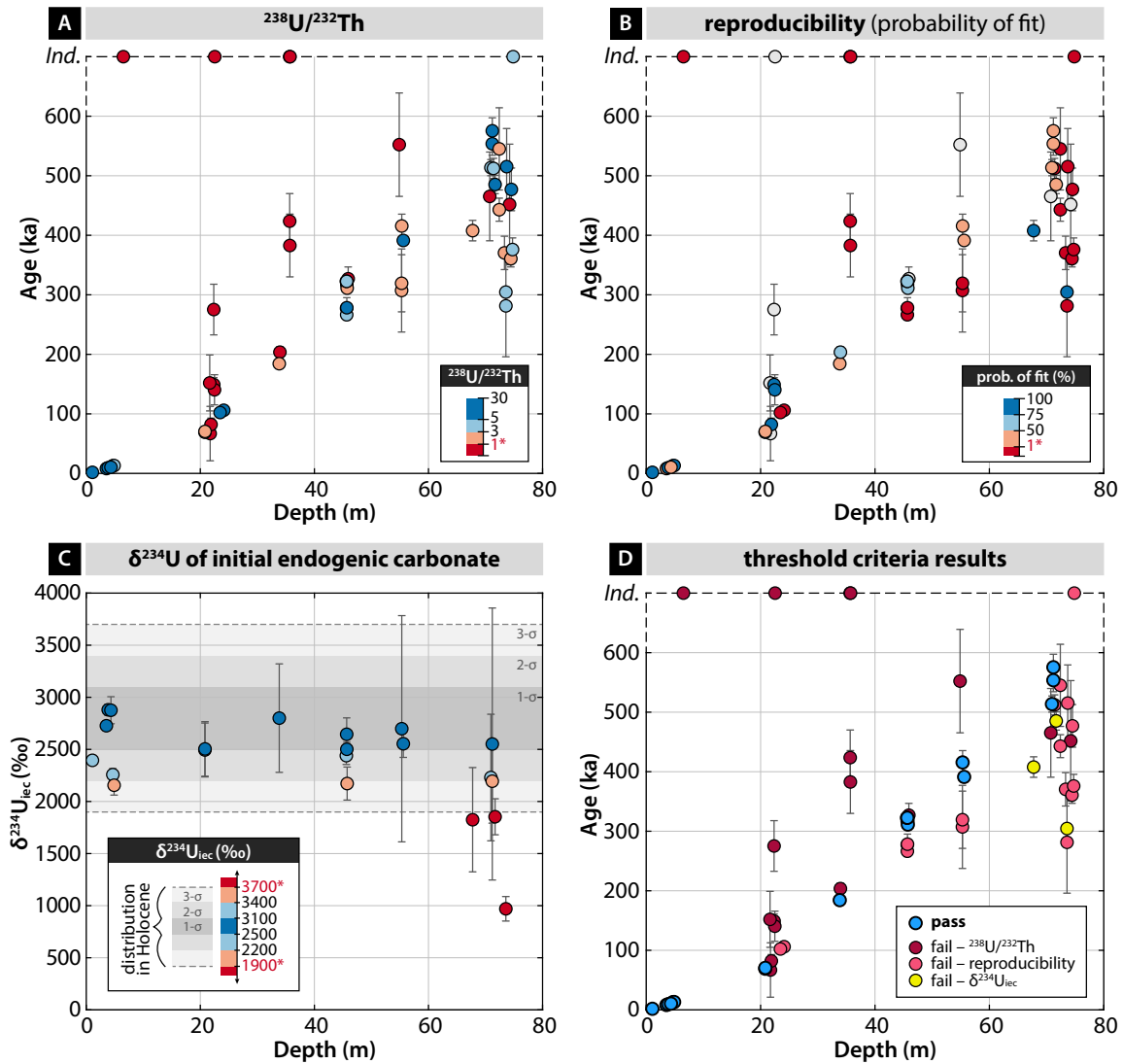
Figure 8: Step-by-step application of thresholding criteria: [**A**] ^{238}U/^{232}Th, [**B**] reproducibility, and [**C**] δ^{234}U of initial endogenic carbonate (δ^{234}U$_{iec}$). [**D**] shows the data that pass and fail the three aforementioned criteria. Note that each point represents the weighted mean and standard deviation of multiple replicate analyses (see Table A1). In Panels A–C, blue/red colors represent values that are more/less ideal for U-Th dating. Values of thresholds are indicated by a red asterisk (*) in each legend. Samples that do not satisfy criteria and were thus subsequently eliminated are colored in dark red. Samples plotted along the uppermost dashed line labeled 'Ind.' refer to analyses that yielded incalculable U-Th dates or were infinite (indeterminate). In Panel B, analyses plotted in light gray are those with only one replicate analysis. Panel C only includes data that pass the ^{238}U/^{232}Th and reproducibility thresholds. Shaded gray areas represent the distribution of δ^{234}U$_{iec}$ values observed in the Holocene, including data from the 1996 core. For Panel D, note that some samples failed both criteria for ^{238}U/^{232}Th and reproducibility; in these instances, the samples were categorized as having failed the ^{238}U/^{232}Th criteria. All error bars in each panel are 2-σ range. Depth refers to the composite core depth below lake floor (CCLF).

21

arbitrary; there is no broad consensus within the geochronology community on how best to treat such data, especially in circumstances in which the total number of subsamples is low (Ludwig, 2012), as is our case. However, most geochronologists would likely agree that samples with a probability of fit less than 1% (especially those much closer to 0%) exhibit an amount of excess scatter that is beyond recovery of practical information about the true age of the sample.

Thus, in the interest of not using too strong of a hand in curating the U-Th data to begin, we apply two conservative threshold criteria: the $^{238}U/^{232}Th$ ratio must be >1 and the probability of fit >1% (Fig. 8A and B). Of the 55 samples, 17 fail the $^{238}U/^{232}Th$ criterion and 22 fail the reproducibility criterion. Of the 17 samples that fail the $^{238}U/^{232}Th$ criterion, eight had more than one replicate analysis, and of those eight, five also fail the reproducibility criterion. In Fig. 8D, we show which criterion each sample fails; for the purposes of simplifying ensuing explorations into the dataset, the five samples that fail both aforementioned criterion are categorized as having failed the $^{238}U/^{232}Th$ criterion.

Next, we consider another screening approach adopted for U-Th dating of marine samples that involves $\delta^{234}U_{initial}$. Because the residence time of uranium in the ocean is very long ($\sim$400 kyrs; Ku et al., 1977), the $\delta^{234}U$ of seawater is thought to have remained relatively constant for at least the last 400 kyrs (Henderson, 2002; Henderson and Anderson, 2003). Thus, assuming that marine samples reliably preserve the $\delta^{234}U$ values of the waters in which they formed, dates from marine samples with $\delta^{234}U$ values that deviate significantly from modern values are considered potentially inaccurate due to diagenesis (Bard et al., 1991; Hamelin et al., 1991; Gallup et al., 1994). In contrast, the $\delta^{234}U$ of surface waters is very diverse and has been found to be sensitive to basin lithology, basin-specific weathering mechanics, riverine and groundwater inputs, and climate (e.g., Sarin et al., 1990; Kronfeld and Vogel, 1991; Plater et al., 1992; Kronfeld et al., 2004; Robinson et al., 2004; Durand et al., 2005; Grzymko et al., 2007; Chabaux et al., 2008). Although few studies examine the long-term history of internal $\delta^{234}U$ variability in lakes and other surface waters (e.g., Kiro et al., 2018), the range of internal $\delta^{234}U$ variability observed in the aforementioned river and groundwater studies suggests that the internal $\delta^{234}U$ of lake waters should not vary significantly without dramatic changes in drainage basin organization. Since the lithology of a lake basin is invariant over the timescales relevant to this study, variability in $\delta^{234}U$ is driven by changes in hydrology. McGee et al. (2012) documented a 300‰ change in the $\delta^{234}U$ of lacustrine cave carbonates during the last deglaciation in Lake Bonneville (Utah, USA), which experienced a $\sim$2× change in precipitation.

Thus, we apply a third threshold criterion using the $\delta^{234}U$ of the initial endogenic carbonate ($\delta^{234}U_{iec}$) of each sample, which we calculate by correcting $\delta^{234}U_{initial}$ values for detrital uranium (see Section S4 for relevant equations). The average $\delta^{234}U_{iec}$ of all samples that yield dates verified by radiocarbon data (including data from the 1996 core) is 2800±300‰. If we compare this average to the $\delta^{234}U_{iec}$ values of the remaining 21 samples, we observe that three samples at $\sim$70–75 m have values that fall well below the average, even outside the range defined by three standard deviations from the mean (Fig. 8C). Because the magnitude of these differences is large, we suggest that these values are unlikely to reflect real changes in the $\delta^{234}U$ of the lake waters, and thus suspect the validity of these dates. Therefore, we mark these three samples as having failed the $\delta^{234}U_{iec}$ criterion (Fig. 8D).

While the remaining 18 dates form a visually pleasing line (Fig. 8D), this observation alone does not intrinsically prove that these remaining dates are accurate. However, the samples generally abide by the rules of stratigraphic order, which is behavior consistent with closed-system dates. Furthermore, the results of applying the threshold criteria may vaguely follow our theoretical ex-

pectations for normally distributed scatter about the mean. That is to say: if you were to ask someone to draw a line through the middle of the original scatter of points, the 18 samples that remain would not stray far from it.

6. Understanding the scatter

Having classified the U-Th data into categories that describe the main flaw of each nominally failed sample (Fig. 8D), we now explore the underlying causes for poor sample behavior and determine if the application of threshold criteria is justified. Essentially, we ask: Is there other evidence that supports our assertion that the threshold criteria failing samples have not remained closed systems? What is special about the 18 passing samples such that they exhibit fewer symptoms of open system behavior?

6.1. Detrital contamination

The first and most obvious hypothesis for poorly behaving dates is detrital contamination that is unaccounted for with the initial ^{230}Th/^{232}Th correction. As stated in Section 2.2, impure sample substrates have been the main obstacle in previous U-Th dating efforts in lake sediments, and there is no evidence to suggest that Lake Junín would be an exception. If detrital contamination does indeed play a large role in the scatter of our U-Th data, we can make certain predictions for how other sedimentological and geochemical data would respond. For example, we would expect that samples with lower $CaCO_3$ content would comprise the eliminated dates, especially those that failed the ^{238}U/^{232}Th criterion. We are able to test this hypothesis directly using co-located measurements of $CaCO_3$ content (weight %) as well as optical lightness from color reflectance spectra (Table 2 and Section S2). Optical lightness, defined here as the sum of spectra in the visible band of the electromagnetic spectrum (400–700 nm), has been shown to be a reasonable proxy for carbonate content in marine sediments (e.g., Nagao and Nakashima, 1992; Mix et al., 1995; Balsam et al., 1999). Data for the PLJ-1 splice also shows that $CaCO_3$ content >50% appears to scale with optical lightness (see gray circles in Fig. 9A). Because color reflectance data were measured on a finer and more regular sampling interval than carbon data, there are more optical lightness data that correspond to U-Th samples than $CaCO_3$ content measurements ($N = 46$ versus 29; Fig. 9).

From Fig. 9, we notice that all but one of our U-Th samples have >50% $CaCO_3$ content, with most passing dates having >70% $CaCO_3$ content. However, many data that failed threshold criteria occupy the same range in $CaCO_3$ content as passing data. Contrary to expectations, each of the five samples with the highest $CaCO_3$ content failed the threshold criteria (Fig. 9B). Likewise, the five samples with the highest optical lightness also failed (not the same five samples; Fig. 9C). Sample C10 is the most extreme case in this comparison, and as a visual check, we can see its sampling location in Fig. 6 and verify its optical lightness value relative to other samples. Again, there is no clear pattern between passing and failing U-Th dates and optical lightness; samples appear to exhibit the entire range of optical lightness values observed in the core. If anything, one could argue that the samples failing the ^{238}U/^{232}Th criterion tend to have higher optical lightness values compared to passing samples, behaving opposite to our predictions. The results are similar when we compare our data with grayscale or luminance (also known as L^*), another "lightness" parameter using the CIE L*a*b* color description system.

Based on these results, we speculate that a high proportion of bedrock carbonate in the detrital component could explain the high $CaCO_3$ content of failed samples; even the darkest gray silt sections in the core with high magnetic susceptibility had 20–50% $CaCO_3$ content. The uranium
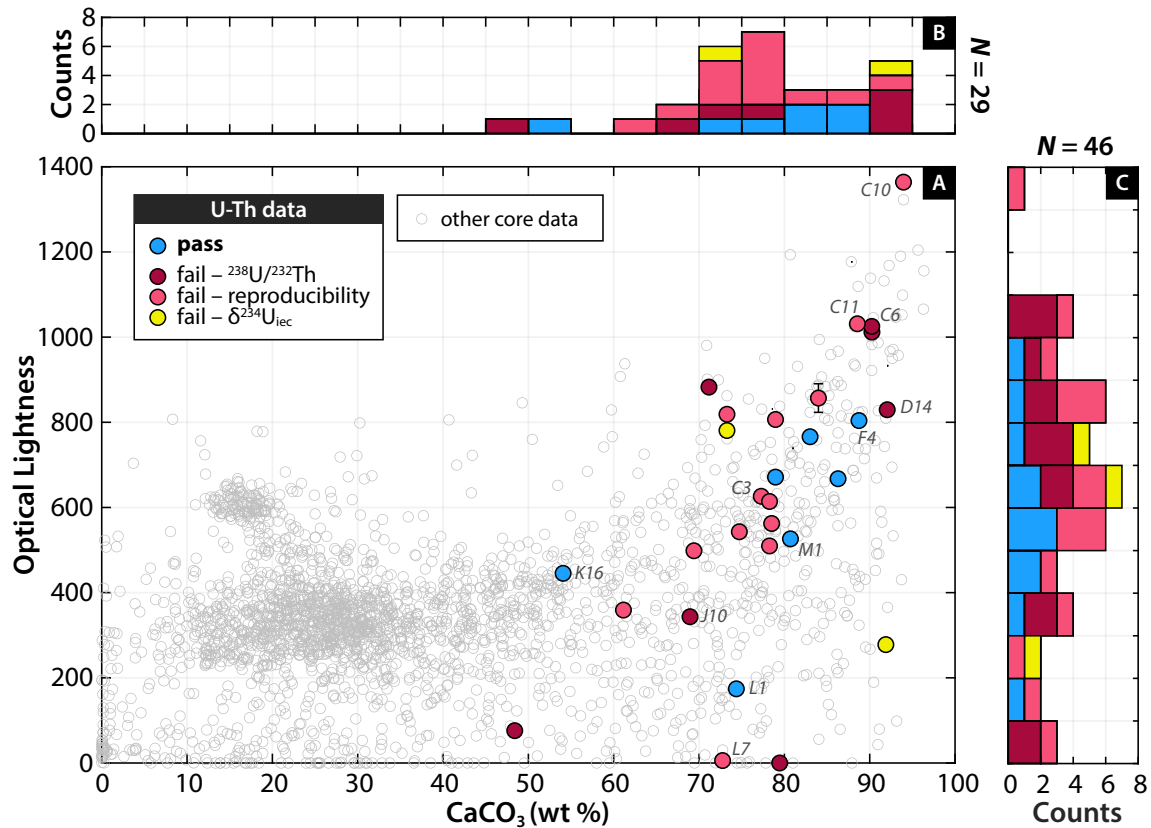
23

Figure 9: Cross-plot [**A**] and histograms of calcium carbonate content [**B**] and optical lightness [**C**], showing the distribution of these values for U-Th samples of each threshold criteria result. In Panel A, there are 29 colored circles which represent the U-Th samples that have both a corresponding $CaCO_3$ analysis (within 1 cm of the sample location) and a color reflectance measurement (within 2.5 mm of the sample location). Since color reflectance data were measured on a finer and more regular sampling interval than carbon data, there are more U-Th samples for which there is a corresponding color reflectance measurement ($N = 46$); thus, there are data plotted in the Panel C histogram that are not shown in Panels A and B. Empty circles with gray outlines represent other pairs of $CaCO_3$ and brightness data throughout the core and are only included if these data correspond to the exact same core depth. Note that this figure does not include any data from the upper 6 m of the core.

from this detrital carbonate would be at secular equilibrium (Fig. 1D) and would adversely impact our We compare the mineralogy of local carbonate bedrock to core sediments to see if mineralogical differences between these carbonates could be used to detect detrital contamination (Section S2). Unfortunately, the results show that there is no discernible difference between the carbonate bedrock and carbonate-bearing lake sediments, even when comparing different grain size groupings. All bedrock samples were dominated by low-Mg calcite, except one sample, which revealed the presence of dolomite. Low-Mg calcite was the dominant carbonate phase in all carbonate-bearing samples from the core, with no evidence of dolomite.

Despite this, elemental ICPMS concentration data support the prediction for detrital contamination in failed samples, in particular, those failing the ^{238}U/^{232}Th criterion. Fig. 10A is a biplot of the orthonormal principal component coefficients for Ca, Mg, Sr, Fe, Mn, Al, Ti, V, and P and the
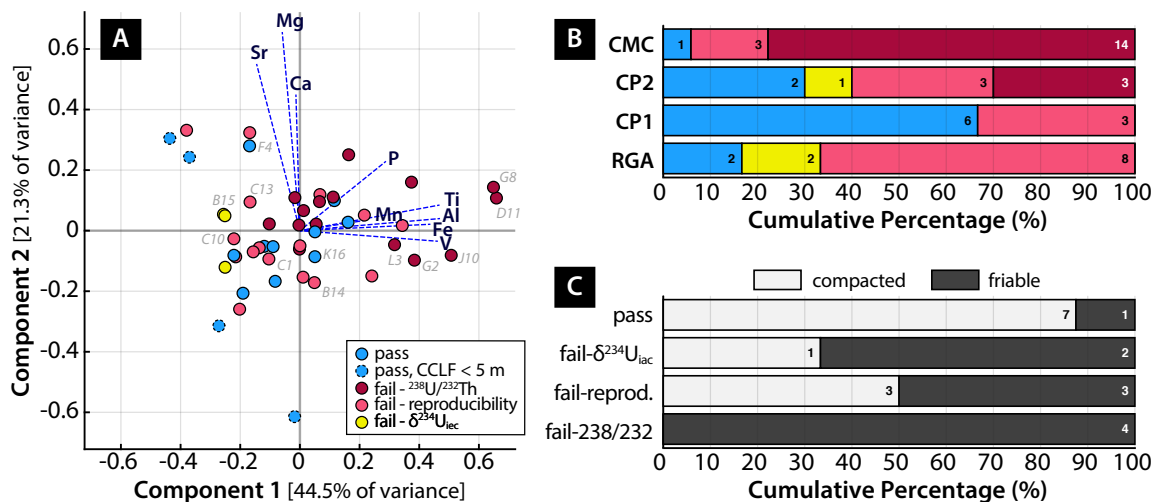
Figure 10: [**A**] Biplot of the orthonormal principal component coefficients for Ca, Mg, Sr, Fe, Mn, Al, Ti, V, and P concentrations (dashed blue lines, labeled by element) and the principal component scores for $N = 48$ samples (circles, color-coded by the threshold criteria result). Light gray labels are corresponding sample IDs of samples that are featured in other figures; we encourage the reader to follow these labels in order to connect these plots with others. [**B**] Bar chart showing, for each facies, the relative proportion of samples that are each of the four threshold criteria results. **CMC** is cream-colored massive carbonate silt (Fig. 6); and **CP1** and **CP2** are cream-colored carbonate silts interbedded with peat layers; and **RGA** is red-green alternating varigated carbonate silt (Fig. 7). See Section 3 for further details. The bar colors follow the legend of Panel A. Numbers within each bar represent the actual number of samples; for example, of the 18 samples categorized as the CMC facies (top row), 1 passed, 3 failed the reproducibility criterion, and 14 failed the $^{238}U/^{232}Th$ criterion. [**C**] Bar chart showing the relative proportion of samples that are compacted (light) versus friable (dark) for samples of each threshold criteria result. Note that we qualitatively assessed sediment hardness for only 21 samples. As with Panel B, numbers within each bar represent the actual number of samples. Note that Panels B and C do not include U-Th samples from the upper 6 m of the core.

principal component scores for each sample. Here, the first principal component (PC1) has positive coefficients for elements that are markers for aluminosilicates (Fe, Mn, Al, and Ti) and explains ~44.5% of the variance in concentration data. Samples failing the $^{238}U/^{232}Th$ criterion generally have positive PC1 scores, indicating that those samples tend to have relatively higher concentrations of these elements. Elemental concentration data from a sample of the dark gray carbonate silt also exhibits higher concentrations of these elements (sample E2; Fig. 6, core at 35 m). As most samples that failed the $^{238}U/^{232}Th$ criterion are of the CMC facies (Fig. 10B), these data are consistent with our visual observations of this facies, in which the lighter-colored carbonates visually appear to have semi-gradational boundaries with the surrounding dark gray glaciogenic silts, suggesting that these samples likely contain some fraction of this material. In addition, the sample with the highest PC1 score, D11, comes from a boundary between cream-colored carbonate and dark gray carbonate silt (Fig. 6).

Despite the clear relationship between high PC1 scores and $^{238}U/^{232}Th$ criterion failing samples, samples with low PC1 scores are not ubiquitously well-behaved, indicating that another factor is influencing our data. Interpreting the meaning of the second principal component (PC2) and the scores for other samples is less clear. PC2 distinguishes among samples that have high values for Mg, Sr, and Ca. Total organic carbon data suggest that samples with negative PC2 scores have

higher organic carbon content, but there are not enough available corresponding carbon data to be convincing. Furthermore, there is no other distinguishable separation of U-Th data by threshold criteria result in the biplot.

6.2. Open system uranium remobilization

While the data comparisons presented thus far broadly confirm that samples with higher $CaCO_3$ content are more likely to yield well-behaved U-Th dates, there remain some inconsistencies with predictions for detrital contamination, mainly that the samples with the highest $CaCO_3$ content and optical lightness fail the threshold criteria, especially the $^{238}U/^{232}Th$ criterion. Regarding the other sample data, there were no patterns distinguishing passing samples from samples failing the reproducibility and $\delta^{234}U_{iec}$ criteria in Figs. 9 and 10A. This information leads us to consider the next probable cause for poor sample behavior: the remobilization of uranium after initial carbonate formation. Using a qualitative assessment of sample hardness, we notice that passing samples were generally more compacted and dense, whereas failing samples were more friable and soft, especially those failing the $^{238}U/^{232}Th$ criterion (Fig. 10C). This observation fits our intuitive expectation that samples with less porosity would be more impervious to diagenesis or secondary deposition of uranium from porewater fluid flow (Fig. 1D).

We now refer back to the facies to which each sample is assigned for further insight. From Fig. 10B, it is clear that facies alone does not dictate how each U-Th sample behaves. Instead, there are some broad tendencies: most CMC samples failed the $^{238}U/^{232}Th$ criterion; most RGA samples failed the reproducibility criterion; and most of the passing samples originate from the CP facies (CP1 and CP2). In considering the reasons behind these patterns, we compare both facies and threshold criteria results with uranium concentration, total organic carbon (TOC), and a*, the red-green color reflectance of sediment, where +a* values are more red and -a* values are more green (Fig. 11). The red or green color of sediments has long been used as a qualitative indicator of *in situ* redox conditions, in which red colors signify oxidizing conditions and green-gray colors suggest reducing conditions, owing to the strong chromophores associated with ferric and ferrous iron (Tomlinson, 1916; Lyle, 1983).

Panels A–F in Fig. 11 (top half) compare the mean a* of all measurements within 5 cm of the U-Th sample to the mean point-to-point difference in a* across the same interval (a measure of the 'volatility' of a* around each sample). For example, having a mean difference of 2 units/cm in a* means that the a* value changes, on average, by a magnitude of 2 along every cm within the 10 cm range surrounding the U-Th sample. Such a value would indicate significant volatility in red-green color, given that the total range of mean a* observed in U-Th samples is ∼3. From these panels, we notice that the CP samples are more red and occupy a relatively narrow range of mean a* values, whereas the CMC samples tend to be less red and exhibit less volatility in red-green color (Fig. 11D, F), especially those failing the $^{238}U/^{232}Th$ criterion (Fig. 11C, E). These results are consistent with our qualitative observations of the CMC facies, in which the lighter colored carbonate occurs in ∼10–50 cm thick beds that are relatively uniform in color (Fig. 6).

Previous studies on sediments have interpreted changes in red-green color intensity as changes in the input of red iron-bearing materials (*e.g.*, Giosan et al., 2002; Helmke et al., 2002; Ji et al., 2005), but because these iron-bearing minerals are highly sensitive to variations in redox environment, reductive diagenesis can subsequently alter sediment color to be more green (Lyle, 1983; König et al., 1999; König et al., 2000). Thus, here we propose that the difference in a* values between the CP and CMC samples is a reflection of diagenesis: the CP samples, being more red, have not been as altered by interactions with post-depositional reducing pore fluids and thus better preserve
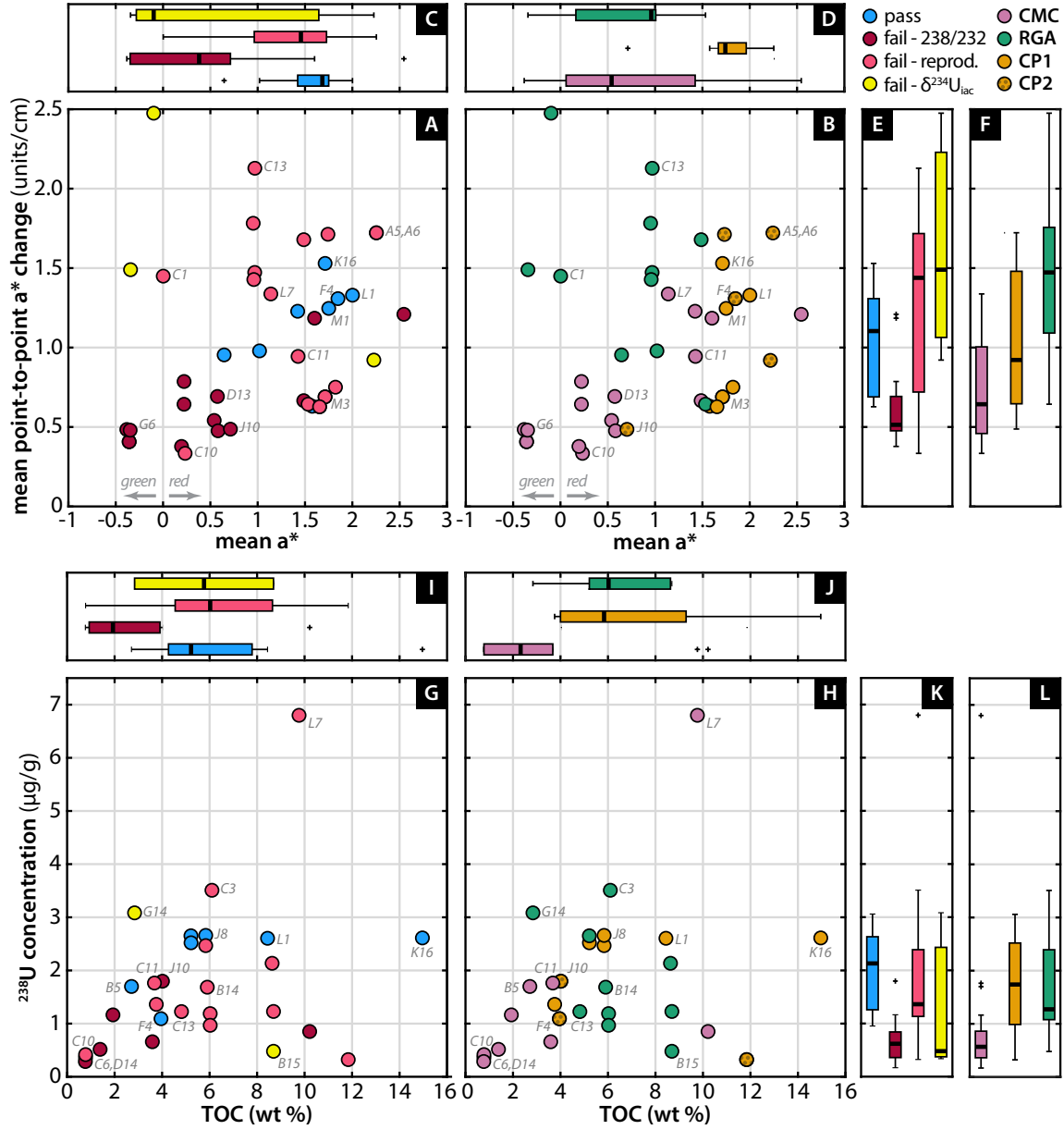
Figure 11: Cross-plots and box-and-whisker plots comparing the red-green color reflectance (a*; from the L*a*b* color space), total organic carbon (TOC) content, and ^{238}U concentration of U-Th samples and showing their relationship to threshold criteria result and facies. In all box-and-whisker plots, the thick central black line represents the median; the top and bottom edges of the box represent the 25th and 75th percentiles, respectively; the whiskers extend to the most extreme points not considered outliers; and the outliers are plotted as '+' symbols. A point is considered an outlier if it has a value >1.5x the interquartile range away from the 25th or 75th percentiles. The top half of the figure compares the mean a* of all measurements within 5 cm of the U-Th sample to the mean point-to-point difference in a* across the same interval. Note that there are some samples for which there is a ^{238}U concentration measurement but no corresponding TOC; thus, Panels K–L include data not shown in the cross-plots of Panels G–H. The bottom half of the figure compares TOC and ^{238}U concentration of each U-Th sample. Note that this figure does not include any data from the upper 5 m of the core.

27

primary isotopic information to produce passing U-Th dates. In contrast, the CMC samples, which may have originally appeared more red like the CP samples, have been altered and as a result, have changed a more green color.

Consistent with this hypothesis is the observation that the CMC and ^{238}U/^{232}Th threshold failing samples generally have much lower ^{238}U concentrations and TOC compared to other samples (Fig. 11G–L). Consider the following scenario: a package of endogenic carbonate containing organic matter is deposited and submerged under oxygenated conditions. After burial, oxygenated porewaters then interact with the organic matter and begin to degrade it, removing from the sediments any uranium associated with the organic matter (Section 2.2; Fig. 1D). This degradation of organic matter may decrease the local pH of pore fluids such that it begins to alter the endogenic carbonate, leaching uranium originally bound within the crystal lattice. At some later point, the pore fluids are no longer recycled, and eventually all oxygen is depleted. The now reducing fluids then begin to reduce the surrounding sediment, shifting its color from red to more green. Any uranium that was removed from the carbonate into the pore fluid has now precipitated as authigenic uranium under these reducing conditions, but is no longer lattice-bound and is thus susceptible to further remobilization (Section 2.2; Fig. 1D). By the time we extract the core and measure the isotopic composition of these sediments, they are green (Fig. 11A–F), easy to physically disaggregate (Fig. 10C), and have low organic matter content and uranium concentrations (Fig. 11G–L).

If uranium loss has occurred from the CMC facies, preferential loss of ^{234}U may be expected, such that replicate analyses produce an inverse relationship between $\delta^{234}U_{initial}$ and ^{238}U concentration (e.g., Robinson et al., 2006). Indeed, such a relationship is observed for some CMC samples (Fig. S1). Furthermore, this proposed mechanism is compatible with the interpretations by Woods et al. (2019) for Lake Junín sediments of the last 50 ka, in which peat layers represent abrupt, ∼25–500 year periods of drought and lake low stands. Dramatic lake level changes would alter water table gradients and change groundwater discharge rates through littoral sediments. Thus, for the CMC facies, while detrital contamination is apparent given the elemental concentration data (Fig. 10), the initial ^{230}Th correction might have compensated to yield an accurate yet imprecise date, were it not for uranium loss.

As for why the CP facies seems not as affected by such pore fluids: we hypothesize that the thick peat beds associated with this facies act as a reductive barrier to the vertical movement of such oxygenated porewaters. This explanation is further bolstered by the observation that samples bounded on top by a thick (>10 cm) peat layer that is laterally continuous across multiple holes at the site (i.e., the CP1 facies) yielded more passing dates with higher ^{238}U/^{232}Th and probability of fit (Fig. 10B and 7). The cream-colored carbonates of the CP1 facies also exhibit faint horizontal banding, possibly representing the preservation of primary fabric. In contrast, samples from the CP2 facies yielded comparatively less ideal U-Th data (Fig. 10B). Sedimentologically, the carbonates of the CP2 facies tend to be darker in color and more massive rather than banded in texture. Fig. 7 features two depth-equivalent core sections from different holes which were classified as the CP2 facies. Examining images of these two core sections, it is clear that the uppermost layer of peat is not laterally continuous. Samples E12 and F4 are the only two samples of this facies that pass the threshold criteria, and are arguably the most tenuous of the passing dates: E12 has a ^{238}U/^{232}Th ratio of 1.02 and F4 has a probability of fit only slightly above 1%, both borderline values.

Thus far, we have multiple lines of evidence that point towards uranium loss as an explanation for the broad behavior of CMC samples, and the basis for that theory can explain the acceptable behavior of the CP samples. As for the RGA samples, these sediments tend to exhibit higher a* volatility (Fig. 11D, F), as one would expect for samples of a facies defined by alternating beds of

28

red and green laminae (Fig. 6). Contrary to the CMC samples, the red-green color of the RGA facies seems to be controlled by sediment composition, given that the laminae are well-defined and the boundaries between color changes are very distinct. The sediment color of RGA facies dulled noticeably a few hours after initial core cutting and exposure, suggesting that iron-bearing minerals again strongly influence color. To explain the general lack of reproducibility of U-Th data from RGA samples (Fig. 10C), we speculate that the green layers containing ferrous iron may be reactive enough to remobilize Fe-Mn hydroxides that complex with uranium (Chappaz et al., 2010), leading to open system behavior that manifests as poor reproducibility.

6.3. Ostracode and mollusc shells

As a demonstration of the utility of paleoecological data for U-Th data interpretation, we compare our U-Th sample data to measures of ostracode color and mollusc shell abundance. During sample processing, we noticed that the color of ostracode shells often varied from sample to sample, ranging from translucent to dark gray or black. Because modern pristine ostracode shells are generally transparent and exhibit only trace pigmentation (Smith and Delorme, 2010), fossil ostracode shells with dark discoloration or coatings are generally thought to be altered and are thus avoided for geochemical analyses as a good practice (Holmes and Chivas, 2002). Many studies have made note of dark coatings on ostracode shells (*e.g.*, Palacios-Fest et al., 2005; Wrozyna et al., 2012; Mackay et al., 2013), but there are few systematic studies that attempt to explain the origin and controls on ostracode discoloration or coatings (*e.g.*, Ainsworth et al., 1990; Schwalb et al., 1995; Holmes, 1998).

The results of our comparison with ostracode shell color are broadly consistent with our hypothesis that the CMC facies has been altered by reductive diagenesis. Fig. 12 compares the threshold criteria result and facies with ostracode color, which we classified on a 7-point scale from translucent to black. Most CMC samples (5 out of 7) and all samples failing the $^{238}U/^{232}Th$ criteria had a higher proportion of darker shells. Sample B5, the only CMC sample that passed threshold criteria, has no ostracode shells with a color > 2. All other samples with different threshold criteria results and facies had ostracode assemblages comprised mainly of light-colored shells, with some exceptions.

Aside from color, there were no conclusive relationships between U-Th data and taphonomy (number of broken versus intact shells; adults versus juvenile counts) or ecology (benthic versus swimmer species; ornamentation). However, we noticed that most of the darker shells (color $>$ 2) belonged to Darwinulidae, a family of benthic ostracodes that are considered an indicator of groundwater discharge. Schwalb et al. (1995) observed dark coatings on *Darwinula stevensoni* valves in Holocene sediments of Williams Lake (Minnesota, USA) and determined via wavelength- and energy-dispersive (WD/ED) spectrometry that the coatings were made of iron sulfide. They proposed that the coatings formed during periods of increased groundwater discharge, in which groundwater supplied additional Fe to the lake while reactive organic matter and sulfate led to reducing conditions that promoted iron sulfide formation. This mechanism is analogous to the one we propose to explain the behavior of U-Th data from the CMC facies. Future investigations should analyze the composition of the surface coatings with either WD/ED spectrometry or scanning electron microscope energy-dispersive X-ray (SEM-EDX) analysis.

Regarding mollusc shells, as discussed in Section 2.3, extensive attempts to U-Th date mollusc shells for paleo-sea level reconstructions have shown that this material does not remain a closed system after burial. We confirm that mollusc shells yield dates that are biased young in sample F14 (∼8200 ka), in which an analysis comprised purely of mollusc shell fragments yielded an age
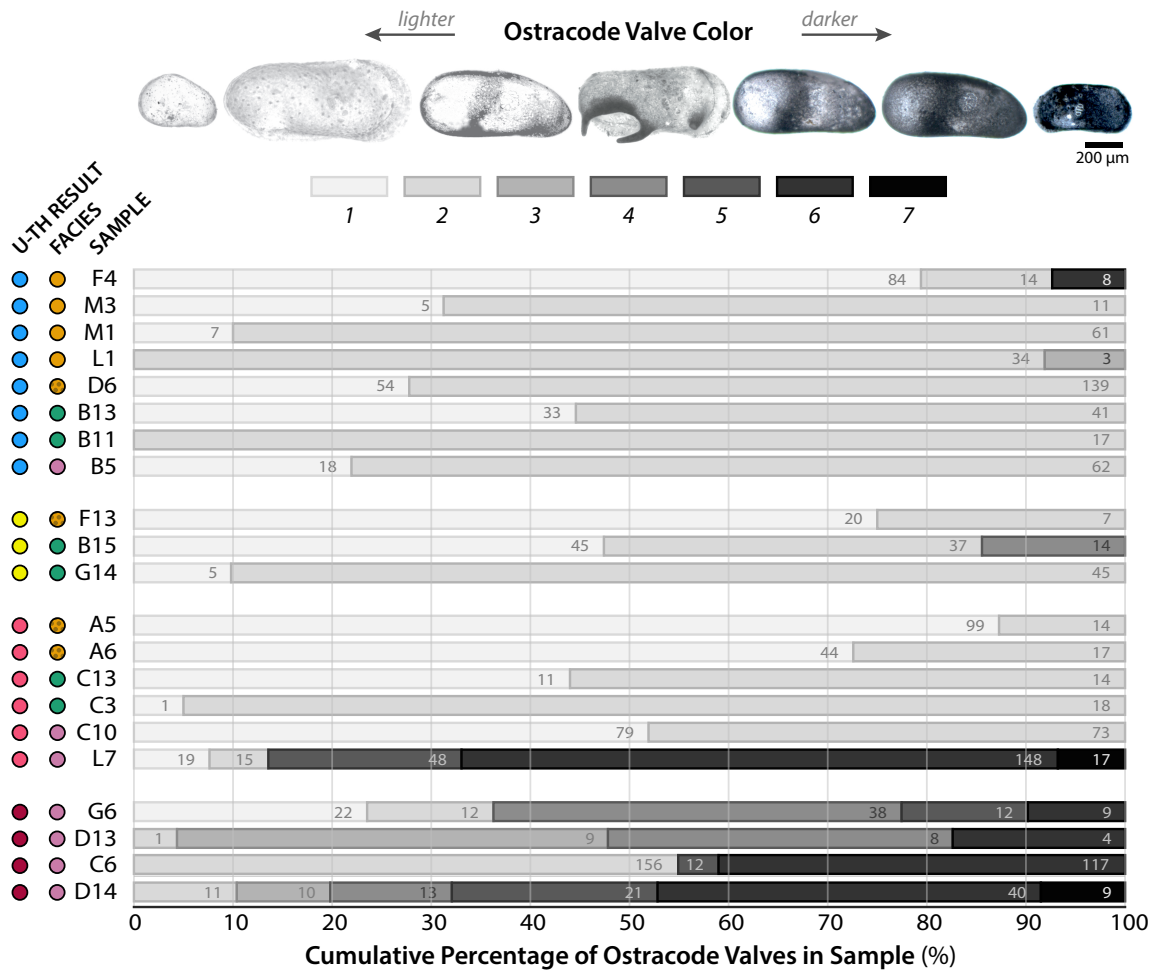
Figure 12: Relationship between ostracode color and U-Th data. Top row of microscope images of ostracode valves illustrate the coloration scale and are arranged from lightest to darkest on a scale of 1 to 7. The bar charts show the relationship between ostracode shell color, threshold criteria result, and facies for 21 samples. Each row in the chart represents ostracode count data from one sample. Rows of data are grouped together vertically by threshold criteria and then sorted within those groups by facies (see colored circles on the left). The length of bars in each row represents the relative proportion of shells in each sample that are of a particular color. The bar color represents the ostracode shell color. Numbers within bars indicate the actual number of valves of each color. From the microscope images (left to right): (1) Translucent (LV, Cyprididae, sample B5); (2) White (RV, Limnocytheridae, sample D14); (3) Partly light gray (RV, Darwinulidae, sample D14); (4) Light gray (RV, Limnocytheridae, sample C6); (5) Partly dark gray (RV, Darwinulidae, sample C6); (6) Dark gray (RV, Darwinulidae, sample C6); (7) Black (LV, Limnocytheridae, sample L7). LV: Left valve external view, RV: Right valve external view.

~3000 yrs younger that the surrounding bulk sediment (Table A2). Although we visually screened for and manually removed identifiable mollusc shell fragments from samples before processing, it is possible that smaller unidentified fragments remained; if differential amounts of mollusc shell fragments were included in replicate analyses, poorly reproducing U-Th data might be an expected result. There is some qualitative indication that the RGA facies is more abundant in mollusc shell fragments than other facies, but the results are not conclusive.

7. Modeling the effects of detrital contamination and uranium remobilization

We have examined various sedimentological and geochemical data to evaluate a few hypotheses for poorly behaved U-Th data. In this section, we simulate the uranium and thorium isotopic evolution of samples with various compositions and uranium loss/gain pathways, and compare these model results with the actual measured isotopic composition of our samples (Figs. 13 and 14). Based on these results, we posit that the balance of evidence from both modeling and the previous data comparisons (Section 6) favors uranium remobilization as the main explanation for the observed scatter, rather than substantial detrital contamination.

To model the effects of detrital contamination, we calculate the impact of mixing varying amounts of detrital material with pure endogenic carbonate. We also test the effects of varying the composition of the detrital material, changing the relative proportions of marine limestone and aluminosilicate. We assume that all detrital material is isotopically homogeneous and at secular equilibrium, in which $[^{230}Th/^{238}U]$ and $[^{234}U/^{238}U]$ are both equal to 1. The uranium and thorium concentrations of the detrital components are set to represent average values for marine limestone and the upper continental crust (Rudnick and Gao, 2003): U conc. = 2 ppm and Th conc. = 1 ppm for marine limestone, and U conc. = 2.7 ppm and Th conc. = 10.5 ppm for the aluminosilicate material. Our measurement of the uranium and thorium concentration of a dark gray silt sample that has ∼30% $CaCO_3$ content (sample E2; Fig. 6) suggests that using these values to simulate the detritus entering Lake Junín is not unrealistic. Although organic matter is a non-negligible constituent of our samples (1–16%; Fig. 11) and is likely a meaningful uranium source (Fig. 1D), we chose to exclude TOC in our model as a necessary simplification for this exercise. As such, the modeling results should be treated as proofs of concept, rather than a serious attempt to precisely quantify the manner by which each deviating U-Th date occurs.

We focus on modeling two groups of data: samples from ∼20–23 m and samples from ∼70–75 m. Taking the passing U-Th dates within these groups at face value, these depth ranges correspond to samples with nominally true ages of ∼75 and ∼550 ka, respectively. The scatter of threshold criteria failing data at ∼20–23 m all originate from the CMC facies and are generally biased older relative to the passing dates, whereas the data at ∼70–75 mostly consists of the RGA facies and are biased younger (Fig. 15B).

7.1. Modeling results for ∼75 ka-aged samples

Fig. 13A compares our U-Th data from the first group (circles) to our simulations of isotopically evolving samples (colored lines) in $^{230}Th/^{238}U$ activity-$\delta^{234}U$ space. All models of samples are evolved for 75 kyrs. To orient the reader: the measured isotopic composition of the two passing samples in this depth range, K16 and L1, are marked by the pair of gray circles located adjacent to the pair of blue circles (see legend). The horizontal offset between the colored and gray circles represents the effect of the initial ^{230}Th correction, the magnitude of which is controlled by the $^{238}U/^{232}Th$ ratio (Eq. 3). The gray shaded region delineates the age range prescribed by the age-depth model (to be shown and discussed in Section 8); for our purposes here, we treat this range as the "true" age range of all samples shown. Thus, any colored circles that do not fall within the gray shaded region are samples that yielded apparent dates that are inconsistent with the true age of these sediments (see straight lines labeled by date). The goal of the subsequent exercises is to explore what pathways of isotopic evolution can explain the isotopic composition of these outlying data.

We first approximate the starting isotopic composition of a representative endogenic carbonate by reverse engineering the isotopic composition of the passing samples. K16 and L1 have an average
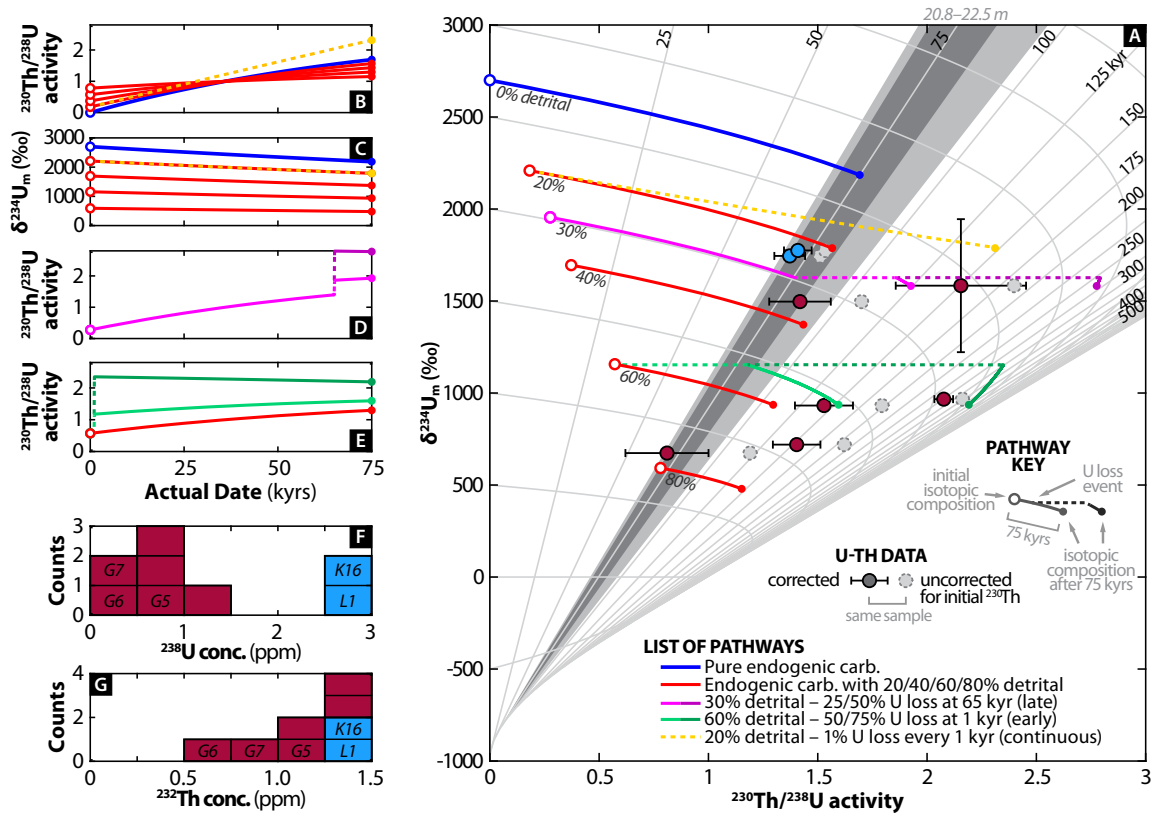
31

Figure 13: Possible pathways of uranium-thorium isotopic evolution that may explain the outlying data at ~20–23 m. [**A**] Plot comparing U-Th data (circles; see legend) with possible pathways (colored lines) in $\delta^{234}U$–$^{230}Th/^{238}U$ activity space, following Fig. 1C. Corrected U-Th ratios (color-coded by threshold criteria result) are each paired with their corresponding uncorrected ratios (gray circles with dashed outlines). The gray triangular wedges represent the expected age range of samples from this depth range based on the age-depth model, where the dark gray area is the range of model means (red line in Fig. 15A) and the light gray area is the maximum and minimum of the uncertainty range (shaded gray area in Fig. 15A). Colored lines represent the isotopic evolution of sample material of mixed composition and uranium loss histories over 75 kyrs (see list of pathways and pathway key for symbology). The simulated samples are mixtures of two isotopically homogeneous end-members: pure endogenic carbonate and detrital material made of 30% limestone and 70% aluminosilicate material. The starting composition of the pure endogenic carbonate is 2.8 ppm ^{238}U and 2700‰ for $\delta^{234}U_{initial}$. These calculations assume that the endogenic carbonate contains no initial ^{230}Th and that uranium loss occurs with no fractionation between ^{234}U and ^{238}U. [**B**] and [**C**] Change in the isotopic evolution as the proportion of detrital material increases (red lines). [**D**] and [**E**] Change in $^{230}Th/^{238}U$ activity after uranium loss. $\delta^{234}U$ is not shown because its evolution is no different from that without uranium loss (compare dashed yellow line with red line of same starting composition in Panel C). [**D**] and [**E**] ^{238}U and ^{232}Th concentrations of U-Th samples in this depth range. K16 and L1 are of the CP1 facies; all other U-Th data featured are of the CMC facies (see Fig. 15B).

uranium concentration of 2.6 ppm, carbonate content of ~60%, and TOC of ~10%. These values indicate that non-carbonate detrital material accounts for ~30% of the sample composition. If we set the detrital end member to be made entirely of aluminosilicate material, we find that a sample consisting of the following material can roughly match the end isotopic composition of K16 and L1 after evolving for 75 kyrs: 20–30% detrital material and 70–80% endogenic carbonate with a starting composition of $\delta^{234}U_{initial}$ = 2700‰ and uranium concentration = 2.8 ppm (Fig. 13A,

32

colored lines labeled 20% and 30%; see legend). The blue pathway represents the isotopic evolution of a pure endogenic carbonate of this composition over the same amount of time, 75 kyrs: with no ^{232}Th, its initial ^{230}Th/^{238}U activity is zero and its final isotopic composition matches its true age. Adding detrital material to this pure endogenic carbonate increases the initial ^{230}Th/^{238}U activity and decreases the initial δ^{234}U of the sample (red pathways in Fig. 13B–C), causing the sample to yield an older apparent date after 75 kyrs (red pathways in Fig. 13A). Note that we tested the sensitivity of these simulations to the composition of the detrital material by varying the proportion of marine limestone, and found that this detail has a small impact compared to that of the total proportion of detrital material.

From the red pathways in Fig. 13A, it is clear that no amount of detrital material is able to explain the samples with high measured ^{230}Th/^{238}U activities, given the composition of the end members being mixed. Furthermore, the ^{232}Th concentrations of these samples place an inexact but actionable upper bound on how much detrital material is reasonable (Fig. 13G); for example, a 30% contribution of detrital material that is 50% limestone already produces a sample with ^{232}Th concentrations of $\sim$1.7 ppm. Thus, we invoke uranium loss to explain these data: yellow, pink, and green pathways in Fig. 13A illustrate the impact of continuous, late, and early uranium loss on the sample isotope composition (see legend and Fig. 13D–E). These samples are also the same low uranium CMC samples failing the ^{238}U/^{232}Th criterion described earlier. We cannot infer which of these uranium loss scenarios is most likely at work from isotopic measurements alone, but our hypothesis for the CMC samples described in Section 6.2 would favor early loss. In addition, the magnitude of uranium loss required to approach the isotopic composition of the outlying samples is similar to the difference in uranium concentration between passing and failing samples (Fig. 13F).

Note that these modeled uranium loss pathways are simplified to assume that loss occurs with no fractionation between ^{234}U and ^{238}U, but preferential leaching of ^{234}U is more likely closer to reality (Section 5).

7.2. Modeling results for ~550 ka-aged samples

Fig. 14 features the U-Th samples from $\sim$70–75 m. At this age, the close spacing of the age isolines in this regime causes the area defining the "true" age range of these samples to occupy a much narrower area in ^{230}Th/^{238}U activity-δ^{234}U space (shaded gray area in Fig. 14B). Here, we start with a pure endogenic carbonate with a composition of δ^{234}U$_{initial}$ = 2700‰ and ^{238}U = 1.8 ppm, values selected via the same reverse engineering steps described in Section 7.1, but using the passing samples in this depth interval. Detrital contamination has much less impact on the accuracy of the dates at this age, as demonstrated by the fact that all the modeled pathways of samples with varied percentages of detrital material still ultimately end in the region defining the true age of the sediments (gray shaded region in Fig. 14B; see Section 2.2 for explanation). In order to produce samples with isotopic compositions that bias dates to be younger, we simulate the impacts of uranium gain.

Similar to detrital contamination, early uranium loss (or gain) has no effect on the final sample date at this age. Thus, in Fig. 14B, we only illustrate the impacts of late or continuous uranium gain (green and yellow pathways). In contrast to the pathways observed for $\sim$75 ka-aged sediments, here very small percent gains in uranium can have measurable impacts. For example, a 1% gain at 540 kyr can cause the sample date to be $\sim$100 kyrs younger (green pathway in Fig. 14B). Thus, the sensitivity of the apparent dates to small alterations in uranium in this regime, in combination with narrowly spaced age isolines, is likely the cause for the large spread of dates at this depth, as well as the poor reproducibility of replicate analyses (Fig. 8D). Because early uranium gain cannot
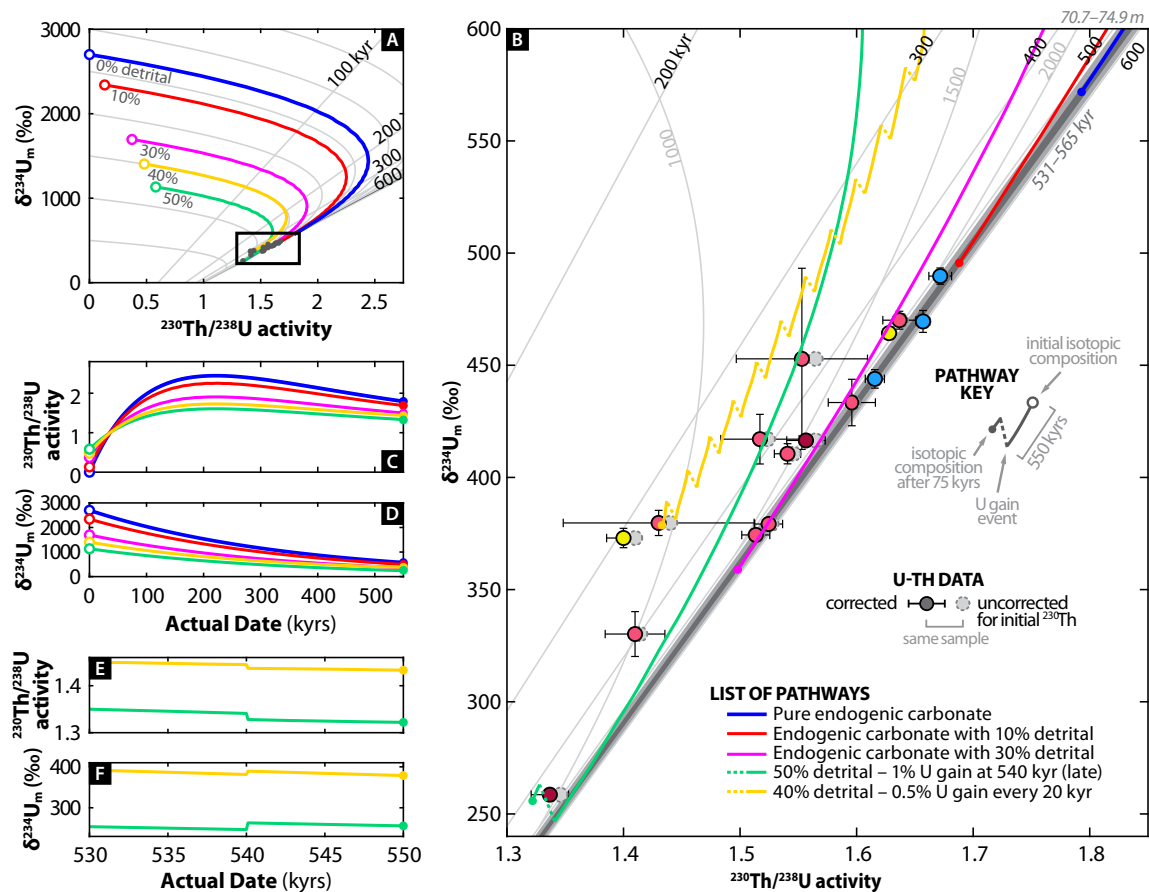
Figure 14: Possible pathways of uranium-thorium isotopic evolution that may explain the outlying data at ∼70–75 m. See caption in Fig. 13 for explanation of symbology. [**A**] Plot showing initial isotopic composition and evolution of pathways over 550 kyrs. [**B**] View of the isotopic evolution of samples within the extent represented by the rectangular box in Panel A. The gray triangular wedges representing the expected age range of samples from this depth range occupies a much narrower area in ^{230}Th/^{238}U activity-δ^{234}U space compared to Fig. 13. The starting composition of the pure endogenic carbonate is 1.8 ppm ^{238}U and 2700‰ for δ^{234}U$_{\text{initial}}$. The detrital component has the same composition as that from Fig. 13, 30% limestone and 70% aluminosilicate material. These calculations assume that uranium gain occurs with a δ^{234}U ratio equal to the δ^{234}U$_{\text{initial}}$ of the sample. [**C**] and [**D**] Change in isotopic evolution as the proportion of detrital material increases. [**E**] and [**F**] Change in isotopic evolution after uranium gain.

explain the young bias of these samples, the hypothesis for post-depositional uranium uptake by gastropod shells seems less convincing; gains would have to be continuous and gradual, and it is unclear from where the continuous supply of uranium would come.

Note that although Figs. 13–14 do not explore compound gain or loss pathways, such scenarios are not outside the realm of possibility.

8. Conclusions: the age-depth model for the PLJ-1 splice

Through the use of threshold criteria that evaluate samples on the basis of their $^{238}U/^{232}Th$ ratio, reproducibility, and $\delta^{234}U_{iec}$, we have conducted a methodical curation of the U-Th data that is justified by comparisons to other sedimentological, geochemical, and paleoecological datasets, as well as modeling of the isotopic evolution of simulated samples. As a result, we deem 18 of the 55 sample dates as satisfactory for use as age constraints. These passing samples generally come from sediments of the CP facies, which we hypothesize have experienced relatively less uranium remobilization because of the thick overlying peat beds that act as reductive barriers to post-depositional fluid flow.

Fig. 15A shows the age-depth model for the PLJ-1 splice using these U-Th ages and radiocarbon data. The model was generated using the R-based Bayesian age-depth modeling software program called Bacon (v2.3; Blaauw and Christen, 2011). On average, the 95% confidence range of this model is ∼30 kyrs. Trachsel and Telford (2017) tested Bacon and other age-depth modeling routines (CLAM, OxCal, BChron) on a varved sediment sequence and found that they all produced mean age-depth models close to the truth, but each program has its own advantages and disadvantages. In the case of Bacon, the application of an accumulation rate prior forces sedimentation rates to be more smooth and linear than is possibly justified. Thus, while the alternating packages of carbonate and glaciogenic silt in the core hint at variability in sedimentation rates, this information is not utilized in the generation of the age-depth model. See Section S5 for details regarding the parameters and priors used for the model run.

Fig. 15A also compares the radiometric age-depth model to geomagnetic relative paleointensity (RPI) tie points made between the PLJ-1 normalized remanence record and well-dated RPI stacks (Hatfield, in prep.). Broadly, these data are consistent with age-depth model and provide further support for its validity. See Section S6 for details on the determination of the RPI tie points.

9. Considerations for future U-Th dating of lake sediments

When it comes to U-Th dating of lake sediments, there are no "silver bullets" or easy answers: no singular facies, carbonate content threshold, color, or any other sedimentological or geochemical data could predict the viability of a U-Th date with certainty in these sediments. In fact, samples that would conventionally be considered ideal were some of the most poorly behaved samples. One wonders what the outcomes might have been if only the nominally choicest samples had been processed, and the dateability of the entire core assessed from those results. Such decision making processes are the norm when less time and fewer resources are available.

Our concern for overlooked but dateable sediments in other records also extends in the opposite direction: other studies may be overly reliant on single-analysis U-Th dates that seem credible but have not been reproduced or tested with stratigraphic coevality constraints. The most glaring example of this can be demonstrated through the results from sample L7, which had the highest uranium concentration (7 ppm, 2 times higher than the next highest) and highest $^{230}Th/^{232}Th$ ratio out of all samples (Table A1). Because of this, individual analyses were rather precise, with 400–700 year uncertainties (2-σ) on ∼100 ka dates. On their own, these dates would be considered excellent, but only after replication is it revealed that none of the precise dates overlap with one another at the 2-σ level. Although a labor intensive strategy, there is no substitute for replication and reproducibility in assessing the quality of U-Th geochronological data.

Furthermore, while the threshold criteria ultimately decided which data would form the foundation of the age-depth model, it was the placement of geochronological data in context of other
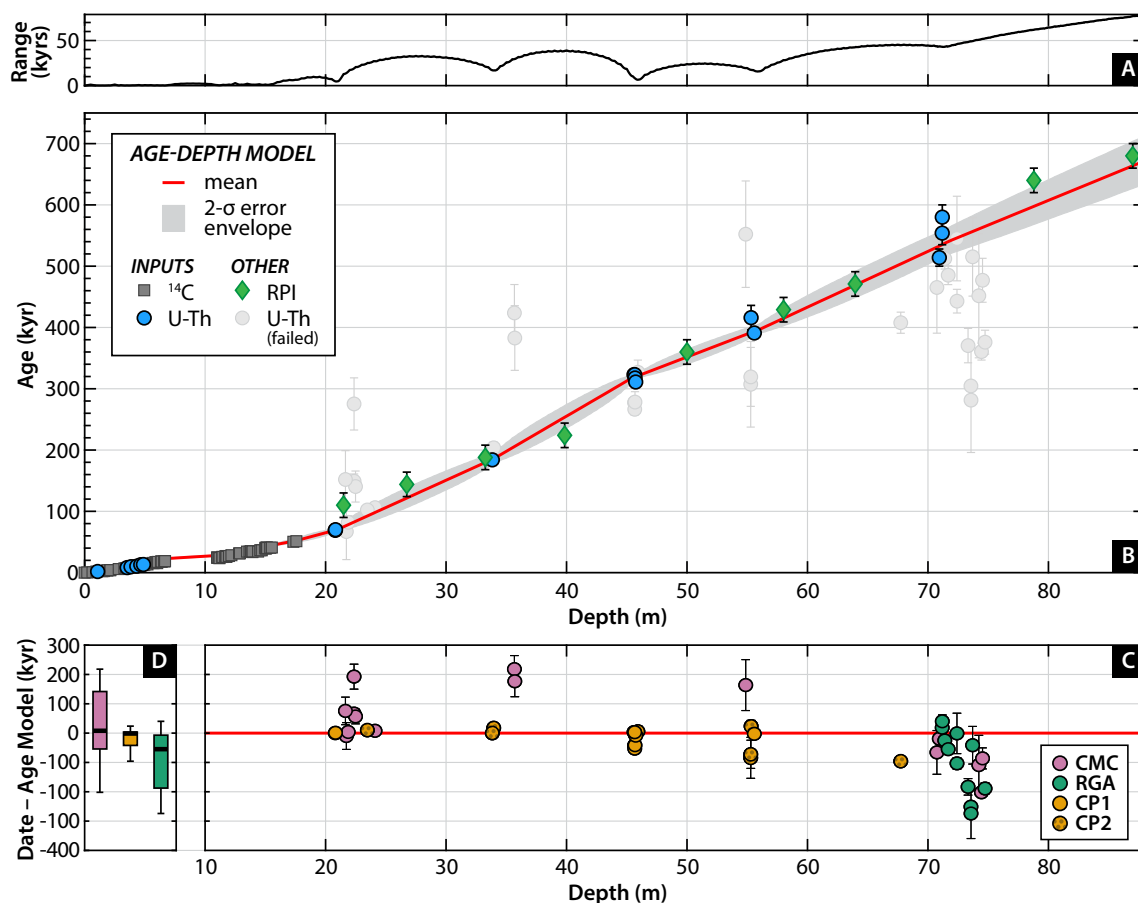
Figure 15: [**A**] and [**B**] Age-depth model for the PLJ-1 splice generated by Bacon (Blaauw and Christen, 2011) using radiocarbon (gray squares) and U-Th (blue circles) data. Red line represents the mean and gray shaded area is the 2-σ range error envelope. U-Th data that did not meet threshold criteria (light gray circles) and relative paleointensity (RPI) tie points (green diamonds) were not used as inputs for the age-depth model and are plotted as an overlay. Section S5 for additional information on the priors and posteriors of the model. Radiocarbon data are from Woods et al. (2019) and RPI data are from Hatfield et al. (in prep.). [**C**] Comparison of all U-Th dates and their departure from the age-depth model mean (thick red line at zero), color-coded by facies. See Fig. 8D to compare with data color-coded by threshold criteria result. [**D**] Box-and-whisker plots showing the distribution by facies of the difference between U-Th dates and the age-depth model mean; see caption of Fig. 11 for description of box-and-whisker plot symbology. All error bars shown are of 2-σ range. Analyses that yielded indeterminant U-Th dates or were infinite are not included in this figure.

sedimentological and geochemical information that provided justification for these thresholds. These data comparisons also provide practical insights on what other characteristics to consider for future U-Th dating attempts on lake sediments: for instance, the aforementioned L7 sample contained some of the darkest ostracode shells categorized (see image of ostracode shell with color = 7 in Fig. 12).

Embracing the noise in our data has led to a richer understanding of the controls on uranium

in these lake sediments. As our ability to resolve this noise increases as the analytical precision of measurements improves, subtle differences in the noise will become interpretable as information on paleoenvironmental processes themselves. This work demonstrates the beginnings of what is possible on this front. Although >150 analyses went into this work, we hope that this number does not intimidate those seeking to apply U-Th dating to their own lake sediment samples. Rather, we seek to showcase strategies for interpreting scattered geochronologic data of any size and encourage similar efforts where better geochronological control would have the most impact. As more high resolution datasets become paired with drill cores by default (*e.g.*, scanning XRF, color reflectance, magnetic susceptibility), there will be more opportunities to use such additional data to test underlying working assumptions for geochronologic tools.

Of all the lessons learned, we hold the following as most important: for the determination of the age of lake sediments, geologic context—in the form of sedimentological observations, geochemical data, and paleoecological descriptions—is of equal importance to the numerical accuracy and precision of geochronological measurements.

10. Author Contributions

Following the Contributor Roles Taxonomy (CRediT; Brand et al., 2015), we provide a statement of the diverse contributions to this published work. **Christine Y. Chen**: Conceptualization, Methodology, Software, Validation, Formal Analysis, Investigation, Writing - Original Draft, Visualization, Project Administration. **David McGee**: Conceptualization, Methodology, Resources, Writing - Review & Editing, Supervision, Funding Acquisition. **Arielle Woods**: Methodology, Writing - Review & Editing. **Liseth Pérez**: Methodology, Investigation, Writing - Review & Editing. **Robert G. Hatfield**: Writing - Review & Editing. **R. Lawrence Edwards**: Conceptualization, Resources, Writing - Review & Editing. **Hai Cheng**: Investigation. **Blas L. Valero-Garcés**: Investigation, Writing - Review & Editing. **Sophie B. Lehmann**: Writing - Review & Editing. **Joseph S. Stoner**: Writing - Review & Editing. **Antje Schwalb**: Methodology, Resources, Writing - Review & Editing. **Irit Tal**: Investigation. **Geoffrey O. Seltzer**: Conceptualization. **Pedro Miguel Tapia**: Project Administration. **Mark B. Abbott**: Conceptualization, Writing - Review & Editing, Supervision, Project Administration, Funding Acquisition. **Donald T. Rodbell**: Conceptualization, Writing - Review & Editing, Supervision, Project Administration, Funding Acquisition.

A more specific description of contributions is as follows: GOS laid the foundation for this work in the 1990s (Siegel et al., 2005). MBA, DTR, and DM conceived of the project and secured funding. CYC and DM formulated the research goals and methodology. CYC collected, processed, and analyzed the U-Th samples from the PLJ-1 splice; made comparisons to the other datasets; and prepared the original draft and figures, all with supervision from DM. IT assisted with processing of U-Th analyses. RLE oversaw U-Th dating of the 1996 piston core, which was conducted by HC. BLVG provided the stratigraphic core description. DM collected the elemental ICPMS concentration data. CYC initiated the ostracode work with LP, who analyzed the ostracodes with input from AS. DTR analyzed carbon and mineralogy data. RH and JS analyzed paleomagnetic data. CYC made the age-depth model, with input from AW, SL, RGH, DM, JSS, MBA, and DTR. CYC, AW, RGH, JSS, PMT, MBA, and DTR contributed to the fieldwork campaign. DM, AW, LP, RGH, RLE, BLVG, SL, AS, MBA, and DTR manuscript feedback. All authors provided expertise.

11. Acknowledgements

Table A1: Average values of various U-Th data for each sample, calculated from replicate analyses. Samples that passed all threshold criteria (Section 5) are listed first; then all samples are sorted by depth (CCLF). All uncertainties listed are 2-σ. N is the total number of replicate analyses made for each sample. MSWD and prob. of fit fields are left blank if there is only 1 replicate analysis or marked with an asterisk (*) if any replicate analyses yielded infinite dates; samples marked with an * are considered to have failed the reproducibility criterion. Weighted Mean Date is reported relative to Before Present (BP), in which the present is defined as January 1, 1950. $\delta^{234}U_m$ is the measured $\delta^{234}U$. Meaning of the abbreviations used for facies can be found in Section 3. For threshold criteria result, numbers indicate which threshold criterion each sample failed: 1 = $^{238}U/^{232}Th$; 2 = reproducibility; and 3 = $\delta^{234}U_{iac}$. See Table A2 for data associated with replicate analyses and Supplementary Materials for raw unrounded data.

Samp. ID	CCLF (m)	N	^{238}U (ng/g)	^{232}Th (ng/g)	MSWD	Prob. of Fit	Weighted Mean Date (yrs BP)	$[^{230}Th/^{238}U]$	$\delta^{234}U_m$ (‰)	$\delta^{234}U_{iac}$ (‰)	$^{238}U/^{232}Th$	$^{230}Th/^{232}Th$	Facies	Threshold Criteria Result
Passing Samples														
F9	1.080	3	2911±70	124±25	0.07	0.93	1810±200	0.0760±0.0027	2355.0±1.6	2395±19	24.1±4.6	28.9±4.5	–	pass
F14	3.530	4	697±58	25.2±5.5	1.38	0.25	8180±150	0.2822±0.0061	2639±11	2727±21	28.5±5.1	127±20	–	pass
F15	3.850	3	980±32	105±13	0.11	0.90	9600±500	0.3665±0.0073	2721±24	2880±53	9.39±0.91	54.5±4.3	–	pass
F16	4.330	2	1150±150	250±140	0.87	0.35	10500±1000	0.4251±0.0076	2630±120	2880±130	5.2±2.3	35±15	–	pass
C16	4.660	3	1580±250	243±32	0.17	0.84	12900±800	0.4181±0.0089	2085.3±3.8	2257±59	6.51±0.18	43.2±0.46	–	pass
D4	4.880	4	1970±71	497±18	0.03	0.99	13200±1200	0.4502±0.0046	1934.3±5.8	2156±95	3.965±0.053	28.34±0.38	CP1	pass
K16	20.806	5	2610±700	1430±350	0.11	0.98	69000±2000	1.512±0.017	1745±20	2490±260	1.824±0.047	43.8±1.0	CP1	pass
L1	20.823	5	2610±540	1300±380	2.77	0.03	70000±4000	1.535±0.067	1774.7±3.4	2500±260	2.04±0.14	49.6±1.7	CP2	pass
D6	33.839	5	1200±110	1000±160	2.06	0.08	184000±6000	2.176±0.075	1288±74	2800±520	1.211±0.096	41.9±4.7	CP1	pass
M1	45.599	4	2520±52	430±23	3.05	0.03	323000±3000	2.1303±0.0061	936.0±2.0	2440±85	5.87±0.21	198.7±7.6	CP1	pass
M3	45.660	5	1740±130	376±25	0.49	0.75	323000±2000	2.212±0.011	999.5±8.0	2650±160	4.63±0.21	162.8±7.5	CP1	pass
J8	45.686	3	2660±110	341±34	0.79	0.46	317500±1700	2.1828±0.0046	985.3±4.8	2501±68	7.83±0.46	271±16	CP1	pass
J9	45.741	3	3059±61	1179±24	0.59	0.56	311000±3000	1.9583±0.0064	807.5±1.6	2170±160	2.594±0.042	80.7±1.6	CP2	pass
E12	55.318	5	953±39	940±110	1.26	0.28	416000±20000	1.828±0.054	631±31	2700±1100	1.017±0.076	29.5±3.0	CP2	pass
F4	55.587	5	1092±80	120±3.6	3.32	0.01	391000±5000	2.0570±0.0064	816.9±4.1	2550±130	9.10±0.40	297±13	CMC	pass
B5	70.941	5	1699±34	364±17	1.00	0.41	514000±14000	1.6727±0.0098	489.7±3.6	2230±610	4.68±0.20	124.2±5.3	RGA	pass
B11	71.182	4	2650±170	353±34	1.70	0.16	554000±19000	1.6160±0.0082	443.9±4.1	2190±400	7.52±0.28	193.1±7.7	RGA	pass
B13	71.190	4	1318±84	134±13	1.69	0.17	580000±20000	1.6572±0.0059	469.5±4.9	2600±1300	9.88±0.41	260±11	CP2	pass
P10	6.505	2	749±33	837±52	*	*	–	0.540±0.013	792.8±2.3	–	0.896±0.028	7.68±0.22	CMC	1,2
L3	21.649	1	619±12	1118±23	–	–	150000±50000	1.621±0.025	719.6±3.0	2200±1300	0.553±0.022	14.25±0.22	CMC	1
G1	21.725	1	851±17	1230±130	–	–	70000±50000	1.19±0.12	673.8±2.0	1340±660	0.69±0.11	13.1±1.9	CMC	1
G2	21.878	2	1164±23	1435±70	0.01	0.92	82000±11000	1.700±0.027	1497±11	2840±860	0.812±0.037	21.91±0.64	CMC	1
G5	22.364	1	635±13	1395±28	–	–	280000±40000	2.162±0.040	966.7±1.7	5200±4200	0.455±0.028	15.61±0.29	CMC	1
G6	22.367	4	351±58	692±81	0.04	0.99	149000±12000	2.40±0.33	1580±360	5300±4600	0.506±0.035	19.2±1.9	CMC	1
G7	22.486	3	418±9	829±17	0.05	0.96	140000±30000	1.794±0.033	932±21	3000±2200	0.504±0.028	14.36±0.19	CMC	1
G8	22.537	1	861±17	2362±48	–	–	–	1.986±0.035	621.9±3.9	–	0.365±0.028	11.50±0.20	CP2	2
M15	23.467	4	323±7	38.3±3	37.0	0.00	102000±3000	2.219±0.043	2302.9±7.0	3175±64	8.46±0.59	298±23	CMC	2
L7	24.105	7	6800±330	400±27	399	0.00	106000±5000	1.829±0.074	1687.6±3.8	2316±47	17.03±0.68	494±24	CP2	1
D7	33.954	2	838±18	997±46	0.24	0.63	204000±9000	2.331±0.020	1328±25	3500±940	0.840±0.028	31.1±0.92	CMC	1,2
D11	35.671	2	392±39	870±210	*	*	–	1.41±0.11	283.9±7.3	–	0.457±0.091	10.2±1.3	CMC	1,2
D12	35.673	2	262±47	440±22	*	*	420000±50000	2.080±0.024	806.1±1.5	4400±1900	0.60±0.14	18.7±5.9	CMC	1,2
D13	35.705	3	168±11	216±15	8.19	0.00	380000±50000	2.078±0.095	823±59	3900±1600	0.778±0.028	25.7±1.5	CMC	1,2
D14	35.733	2	287±6	291±12	*	*	–	2.663±0.040	1019.2±4.4	–	0.987±0.028	41.71±0.21	CMC	1,2

Table A1 continued from previous page

Samp. ID	CCLF (m)	N	^{238}U (ng/g)	^{232}Th (ng/g)	MSWD	Prob. of Fit	Weighted Mean Date (yrs BP)	[^{230}Th/^{238}U]	δ^{234}U$_m$ (‰)	δ^{234}U$_{iac}$ (‰)	^{238}U/^{232}Th	^{230}Th/^{232}Th	Facies	Threshold Criteria Result
J5	45.640	4	1360±120	377±83	5.51	0.00	277000±5000	2.131±0.043	1002±40	2370±130	3.71±0.60	126±22	CP1	2
J6	45.661	3	1202±80	389±36	14.0	0.00	266000±9000	2.129±0.023	1016.9±5.4	2380±140	3.095±0.095	104.6±4.3	CP1	2
J7	45.683	2	2467±83	389.8±8.9	97.2	0.00	278000±17000	2.162±0.028	1027.3±1.1	2367±88	6.33±0.36	217.3±9.5	CP1	2
J10	45.921	1	1798±36	2117±42	–	–	327000±20000	1.977±0.016	789.8±0.8	2930±800	0.849±0.028	26.66±0.21	CP2	1
K1	54.873	1	659±13	654±13	–	–	550000±90000	1.798±0.014	571.8±1.4	3700±2100	1.000±0.028	28.76±0.23	CMC	1
A5	55.288	2	2360±140	1496±30	72.6	0.00	310000±70000	1.907±0.044	751±19	2290±380	1.578±0.071	47.8±1.0	CP2	2
A6	55.292	3	2520±190	1143±75	105	0.00	320000±50000	1.996±0.064	819.3±6.5	2400±370	2.202±0.028	69.8±2.0	CP2	2
F13	67.741	4	338±7	278±21	0.29	0.84	408000±17000	1.584±0.057	448±45	1820±500	1.219±0.082	30.7±3.1	CP2	3
B2	70.741	1	516±10	615±12	–	–	470000±70000	1.565±0.017	416.5±2.1	2300±1200	0.839±0.028	20.84±0.22	CMC	1
G13	71.394	4	734±15	159.6±6.0	*	*	512000±17000	1.597±0.020	433±10	2060±770	4.60±0.21	117.5±7.3	RGA	2
G14	71.679	2	3084±62	206.0±7.1	2.11	0.15	485000±15000	1.6282±0.0046	464.3±1.8	1850±170	14.98±0.64	387±17	RGA	3
H6	72.406	3	1188±89	887±33	*	*	550000±70000	1.527±0.012	379.2±2.9	2200±1700	1.34±0.12	33.3±1.6	RGA	2
H7	72.409	4	968±51	607±47	*	*	443000±19000	1.546±0.011	410.5±4.5	1730±460	1.60±0.10	39.7±2.6	RGA	2
B14	73.327	4	1685±35	698±57	12.0	0.00	370000±30000	1.524±0.034	417±11	1420±620	2.43±0.20	58.7±5.2	RGA	2
B15	73.566	4	479±10	161±10	0.19	0.90	305000±5000	1.410±0.015	373.0±4.3	970±120	2.98±0.15	66.8±3.5	RGA	3
C1	73.573	4	1230±440	330±130	195	0.00	280000±90000	1.440±0.082	379.7±5.6	1270±460	3.8±0.66	87±13	RGA	2
C3	73.704	2	3508±71	673±20	8.62	0.00	520000±60000	1.514±0.012	374.4±2.5	1770±470	5.213±0.054	125.3±2.3	RGA	2
C6	74.222	1	361±7	422.6±8.5	–	–	450000±100000	1.346±0.016	258.6±2.8	1360±920	0.855±0.028	18.27±0.22	CMC	1
C10	74.444	8	417±37	275±31	3.69	0.00	361000±14000	1.565±0.057	453±40	1540±340	1.521±0.095	37.8±3.4	CMC	2
C11	74.529	2	1763±36	339±11	8.18	0.00	480000±40000	1.638±0.014	470.1±4.0	1980±330	5.202±0.088	135.3±3.5	CMC	2
C13	74.739	4	1226±42	356±32	7.11	0.00	376000±20000	1.414±0.026	330±10	1100±230	3.46±0.25	77.9±6.8	RGA	2
C14	74.851	2	2135±43	525±12	*	*	–	1.5881±0.0049	364.4±3.8	–	4.069±0.088	102.6±2.5	RGA	2

Table A2: U-Th data for replicate analyses of each sample. All uncertainties listed are 2-σ. **Rep. ID** refers to a unique identifier for each replicate analysis. Note that sample 'F14(s)' refers to an analysis of gastropod shells from the same horizon as F14. Reported errors for ^{238}U and ^{232}Th concentrations are estimated to be $\pm$2% due to uncertainties in spike concentration; analytical uncertainties are smaller. **Date Uncorr.** indicates that no correction has been made for initial ^{230}Th. **Date Corr.** are corrected for initial detrital ^{230}Th assuming an initial ^{230}Th/^{232}Th of 8.0$\pm$4.0$\times$10^{-6} (Section 4), and are reported relative to Before Present (BP), in which the present is defined as January 1, 1950. Decay constants for ^{230}Th and ^{234}U are from Cheng et al. (2013); decay constant for ^{238}U is 1.55125$\times$10^{-10} yr^{-1} (Jaffey et al., 1971). See Eqs. 1–3 for equations for the calculation of dates. See Eq. 2 for the calculation of δ^{234}U$_{initial}$ and Section S4 for the calculation of δ^{234}U$_{iac}$.

Samp. ID	Rep. ID	^{238}U (ng/g)	^{232}Th (ng/g)	δ^{234}U$_m$ (‰)	[^{230}Th/^{238}U]	^{230}Th/^{232}Th	Date Uncorr. (yrs)	Date Corr. (yrs BP)	δ^{234}U$_{initial}$ (‰)	δ^{234}U$_{iac}$ (‰)
Replicate Analyses of Passing Samples										
F9	F9(1)	2831±57	97.5±2.0	2356.7±1.1	0.07300±0.00060	33.67±0.29	2392±20	1830±280	2368.9±2.2	2391±13
	F9(2)	2940±59	147.4±3.0	2354.87±0.95	0.07805±0.00082	24.71±0.26	2560±27	1740±410	2366.5±2.9	2399±19
	F9(3)	2962±59	127.8±2.6	2353.5±1.1	0.07708±0.00082	28.36±0.30	2529±27	1820±360	2365.6±2.6	2394±16
F14	F14(1)	737±15	26.29±0.53	2635.37±0.68	0.28880±0.00099	128.59±0.49	8942±32	8410±270	2698.7±2.2	2725±15
	F14(2)	715±14	29.16±0.59	2640.01±0.82	0.2838±0.0016	110.42±0.62	8769±50	8160±310	2701.5±2.5	2732±17
	F14(3)	725±15	28.26±0.57	2652.8±6.3	0.2823±0.0014	114.98±0.57	8690±46	8110±290	2714.3±6.8	2743±21
	F14(4)	611±12	17.08±0.34	2625.96±0.69	0.27407±0.00084	155.78±0.42	8494±27	8080±210	2686.5±1.7	2707±12
	F14(s)	292±5.8	5.48±0.11	2636.3±3.6	0.1765±0.0012	149.3±1.3	5395±39	5110±150	2674.6±3.8	2688±11
F15	F15(1)	1000±20	119.7±2.4	2694.2±2.2	0.3748±0.0019	49.72±0.23	11524±61	9770±890	2769.5±7.3	2863±53
	F15(2)	997±20	99.0±2.0	2741.1±1.0	0.3624±0.0019	57.96±0.30	10980±61	9540±730	2815.9±5.9	2894±44
	F15(3)	944±19	96.9±1.9	2728.17±0.97	0.3621±0.0022	55.96±0.33	11010±70	9520±760	2802.4±6.1	2883±46
F16	F16(1)	1259±25	353.7±7.1	2546.1±1.6	0.4304±0.0049	24.33±0.28	13900±170	9600±2200	2616±17	2830±130
	F16(2)	1048±21	155.4±3.1	2717.5±6.4	0.4197±0.0025	44.96±0.22	12884±83	10700±1100	2801±11	2919±69
C16	C16(1)	1305±26	205.5±4.1	2084.2±2.5	0.4278±0.0024	43.12±0.23	16021±96	13300±1400	2163.6±9.0	2261±59
	C16(2)	1673±33	258.2±5.2	2088.26±0.47	0.4159±0.0023	42.78±0.22	15529±90	12800±1400	2165.2±8.4	2260±57
	C16(3)	1773±35	264.5±5.3	2083.6±3.8	0.4105±0.0023	43.69±0.23	15338±95	12700±1300	2159.8±9.0	2251±56
D4	D4(1)	1946±39	500±10	1930.39±0.61	0.4514±0.0034	27.87±0.20	17920±140	13100±2500	2003±14	2154±95
	D4(2)	2073±41	520±10	1929.5±2.5	0.4549±0.0033	28.78±0.21	18070±140	13400±2400	2004±14	2151±92
	D4(3)	1943±39	489.1±9.8	1935.47±0.82	0.4508±0.0038	28.44±0.24	17860±160	13200±2400	2009±14	2157±92
	D4(4)	1916±38	477.4±9.6	1942±1.2	0.4438±0.0040	28.28±0.25	17520±170	12900±2400	2014±14	2161±92
K16	K16(1)	3861±77	2049±41	1768±1.0	1.5022±0.0068	44.95±0.19	77570±470	68000±5100	2142±31	2500±240
	K16(4)	2258±45	1257±25	1750.7±2.2	1.520±0.017	43.35±0.48	79500±1200	69300±5500	2129±33	2510±250
	K16(5)	2357±47	1267±25	1713.3±1.9	1.506±0.016	44.48±0.48	80100±1200	70100±5400	2088±32	2450±240
	K16(6)	2293±46	1266±25	1746.5±1.9	1.524±0.017	43.81±0.48	79900±1200	69800±5500	2127±33	2500±250
	K16(7)	2290±46	1294±26	1746.9±1.8	1.509±0.017	42.39±0.48	78900±1200	68500±5600	2120±34	2510±260
L1	L1(2)	3570±71	1984±40	1780.6±1.1	1.6487±0.0075	47.09±0.21	87550±560	77700±5200	2217±33	2610±260
	L1(5)	2358±47	1113±22	1772.4±2.0	1.528±0.015	51.40±0.49	79200±1000	70700±4600	2164±28	2480±210
	L1(6)	2314±46	1106±22	1774.2±1.9	1.529±0.015	50.79±0.51	79200±1100	70600±4600	2166±28	2490±210
	L1(7)	2381±48	1115±22	1772.8±1.8	1.473±0.015	49.91±0.50	75350±1000	66800±4500	2141±28	2450±200
	L1(8)	2403±48	1171±24	1773.6±2.3	1.499±0.015	48.83±0.50	77100±1100	68300±4700	2151±29	2480±220
D6	D6(1)	1091±22	841±17	1347.5±1.2	2.209±0.013	45.48±0.27	193800±2600	180000±7900	2240±50	2840±420
	D6(2)	1070±21	806±16	1385.4±1.7	2.291±0.013	48.28±0.26	202300±2700	189400±7500	2364±50	2980±430
	D6(3)	1259±25	1141±23	1212.9±2.7	2.151±0.027	37.69±0.47	211600±6500	194000±12000	2100±69	2790±520
	D6(4)	1283±26	1104±22	1241.5±2.0	2.111±0.026	38.94±0.47	196100±5400	180000±11000	2061±62	2690±470
	D6(5)	1288±26	1103±22	1252.2±1.8	2.117±0.018	39.23±0.33	195000±3800	178700±9800	2074±58	2710±470

Table A2 continued from previous page

Samp. ID	Rep. ID	^{238}U (ng/g)	^{232}Th (ng/g)	δ^{234}U$_m$ (‰)	[^{230}Th/^{238}U]	^{230}Th/^{232}Th	Date Uncorr. (yrs)	Date Corr. (yrs BP)	δ^{234}U$_{initial}$ (‰)	δ^{234}U$_{iac}$ (‰)
M1	M1(1)	2505±50	427.0±8.5	935.7±2.0	2.1324±0.0049	198.65±0.37	327100±3600	324300±3900	2337±26	2451±85
	M1(2)	2497±50	411.7±8.2	938.4±1.1	2.1321±0.0046	205.34±0.34	324700±3100	322000±3400	2328±23	2438±78
	M1(3)	2496±50	417.4±8.4	936.29±0.6	2.1351±0.0044	202.73±0.29	328400±2900	325600±3300	2347±22	2459±78
	M1(4)	2582±52	462.2±9.2	933.7±1.0	2.1213±0.0050	188.15±0.35	321600±3300	318600±3600	2295±24	2412±84
M3	M3(1)	1828±37	373.8±7.5	1004.66±0.81	2.2154±0.0051	172.03±0.31	324600±3200	321300±3600	2488±25	2635±99
	M3(2)	1820±36	384.4±7.7	1010.6±2.2	2.2234±0.0051	167.10±0.27	324900±3500	321600±4000	2504±29	2660±110
	M3(3)	1854±37	410.1±8.2	991.3±1.2	2.2034±0.0051	158.19±0.28	327600±3300	324100±3800	2474±27	2630±110
	M3(4)	1599±32	342.6±6.9	993.9±5.6	2.207±0.011	163.54±0.69	328000±8300	324500±8500	2484±61	2640±160
	M3(5)	1596±32	366.7±7.4	997.2±4.0	2.213±0.011	152.93±0.70	328700±7700	325000±8000	2496±58	2660±160
J8	J8(1)	2590±52	315.1±6.3	987.7±1.6	2.1837±0.0041	285.00±0.34	318300±2700	316300±2900	2412±20	2494±62
	J8(2)	2607±52	328.0±6.6	988.5±1.6	2.1862±0.0046	275.81±0.43	319300±3000	317200±3100	2420±22	2506±66
	J8(3)	2782±56	379.5±7.6	979.8±1.3	2.1785±0.0043	253.53±0.34	321100±2800	318900±3000	2410±21	2503±68
J9	J9(1)	3055±61	1156±23	810.79±0.64	1.9655±0.0064	82.48±0.25	320700±4500	313500±5900	1964±33	2190±160
	J9(2)	3058±61	1191±24	804.54±0.79	1.9548±0.0060	79.71±0.22	318700±4100	311200±5700	1936±31	2170±160
	J9(3)	3064±61	1192±24	807.1±1.3	1.9547±0.0058	79.79±0.20	316600±4000	309100±5700	1931±31	2160±160
E12	E12(1)	907±18	845±17	664.1±2.8	1.890±0.014	32.23±0.27	454000±31000	437000±34000	2280±220	3060±810
	E12(2)	913±18	821±16	663.9±2.8	1.880±0.012	33.20±0.21	436000±23000	419000±26000	2170±160	2870±650
	E12(3)	977±20	1053±21	606.4±3.5	1.779±0.035	26.22±0.52	397000±54000	373000±59000	1740±300	2500±1000
	E12(4)	991±20	1024±21	599.3±4.5	1.780±0.034	27.34±0.52	412000±60000	390000±64000	1800±340	2500±1100
	E12(5)	976±20	975±20	620.7±3.5	1.809±0.033	28.74±0.52	414000±56000	393000±60000	1880±330	2600±1100
F4	F4(1)	1006±20	116.2±2.3	818.5±2.1	2.0592±0.0054	283.16±0.61	394900±7100	393000±7200	2482±51	2560±110
	F4(2)	1003±20	115.9±2.3	811.9±2.2	2.0516±0.0049	281.86±0.51	396300±6800	394400±6900	2471±49	2550±110
	F4(3)	1140±23	122.3±2.4	822.0±1.1	2.0557±0.0044	304.29±0.52	385700±5000	384000±5100	2430±35	2503±83
	F4(4)	1157±23	122.1±2.4	813.5±1.8	2.0545±0.0057	309.03±0.78	397200±7400	395400±7400	2484±53	2560±120
	F4(5)	1154±23	123.2±2.5	818.6±1.9	2.0638±0.0064	306.99±0.87	400200±8300	398400±8400	2520±60	2600±130
B5	B5(1)	1693±34	352.7±7.1	494.4±2.1	1.6751±0.0050	127.68±0.30	503000±21000	499000±21000	2020±120	2150±270
	B5(2)	1702±34	393.9±7.9	488.2±1.1	1.6745±0.0052	114.89±0.33	536000±25000	532000±26000	2190±160	2340±360
	B5(3)	1687±34	355.4±7.1	488.7±2.5	1.6726±0.0087	126.04±0.63	525000±41000	521000±41000	2130±250	2250±540
	B5(4)	1690±34	354.2±7.1	490.6±2.2	1.6727±0.0088	126.71±0.65	514000±37000	510000±38000	2070±230	2200±480
	B5(5)	1721±34	362.0±7.3	486.7±3.6	1.6686±0.0098	125.93±0.69	519000±46000	515000±47000	2090±280	2210±610
B11	B11(1)	2501±50	331.3±6.6	447.3±1.2	1.6230±0.0041	194.52±0.37	567000±28000	565000±28000	2200±180	2290±370
	B11(2)	2501±50	318.5±6.4	445.21±0.84	1.6214±0.0043	202.18±0.46	576000±30000	574000±30000	2250±190	2330±400
	B11(3)	2787±56	389.2±7.8	445.3±2.8	1.6149±0.0048	183.58±0.47	538000±31000	535000±31000	2020±180	2100±380
	B11(4)	2819±56	374.2±7.5	437.9±1.9	1.6049±0.0053	191.98±0.59	540000±30000	537000±30000	1990±180	2070±370
B13	B13(1)	1280±26	131.9±2.6	468.4±1.1	1.6559±0.0041	255.10±0.46	588000±31000	587000±31000	2450±220	2520±450
	B13(2)	1218±24	116.1±2.3	471.6±4.9	1.6556±0.0059	275.87±0.65	558000±51000	557000±52000	2270±340	2330±710
	B13(3)	1401±28	145.5±2.9	471.25±0.86	1.6568±0.0036	253.31±0.46	568000±23000	567000±23000	2330±150	2400±320
	B13(5)	1372±27	141.3±2.8	466.9±3.0	1.6605±0.0053	256.07±0.72	645000±74000	644000±74000	2870±630	3000±1300

Replicate Analyses of Failing Samples

Samp. ID	Rep. ID	^{238}U (ng/g)	^{232}Th (ng/g)	δ^{234}U$_m$ (‰)	[^{230}Th/^{238}U]	^{230}Th/^{232}Th	Date Uncorr. (yrs)	Date Corr. (yrs BP)	δ^{234}U$_{initial}$ (‰)	δ^{234}U$_{iac}$ (‰)
P10	P10(1)	726±15	800±16	794.4±1.5	0.543±0.013	7.83±0.18	38300±1000	-1000±25000	792±57	1130±360
	P10(2)	772±15	874±18	791.2±1.0	0.536±0.013	7.52±0.18	37700±1100	-3000±26000	785±59	1130±380

Table A2 continued from previous page

Samp. ID	Rep. ID	^{238}U (ng/g)	^{232}Th (ng/g)	δ^{234}U$_m$ (‰)	[^{230}Th/^{238}U]	^{230}Th/^{232}Th	Date Uncorr. (yrs)	Date Corr. (yrs BP)	δ^{234}U$_{initial}$ (‰)	δ^{234}U$_{iac}$ (‰)
L3	L3(1)	619±12	1118±23	719.6±3.0	1.621±0.025	14.25±0.22	210400±8200	152000±47000	1100±150	2200±1300
G1	G1(1)	851±17	1230±130	673.8±2.0	1.190±0.120	13.1±1.9	121000±21000	67000±46000	810±110	1340±660
G2	G2(1)	1167±23	1485±30	1504.84±0.76	1.720±0.020	21.46±0.25	109200±2000	83000±16000	1900±86	2910±860
	G2(2)	1161±23	1386±28	1488.7±2.8	1.681±0.020	22.37±0.26	106600±1900	82000±15000	1875±79	2780±750
G5	G5(1)	635±13	1395±28	966.7±1.7	2.162±0.040	15.61±0.29	321000±25000	275000±43000	2100±260	5200±4200
G6	G6(1)	435.9±8.7	792±16	1041.8±2.3	1.902±0.025	16.62±0.22	195100±5800	150000±32000	1590±150	3200±1700
	G6(2)	315.3±6.3	614±12	1772.4±6.1	2.567±0.029	20.93±0.23	182200±4300	150000±21000	2710±160	5800±3400
	G6(3)	316.0±6.3	639±13	1777.8±1.8	2.586±0.031	20.30±0.24	184300±4600	151000±22000	2720±170	6100±3900
	G6(4)	336.2±6.7	721±14	1741.8±4.0	2.539±0.033	18.79±0.24	182500±4900	146000±24000	2630±180	6300±4600
G7	G7(1)	414.1±8.3	831±17	955.3±5.9	1.831±0.025	14.48±0.19	199500±6400	144000±43000	1440±180	3200±2200
	G7(2)	426.5±8.5	839±17	925.6±3.7	1.768±0.024	14.27±0.19	191400±5800	135000±44000	1360±170	2900±1900
	G7(3)	413.7±8.3	818±16	915.1±6.0	1.784±0.024	14.32±0.19	198100±6300	142000±44000	1370±180	3000±2000
G8	G8(1)	861±17	2362±48	621.9±3.9	1.986±0.035	11.50±0.20	–	–	–	–
M15	M15(1)	327.4±6.5	38.91±0.78	2306.98±0.78	2.2407±0.0058	299.35±0.64	105080±410	103470±910	3089.3±8.0	3193±58
	M15(2)	313.5±6.3	35.45±0.71	2310.06±0.98	2.2675±0.0057	318.39±0.64	106800±400	105280±870	3109.2±7.7	3208±56
	M15(3)	322.6±6.5	42.20±0.85	2300.3±1.5	2.1937±0.0065	266.23±0.65	102160±450	100400±1000	3053.5±8.9	3166±64
	M15(4)	327.3±6.5	36.66±0.73	2294.4±1.5	2.1731±0.0055	308.04±0.61	101030±380	99490±860	3038.2±7.6	3134±54
L7	L7(1)	6960±140	383.1±7.8	1690±1.4	1.8670±0.0044	538.4±2.5	110430±410	109510±620	2302.0±4.4	2337±21
	L7(2)	6430±130	372.4±7.6	1686.3±1.5	1.7499±0.0042	479.5±2.0	100410±370	99420±620	2232.4±4.4	2268±22
	L7(3)	7340±150	451.5±9.2	1691.47±0.64	1.9770±0.0046	510.6±1.9	120680±450	119670±680	2371.0±4.6	2411±24
	L7(4)	6460±130	392.9±8.0	1687.04±0.74	1.8028±0.0041	470.4±1.9	104900±360	103870±630	2261.7±4.2	2305±23
	L7(5)	6920±140	417.7±8.4	1692.2±1.5	1.8034±0.0041	474.2±1.3	104640±370	103620±630	2267.1±4.5	2305±23
	L7(6)	6590±130	388.6±7.8	1682.24±0.70	1.8101±0.0040	487.5±1.2	105840±350	104850±610	2261.5±4.0	2298±22
	L7(7)	6900±140	393.6±7.9	1684.15±0.78	1.7943±0.0047	499.6±1.4	104340±420	103370±640	2254.6±4.2	2290±22
D7	D7(1)	850±17	1029±21	1310.5±1.5	2.322±0.020	30.45±0.26	227500±5100	206000±13000	2344±89	3500±940
	D7(2)	825±17	965±19	1346.2±1.7	2.339±0.019	31.76±0.25	222000±4600	202000±13000	2378±85	3490±890
D11	D11(1)	365.0±7.3	725±64	289.1±1.1	1.330±0.110	10.7±1.3	–	–	–	–
	D11(2)	419.7±8.4	1025±21	278.7±2.1	1.493±0.039	9.71±0.26	–	–	–	–
D12	D12(1)	228.8±4.6	456.0±9.2	596.8±1.8	1.829±0.036	14.57±0.29	–	–	–	–
	D12(2)	294.8±5.9	424.9±8.5	806.1±1.5	2.080±0.024	22.91±0.26	447000±42000	424000±46000	2670±360	4400±1900
D13	D13(1)	161.4±3.2	204.2±4.1	862.8±2.5	2.168±0.018	27.20±0.22	467000±35000	448000±38000	3060±340	4700±1600
	D13(2)	161.8±3.2	210.5±4.2	851.3±1.8	2.087±0.022	25.46±0.27	378000±23000	354000±28000	2310±180	3600±1200
	D13(3)	180.4±3.6	233.1±4.7	755.1±2.2	1.979±0.021	24.31±0.26	399000±28000	375000±33000	2180±210	3400±1100
D14	D14(1)	291.2±5.8	299.1±6.0	1022.3±1.6	2.691±0.014	41.60±0.21	–	–	–	–
	D14(2)	282.0±5.6	282.1±5.7	1016.1±2.3	2.634±0.014	41.82±0.21	–	–	–	–
J5	J5(1)	1310±26	411.7±8.2	946.8±1.7	2.0688±0.0067	104.48±0.27	284200±3300	278500±4500	2078±27	2270±130
	J5(2)	1383±28	336.9±6.8	1031.87±0.62	2.1567±0.0078	140.58±0.54	277800±3300	273600±4000	2233±25	2390±110
	J5(3)	1238±25	285.7±5.7	1032.3±1.5	2.1597±0.0059	148.57±0.32	278800±2600	274800±3300	2242±21	2393±99
	J5(4)	1518±30	473.5±9.5	997.5±1.4	2.1404±0.0054	108.97±0.22	289100±2700	283600±3900	2221±25	2430±130
J6	J6(1)	1110±22	348.2±7.0	1019±1.9	2.1544±0.0089	109.03±0.40	283500±4100	278100±5000	2234±32	2440±140
	J6(2)	1247±25	402.2±8.0	1021±1.2	2.1230±0.0057	104.53±0.24	269200±2400	263400±3800	2147±23	2350±130
	J6(3)	1248±25	416.3±8.3	1010.8±1.6	2.1089±0.0061	100.38±0.25	268300±2600	262300±4100	2119±25	2330±140

43

Table A2 continued from previous page

Samp. ID	Rep. ID	238U (ng/g)	232Th (ng/g)	δ234U_m (‰)	[230Th/238U]	230Th/232Th	Date Uncorr. (yrs)	Date Corr. (yrs BP)	δ234U_initial (‰)	δ234U_iac (‰)
J7	J7(1)	2526±51	383.5±7.7	1027.16±0.9	2.1421±0.0041	224.01±0.27	274000±1800	271400±2200	2209±14	2305±62
	J7(2)	2408±48	396.1±7.9	1027.4±1.1	2.1816±0.0047	210.61±0.33	291400±2300	288600±2700	2320±18	2429±72
J10	J10(2)	1798±36	2117±42	789.80±0.77	1.977±0.016	26.66±0.21	351000±14000	327000±20000	1990±110	2930±800
K1	K1(1)	659±13	654±13	571.8±1.4	1.798±0.014	28.76±0.23	568000±84000	552000±87000	2720±710	3700±2100
A5	A5(1)	2260±45	1479±30	737.1±1.3	1.938±0.013	47.01±0.31	379000±14000	366000±16000	2073±96	2520±380
	A5(2)	2464±49	1513±30	764.48±0.95	1.876±0.010	48.50±0.25	299700±6300	286700±9500	1717±46	2060±260
A6	A6(2)	2442±49	1117±22	812.2±1.9	1.9609±0.0081	68.09±0.28	316400±5600	307500±7400	1935±41	2210±200
	A6(3)	2376±48	1086±22	825.1±1.3	2.0697±0.0083	71.91±0.27	396900±9900	389000±11000	2477±76	2830±280
	A6(4)	2737±55	1227±25	820.6±2.2	1.9575±0.0087	69.31±0.28	307500±5600	298700±7300	1907±40	2170±190
F13	F13(1)	339.3±6.8	308.3±6.2	380.6±2.0	1.499±0.013	26.20±0.22	442000±36000	418000±40000	1240±150	1640±500
	F13(2)	339.2±6.8	265.6±5.3	467.8±2.6	1.606±0.015	32.57±0.30	417000±31000	398000±34000	1440±140	1830±460
	F13(3)	342.1±6.8	278.5±5.6	469.4±1.7	1.611±0.014	31.41±0.26	422000±29000	403000±32000	1460±140	1880±460
	F13(4)	330.7±6.6	260.6±5.2	472.6±1.8	1.621±0.013	32.66±0.27	434000±30000	416000±33000	1530±150	1940±480
B2	B2(1)	516±10	615±12	416.5±2.1	1.565±0.017	20.84±0.22	494000±68000	465000±75000	1550±340	2300±1200
G13	G13(1)	728±15	166.4±3.3	428.3±1.8	1.5828±0.0049	109.95±0.31	501000±22000	496000±22000	1740±110	1850±240
	G13(2)	727±15	163.0±3.3	426.5±2.1	1.5877±0.0052	112.52±0.32	533000±30000	528000±30000	1900±160	2020±360
	G13(3)	742±15	155.6±3.1	445.6±5.7	1.640±0.010	124.22±0.68	–	–	–	–
	G13(4)	737±15	153.6±3.1	445.3±2.1	1.6200±0.0082	123.40±0.60	566000±56000	563000±56000	2180±360	2310±770
G14	G14(1)	3066±61	211.1±4.2	465.4±1.8	1.6273±0.0046	375.25±0.92	477000±16000	476000±16000	1784±84	1820±170
	G14(2)	3101±62	201.0±4.0	463.2±1.0	1.6290±0.0037	399.07±0.58	493000±14000	492000±14000	1855±73	1890±150
H6	H6(1)	1115±22	918±18	364.6±1.7	1.648±0.016	31.79±0.30	–	–	–	–
	H6(2)	1288±26	891±18	378.4±2.9	1.523±0.012	34.95±0.27	547000±82000	532000±85000	1700±430	2100±1100
	H6(3)	1161±23	852±17	380.1±1.6	1.531±0.012	33.11±0.25	580000±110000	570000±120000	1900±690	2400±1700
H7	H7(1)	893±18	565±11	404.74±0.75	1.607±0.012	40.31±0.30	–	–	–	–
	H7(2)	1003±20	597±12	413.5±1.5	1.551±0.010	41.34±0.26	463000±31000	449000±33000	1470±140	1750±390
	H7(3)	988±20	675±14	405.4±1.7	1.5410±0.0110	35.85±0.26	466000±37000	449000±39000	1440±160	1770±460
	H7(4)	989±20	589±12	412.8±2.2	1.5452±0.0099	41.20±0.26	448000±28000	434000±30000	1400±120	1680±350
B14	B14(1)	1676±34	739±15	410.00±0.93	1.5156±0.0067	54.60±0.24	392000±12000	380000±14000	1200±47	1360±160
	B14(2)	1664±33	614±12	433.5±1.1	1.5425±0.0064	66.35±0.26	385000±11000	376000±12000	1251±43	1390±130
	B14(3)	1669±33	727±15	413.2±2.8	1.557±0.015	56.78±0.54	482000±57000	472000±58000	1570±270	1780±620
	B14(4)	1730±35	712±14	411.5±4.2	1.480±0.014	57.15±0.53	338000±18000	327000±19000	1035±58	1170±160
B15	B15(1)	477±10	155.4±3.1	373.5±1.9	1.4102±0.0058	68.70±0.30	314400±6400	304500±8300	882±21	968±82
	B15(2)	482±10	171.7±3.4	375.5±2.1	1.4136±0.0061	62.94±0.27	314900±6900	304000±9000	886±23	982±91
	B15(3)	471.0±9.4	149.8±3.0	375.3±3.6	1.416±0.011	70.72±0.55	318000±13000	309000±14000	897±37	980±100
	B15(4)	488±10	167.1±3.4	367.4±4.3	1.400±0.015	64.94±0.62	311000±16000	301000±17000	859±43	950±120
C1	C1(1)	1628±33	442.8±8.9	375.2±3.3	1.5121±0.0058	88.27±0.30	513000±35000	508000±35000	1570±160	1700±360
	C1(2)	1582±32	431.3±8.6	374.6±1.4	1.5083±0.0048	87.83±0.25	500000±22000	494000±23000	1509±98	1630±230
	C1(3)	865±17	276.2±5.5	385.3±5.4	1.389±0.012	69.06±0.55	283000±11000	273000±12000	831±31	911±93
	C1(4)	839±17	177.9±3.6	383.8±4.9	1.3509±0.0089	101.12±0.62	256800±6800	250000±7700	777±20	825±58
C3	C3(2)	3557±71	687±14	372.94±0.95	1.5058±0.0059	123.71±0.48	499000±26000	495000±26000	1510±110	1590±240
	C3(3)	3460±69	659±13	375.8±2.5	1.5228±0.0045	126.96±0.27	569000±40000	566000±41000	1850±220	1960±470
C6	C6(1)	361.3±7.2	422.6±8.5	258.6±2.8	1.346±0.016	18.27±0.22	490000±92000	450000±100000	930±280	1360±920

Table A2 continued from previous page

Samp. ID	Rep. ID	^{238}U (ng/g)	^{232}Th (ng/g)	δ^{234}U$_m$ (‰)	[^{230}Th/^{238}U]	^{230}Th/^{232}Th	Date Uncorr. (yrs)	Date Corr. (yrs BP)	δ^{234}U$_{initial}$ (‰)	δ^{234}U$_{iac}$ (‰)
C10	C10(1)	381.9±7.6	267.9±5.4	414.3±1.6	1.525±0.010	34.51±0.22	398000±19000	379000±23000	1208±79	1490±290
	C10(2)	382.6±7.7	256.7±5.2	518.2±3.8	1.659±0.012	39.25±0.29	392000±21000	376000±23000	1497±100	1830±340
	C10(3)	379.9±7.6	218.5±4.4	515.5±1.9	1.6498±0.0099	45.53±0.27	384000±15000	370000±17000	1465±71	1740±250
	C10(4)	404.4±8.1	271.5±5.5	443.1±1.5	1.552±0.011	36.70±0.27	380000±18000	362000±21000	1232±74	1510±270
	C10(5)	431.3±8.6	277.9±5.6	427.2±1.6	1.530±0.011	37.71±0.27	379000±18000	361000±21000	1184±70	1440±250
	C10(6)	431.7±8.6	295.1±5.9	434.9±1.9	1.555±0.012	36.13±0.27	404000±23000	387000±25000	1296±94	1590±320
	C10(7)	483±10	325.0±6.5	433.1±2.6	1.528±0.012	36.02±0.28	364000±17000	345000±20000	1147±67	1400±250
	C10(8)	443.3±8.9	290.6±5.8	436.4±1.4	1.519±0.011	36.80±0.27	347000±14000	329000±17000	1104±55	1340±230
C11	C11(1)	1781±36	346.6±6.9	467.3±1.1	1.6278±0.0045	132.84±0.32	471000±14000	467000±14000	1747±71	1850±160
	C11(2)	1746±35	331.6±6.7	472.91±0.98	1.6480±0.0063	137.73±0.54	514000±26000	510000±26000	2000±150	2110±330
C13	C13(1)	1229±25	387.3±7.8	321.3±1.9	1.3946±0.0052	70.28±0.24	385000±11000	376000±12000	928±33	1015±98
	C13(2)	1281±26	378.0±7.6	322.1±1.5	1.3899±0.0048	74.77±0.22	374500±9000	366000±10000	904±27	983±84
	C13(3)	1214±24	322.1±6.5	341.3±2.6	1.4390±0.0098	86.11±0.58	424000±26000	417000±27000	1106±86	1190±190
	C13(4)	1180±24	334.8±6.7	336.1±3.6	1.434±0.011	80.24±0.59	429000±31000	421000±32000	1100±100	1200±230
C14	C14(1)	2133±43	516±10	367.09±0.91	1.5908±0.0047	104.35±0.25	–	–	–	–
	C14(2)	2136±43	533±11	361.7±1.2	1.5855±0.0049	100.87±0.26	–	–	–	–

References

Ainsworth, N.R., Burnett, R.D., Kontrovitz, M., 1990. Ostracod colour change by thermal alteration, offshore Ireland and Western UK. Marine and Petroleum Geology 7, 288–297.

Alam, M.S., Cheng, T., 2014. Uranium release from sediment to groundwater: Influence of water chemistry and insights into release mechanisms. Journal of Contaminant Hydrology 164, 72–87. doi:10.1016/j.jconhyd.2014.06.001.

Ames, L.L., McGarrah, J.E., Walker, B.A., 1983a. Sorption of Trace Constituents from Aqueous Solutions onto Secondary Minerals. II. Radium. Clays and Clay Minerals 31, 321–334.

Ames, L.L., McGarrah, J.E., Walker, B.A., 1983b. Sorption of Uranium and Radium by Biotite, Muscovite, and Phlogopite. Clays and Clay Minerals 31, 343–351.

Ames, L.L., McGarrah, J.E., Walker, B.A., Salter, P.F., 1983c. Uranium and radium sorption on amorphous ferric oxyhydroxide. Chemical Geology 40, 135–148. doi:10.1016/0009-2541(83)90095-5.

Balch, D.P., Cohen, A.S., Schnurrenberger, D.W., Haskell, B.J., Valero-Garcés, B.L., Beck, J.W., Cheng, H., Edwards, R.L., 2005. Ecosystem and paleohydrological response to Quaternary climate change in the Bonneville Basin, Utah. Palaeogeography, Palaeoclimatology, Palaeoecology 221, 99–122. doi:10.1016/j.palaeo.2005.01.013.

Balsam, W.L., Deaton, B.C., Damuth, J.E., 1999. Evaluating optical lightness as a proxy for carbonate content in marine sediment cores. Marine Geology 161, 141–153. doi:10.1016/S0025-3227(99)00037-7.

Bar-Matthews, M., Ayalon, A., Gilmour, M., Matthews, A., Hawkesworth, C.J., 2003. Sea-land oxygen isotope relationships from planktonic foraminifera and speleothems in the Eastern Mediterranean region and their implication for paleorainfall during interglacial intervals. Geochimica et Cosmochimica Acta 67, 3181–3199.

Bard, E., Fairbanks, R.G., Hamelin, B., Zindler, A., Chi Track Hoang, 1991. Uranium-234 anomalies in corals older than 150,000 years. Geochimica et Cosmochimica Acta 55, 2385–2390. URL: https://linkinghub.elsevier.com/retrieve/pii/001670379190115L, doi:10.1016/0016-7037(91)90115-L.

Bateman, H., 1910. The solution of a system of differential equations occurring in the theory of radio-active transformations. Proc. Cambridge Phil. Soc. 15, 423–427.

Bischoff, J.L., Fitzpatrick, J.a., 1991. U-series dating of impure carbonates: An isochron technique using total-sample dissolution. Geochimica et Cosmochimica Acta 55, 543–554. doi:10.1016/0016-7037(91)90011-S.

Bischoff, J.L., Rosenbauer, R.J., Smith, G.I., 1985. Uranium-Series Dating of Sediments from Searles Lake: Differences Between Continental and Marine Climate Records. Science 227, 1222–1224.

Blaauw, M., Christen, J.A., 2011. Flexible paleoclimate age-depth models using an autoregressive gamma process. Bayesian Analysis 6, 457–474. URL: http://projecteuclid.org/euclid.ba/1339616472, doi:10.1214/11-BA618.

Blanchard, R.L., Cheng, M.H., Potratz, H.A., 1967. Uranium and Thorium Series Disequilibria in Recent and Fossil Marine Molluscan Shells. Journal of Geophysical Research 72, 4745–4757.

Bobst, A.L., Lowenstein, T.K., Jordan, T.E., Godfrey, L.V., Ku, T.L., Luo, S., 2001. A 106 ka paleoclimate record from drill core of the Salar de Atacama, northern Chile. Palaeogeography, Palaeoclimatology, Palaeoecology 173, 21–42. URL: http://linkinghub.elsevier.com/retrieve/pii/S003101820100308X, doi:10.1016/S0031-0182(01)00308-X.

Bone, S.E., Dynes, J.J., Cliff, J., Bargar, J.R., 2017. Uranium(IV) adsorption by natural organic matter in anoxic sediments. Proceedings of the National Academy of Sciences 114, 201611918. URL: http://www.pnas.org/lookup/doi/10.1073/pnas.1611918114, doi:10.1073/pnas.1611918114.

Bourdon, B., Henderson, G.M., Lundstrom, C.C., Turner, S.P. (Eds.), 2003. Uranium-Series Geochemistry. volume 52. The Mineralogical Society of America.

Brand, A., Allen, L., Altman, M., Hlava, M., Scott, J., 2015. Beyond authorship: attribution, contribution, collaboration, and credit. Learned Publishing 28, 151–155.

Broecker, W.S., 1963. A Preliminary Evoluation of Uranium Series Inequilibrium as a Tool for Absolute Age Measurement on Marine Carbonates. Journal of Geophysical Research 68, 2817–2834.

Chabaux, F., Bourdon, B., Riotte, J., 2008. Chapter 3 U-Series Geochemistry in Weathering Profiles, River Waters and Lakes, in: Radioactivity in the Environment. volume 13, pp. 49–104. URL: https://linkinghub.elsevier.com/retrieve/pii/S1569486007000034, doi:10.1016/S1569-4860(07)00003-4.

Chabaux, F., Riotte, J., Dequincey, O., 2003. U-Th-Ra Fractionation During Weathering and River Transport. Reviews in Mineralogy and Geochemistry 52, 533–576. URL: https://pubs.geoscienceworld.org/rimg/article/52/1/533-576/87464, doi:10.2113/0520533.

Chappaz, A., Gobeil, C., Tessier, A., 2010. Controls on uranium distribution in lake sediments. Geochimica et Cosmochimica Acta 74, 203–214. doi:10.1016/j.gca.2009.09.026.

Cheng, H., Adkins, J., Edwards, R., Boyle, E.A., 2000. U-Th dating of deep-sea corals. Geochimica et Cosmochimica Acta 64, 2401–2416. URL: http://linkinghub.elsevier.com/retrieve/pii/S0016703799004226, doi:10.1016/S0016-7037(99)00422-6.

Cheng, H., Edwards, R.L., Sinha, A., Spötl, C., Yi, L., Chen, S., Kelly, M., Kathayat, G., Wang, X., Li, X., Kong, X., Wang, Y., Ning, Y., Zhang, H., 2016. The Asian monsoon over the past 640,000 years and ice age terminations. Nature 534, 640–646. URL: http://www.nature.com/doifinder/10.1038/nature18591, doi:10.1038/nature18591.

Cheng, H., Lawrence Edwards, R., Shen, C.C., Polyak, V.J., Asmerom, Y., Woodhead, J., Hellstrom, J., Wang, Y., Kong, X., Spötl, C., Wang, X., Calvin Alexander, E., 2013. Improvements in 230Th dating, 230Th and 234U half-life values, and U-Th isotopic measurements by multi-collector inductively coupled plasma mass spectrometry. Earth and Planetary Science Letters 371-372, 82–91. URL: http://dx.doi.org/10.1016/j.epsl.2013.04.006, doi:10.1016/j.epsl.2013.04.006.

Cobbing, E.J., Pitcher, W.S., WIlson, J.J., Baldock, J.W., Taylor, W.P., McCourt, W., Snelling, N.J., 1981. The geology of the Western Cordillera of northern Peru. volume 5. Great Britain Institute of Geological Sciences, Natural Environmental Research Council.

Colman, S., Kaufman, D., Bright, J., Heil, C., King, J., Dean, W., Rosenbaum, J., Forester, R., Bischoff, J., Perkins, M., McGeehin, J., 2006. Age model for a continuous, ca 250-ka Quaternary lacustrine record from Bear Lake, Utah–Idaho. Quaternary Science Reviews 25, 2271–2282. URL: http://linkinghub.elsevier.com/retrieve/pii/S0277379106001806, doi:10.1016/j.quascirev.2005.10.015.

Colman, S.M., 1996. Continental Drilling for Paleoclimatic Records: Recommendations from an International Workshop. Technical Report. GeoForschungsZentrum. Potsdam, Germany.

Durand, S., Chabaux, F., Rihs, S., Duringer, P., Elsass, P., 2005. U isotope ratios as tracers of groundwater inputs into surface waters: example of the upper rhine hydrosystem. Chemical Geology 220, 1–19.

Dutton, A., Rubin, K., McLean, N., Bowring, J., Bard, E., Edwards, R.L., Henderson, G.M., Reid, M.R., Richards, D.A., Sims, K., Walker, J.D., Yokoyama, Y., 2017. Data reporting standards for publication of U-series data for geochronology and timescale assessment in the earth sciences. Quaternary Geochronology 39, 142–149. URL: http://dx.doi.org/10.1016/j.quageo.2017.03.001, doi:10.1016/j.quageo.2017.03.001.

Edwards, R., Gallup, C., Cheng, H., 2003. Uranium-series Dating of Marine and Lacustrine Carbonates. Reviews in Mineralogy and Geochemistry 52, 363–405. URL: http://rimg.geoscienceworld.org/cgi/doi/10.2113/0520363, doi:10.2113/0520363.

Edwards, R.L., 1988. High Precition Thorium-230 Ages of Corals and the Timing of Sea Level Fluctuations in the Late Quaternary. Ph.D. thesis. California Insititute of Technology.

Edwards, R.L., Chen, J., Wasserburg, G., 1987. 238U-234U-230Th-232Th systematics and the precise measurement of time over the past 500,000 years. Earth and Planetary Science Letters 81, 175–192. doi:10.1016/0012-821X(87)90154-3.

Fleischer, R.L., 1982. Alpha-recoil damage and solution effects in minerals: uranium isotopic disequilibrium and radon release. Geochimica et Cosmochimica Acta 46, 2191–2201. URL: https://linkinghub.elsevier.com/retrieve/pii/0016703782901946, doi:10.1016/0016-7037(82)90194-6.

Flusche, M.A., Seltzer, G., Rodbell, D., Siegel, D., Samson, S., 2005. Constraining water sources and hydrologic processes from the isotopic analysis of water and dissolved strontium, Lake Junin, Peru. Journal of Hydrology 312, 1–13. URL: https://linkinghub.elsevier.com/retrieve/pii/S0022169405000727, doi:10.1016/j.jhydrol.2005.02.021.

Francke, A., Wagner, B., Just, J., Leicher, N., Gromig, R., Baumgarten, H., Vogel, H., Lacey, J.H., Sadori, L., Wonik, T., Leng, M.J., Zanchetta, G., Sulpizio, R., Giaccio, B., 2016. Sedimentological processes and environmental variability at Lake Ohrid (Macedonia, Albania) between 637 ka and the present. Biogeosciences 13, 1179–1196. doi:10.5194/bg-13-1179-2016.

Frechen, M., Sierralta, M., Oezen, D., Urban, B., 2007. Uranium-series dating of peat from central and Northern Europe, in: Sirocko, F., Claussen, M., Goñi, M.F.S., Litt, T. (Eds.), Developments in Quaternary Science: The Climate of Past Interglacials. Elsevier. volume 7. chapter 8, pp. 83–117. doi:10.1016/S1571-0866(07)80033-9.

Fritz, S.C., Baker, P.a., Lowenstein, T.K., Seltzer, G.O., Rigsby, C.a., Dwyer, G.S., Tapia, P.M., Arnold, K.K., Ku, T.L., Luo, S., 2004. Hydrologic variation during the last 170,000 years in the southern hemisphere tropics of South America. Quaternary Research 61, 95–104. doi:10.1016/j.yqres.2003.08.007.

Fritz, S.C., Baker, P.A., Seltzer, G.O., Ballantyne, A., Tapia, P., Cheng, H., Edwards, R.L., 2007. Quaternary glaciation and hydrologic variation in the South American tropics as reconstructed from the Lake Titicaca drilling project. Quaternary Research 68, 410–420. doi:10.1016/j.yqres.2007.07.008.

Gallup, C.D., Edwards, R.L., Johnson, R.G., 1994. The timing of high sea levels over the past 200,000 years. Science 263, 796–800.

Geyh, M.A., Mu, H., 2005. Numerical 230Th/U dating and a palynological review of the Holsteinian/Hoxnian Interglacial. Quaternary Science Reviews 24, 1861–1872. doi:10.1016/j.quascirev.2005.01.007.

Giosan, L., Flood, R.D., Aller, R.C., 2002. Paleoceanographic significance of sediment color on western North Atlantic drifts: I. Origin of color. Marine Geology 189, 25–41. URL: https://linkinghub.elsevier.com/retrieve/pii/S0025322702003225https://linkinghub.elsevier.com/retrieve/pii/S0025322702003213, doi:10.1016/S0025-3227(02)00321-3.

Groot, M.H.M., Bogotá, R.G., Lourens, L.J., Hooghiemstra, H., Vriend, M., Berrio, J.C., Tuenter, E., Van Der Plicht, J., Van Geel, B., Ziegler, M., Weber, S.L., Betancourt, A., Contreras, L., Gaviria, S., Giraldo, C., González, N., Jansen, J.H.F., Konert, M., Ortega, D., Rangel, O., Sarmiento, G., Vandenberghe, J., Van Der Hammen, T., Van Der Linden, M., Westerhoff, W., 2011. Ultra-high resolution pollen record from the northern Andes reveals rapid shifts in montane climates within the last two glacial cycles. Climate of the Past 7, 299–316. doi:10.5194/cp-7-299-2011.

Grzymko, T.J., Marcantonio, F., McKee, B.A., Mike Stewart, C., 2007. Temporal variability of uranium concentrations and 234U/238U activity ratios in the Mississippi river and its tributaries. Chemical Geology 243, 344–356. URL: https://linkinghub.elsevier.com/retrieve/pii/S0009254107002434, doi:10.1016/j.chemgeo.2007.05.024.

Haase-Schramm, A., Goldstein, S.L., Stein, M., 2004. U-Th dating of Lake Lisan (late Pleistocene dead sea) aragonite and implications for glacial east Mediterranean climate change. Geochimica et Cosmochimica Acta 68, 985–1005. URL: http://linkinghub.elsevier.com/retrieve/pii/S0016703703005647, doi:10.1016/j.gca.2003.07.016.

Halbach, P., Von Borstel, D., Gundermann, K.d., 1980. The uptake of uranium by organic substances in a peat bog environment on a granitic bedrock. Chemical Geology 29, 117–138.

Hamelin, B., Bard, E., Zindler, A., Fairbanks, R.G., 1991. 234U/238U mass spectrometry of corals: How accurate is the UTh age of the last interglacial period? Earth and Planetary Science Letters 106, 169–180. URL: https://linkinghub.elsevier.com/retrieve/pii/0012821X9190070X, doi:10.1016/0012-821X(91)90070-X.

Hansen, B.C.S., Wright, H.E., Bradbury, J.P., 1984. Pollen studies in the Junín area, central Peruvian Andes. Geological Society of America Bulletin 95, 1454. URL: https://pubs.geoscienceworld.org/gsabulletin/article/95/12/1454-1465/186834, doi:10.1130/0016-7606(1984)95<1454:PSITJA>2.0.CO;2.

Hatfield, R., Woods, A., Lehmann, S., Weidhaas, N., Chen, C., Kück, J., Pierdominici, S., Stoner, J., Abbott, M., Rodbell, D., 2019. Stratigraphic correlation and splice generation for sediments recovered from a large-lake drilling project: an example from lake junín, peru. Journal of Paleolimnology , 1–18doi:10.1007/s10933-019-00098-w.

Helmke, J.P., Schulz, M., Bauch, H.A., 2002. Sediment-Color Record from the Northeast Atlantic Reveals Patterns of Millennial-Scale Climate Variability during the Past 500,000 Years. Quaternary Research 57, 49–57. URL: https://www.cambridge.org/core/product/identifier/S0033589400010565/type/journal{_}article, doi:10.1006/qres.2001.2289.

Henderson, G.M., 2002. Seawater (234U/238U) during the last 800 thousand years. Earth and Planetary Science Letters 199, 97–110. URL: https://linkinghub.elsevier.com/retrieve/pii/S0012821X02005563, doi:10.1016/S0012-821X(02)00556-3.

Henderson, G.M., Anderson, R.F., 2003. The U-series Toolbox for Paleoceanography. Reviews in Mineralogy and Geochemistry 52, 493–531. URL: https://pubs.geoscienceworld.org/rimg/article/52/1/493-531/87463, doi:10.2113/0520493.

Henderson, G.M., Robinson, L.F., Cox, K., Thomas, A.L., 2006. Recognition of non-Milankovitch sea-level highstands at 185 and 343 thousand years ago from U-Th dating of Bahamas sediment. Quaternary Science Reviews 25, 3346–3358. URL: https://linkinghub.elsevier.com/retrieve/pii/S0277379106001363, doi:10.1016/j.quascirev.2006.03.003.

Holmes, J., 1998. Chapter 10: The palaeoenvironmental significance of iron and manganese in non-marine ostracod shells: a preliminary analysis, in: Holmes, J., Lynch, K. (Eds.), The Kingston Papers: a geographical perspective on the environment, economy, and society. Kingston University School of Geography. chapter Holmes, pp. 198–212.

Holmes, J.A., Chivas, A.R., 2002. Ostracod shell chemistry - overview. Geophysical Monograph Series 131, 185–204. doi:10.1029/131GM10.

Israelson, C., Björck, S., Hawkesworth, C.J., Possnert, G., 1997. Direct U-Th dating of organic- and carbonate-rich lake sediments from southern Scandinavia. Earth and Planetary Science Letters 153, 251–263. doi:10.1016/S0012-821X(97)00184-2.

Ivanovich, M., Harmon, R., 1992. Uranium-series Disequilibrium: Applications to Earth, Marine, and Environmental Sciences. Oxford University Press, New York.

Jaffey, A.H., Flynn, K.F., Glendenin, L.E., Bentley, W.C., Essling, A.M., 1971. Precision measurement of half-lives and specific activities of U235 and U238. Physical Review C 4, 1889–1906. doi:10.1103/PhysRevC.4.1889.

Ji, J., Shen, J., Balsam, W.L., Chen, J., Liu, L., Liu, X., 2005. Asian monsoon oscillations in the northeastern Qinghai–Tibet Plateau since the late glacial as interpreted from visible reflectance of Qinghai Lake sediments. Earth and Planetary Science Letters 233, 61–70. URL: https://linkinghub.elsevier.com/retrieve/pii/S0012821X05001275, doi:10.1016/j.epsl.2005.02.025.

Karanovic, I., 2012. Recent freshwater ostracods of the world: Crustacea, Ostracoda, Podocopida. Springer Science & Business Media.

Kaufman, A., Broecker, W.S., Ku, T.L., Thurber, D.L., 1971. The status of U-series methods of mollusk dating. Geochimica et Cosmochimica Acta 35, 1155–1183. doi:10.1016/0016-7037(71)90031-7.

Kaufman, A., Yechieli, Y., Gardosh, M., 1992. Reevaluation of the Lake-Sediment Chronology in the Dead-Sea Basin, Israel, Based on New Th-230/U Dates. Quaternary Research 38, 292–304.

Kelly, S.D., Newville, M.G., Cheng, L., Kemner, K.M., Sutton, S.R., Fenter, P., Sturchio, N.C., Spötl, C., 2003. Uranyl Incorporation in Natural Calcite. Environmental Science & Technology 37, 1284–1287. URL: https://pubs.acs.org/doi/10.1021/es025962f, doi:10.1021/es025962f.

Kelly, S.D., Rasbury, E.T., Chattopadhyay, S., Kropf, A.J., Kemner, K.M., 2006. Evidence of a Stable Uranyl Site in Ancient Organic-Rich Calcite. Environmental Science & Technology 40, 2262–2268. URL: https://pubs.acs.org/doi/10.1021/es051970v, doi:10.1021/es051970v.

Kigoshi, K., 1971. Alpha-Recoil Thorium-234: Dissolution into Water and the Uranium-234/Uranium-238 Disequilibrium in Nature. Science 173, 47–48. URL: http://www.sciencemag.org/cgi/doi/10.1126/science.173.3991.47, doi:10.1126/science.173.3991.47.

Kiro, Y., Goldstein, S., Kushnir, Y., Stein, M., Lazar, B., 2018. Droughts and tropical-induced rainfall in the east mediterranean during warm periods, in: Goldschmidt Abstracts.

Kliem, P., Enters, D., Hahn, A., Ohlendorf, C., Lisé-Pronovost, A., St-Onge, G., Wastegård, S., Zolitschka,

B., the Pasado Science Team, 2013. Lithology, radiocarbon chronology and sedimentological interpretation of the lacustrine record from Laguna Potrok Aike, southern Patagonia. Quaternary Science Reviews 71, 54–69. doi:10.1016/j.quascirev.2012.07.019.

König, I., Haeckel, M., Drodt, M., Suess, E., Trautwein, A.X., 1999. Reactive Fe(II) layers in deep-sea sediments. Geochimica et Cosmochimica Acta 63, 1517–1526. URL: https://linkinghub.elsevier.com/retrieve/pii/S0016703799001040, doi:10.1016/S0016-7037(99)00104-0.

König, I., Lougear, A., Bruns, P., Grützner, J., Trautwein, A., Dullo, W.C., 2000. Iron oxidation in sediment cores (Site 1062) during six months of storage in the Ocean Drilling Program archive. Proceedings of the Ocean Drilling Program, Scientific Results. volume 172. pp. 1–11.

Kronfeld, J., 1974. Uranium deposition and Th-234 alpha-recoil: An explanation for extreme U-234/U-238 fractionation within the Trinity aquifer. Earth and Planetary Science Letters 21, 327–330. URL: https://linkinghub.elsevier.com/retrieve/pii/0012821X74901691, doi:10.1016/0012-821X(74)90169-1.

Kronfeld, J., Godfrey-Smith, D., Johannessen, D., Zentilli, M., 2004. Uranium series isotopes in the avon valley, nova scotia. Journal of Environmental Radioactivity 73, 335–352.

Kronfeld, J., Vogel, J.C., 1991. Uranium isotopes in surface waters from southern Africa. Earth and Planetary Science Letters 105, 191–195. doi:10.1016/0012-821X(91)90130-A.

Ku, T.L., Knauss, K.G., Mathieu, G.G., 1977. Uranium in open ocean: concentration and isotopic composition. Deep Sea Research 24, 1005 – 1017. URL: http://www.sciencedirect.com/science/article/pii/0146629177905719, doi:https://doi.org/10.1016/0146-6291(77)90571-9.

Ku, T.L., Liang, Z.C., 1984. The Dating of Impure Carbonates with Decay-Series Isotopes. Nuclear Instruments and Methods in Physics Research 223, 563–571. doi:10.1360/zd-2013-43-6-1064.

Ku, T.L., Luo, S., Lowenstein, T.K., Li, J., Spencer, R.J., 1998. U-Series Chronology of Lacustrine Deposits in Death Valley, California. Quaternary Research 50, 261–275.

Kutterolf, S., Schindlbeck, J.C., Anselmetti, F.S., Ariztegui, D., Brenner, M., Curtis, J., Schmid, D., Hodell, D., Mueller, A., Pérez, W., Schwalb, A., Frische, M., Wang, K.L., 2016. A 400-ka tephrochronological framework for Central America from Lake Petén Itzá (Guatemala) sediments. Quaternary Science Reviews 150, 200–220. doi:10.1016/j.quascirev.2016.08.023.

Lambert, F., Delmonte, B., Petit, J., Bigler, M., Kaufmann, P., Hutterli, M., Stocker, T., Ruth, U., Steffensen, J., Maggi, V., 2008. Dust-climate couplings over the past 800,000 years from the EPICA Dome C ice core. Nature 452, 616–619. doi:10.1038/nature06763.

Langmuir, D., 1978. Uranium solution-mineral equilibria at low temperatures with applications to sedimentary ore deposits. Geochimica et Cosmochimica Acta 42, 547–569.

Langmuir, D., Herman, J.S., 1980. The mobility of thorium in natural waters at low temperatures. Geochimica et Cosmochimica Acta 44, 1753–1766. URL: papers2://publication/uuid/5E9E5D34-242B-4117-8B39-BF4464A10B4B.

Lenhart, J.J., Cabaniss, S.E., MacCarthy, P., Honeyman, B.D., 2000. Uranium (VI) complexation with citric, humic and fulvic acids. Radiochimica Acta 88, 345–353.

Li, J., Lowenstein, T.K., Brown, C.B., Ku, T.L., Luo, S., 1996. A 100 ka record of water tables and paleoclimates from salt cores, Death Valley, California. Palaeogeography, Palaeoclimatology, Palaeoecology 123, 179–203.

Lin, J.C., Broecker, W.S., Hemming, S.R., Hajdas, I., Anderson, R.F., Smith, G.I., Kelley, M., Bonani, G., 1998. A Reassessment of U-Th and 14C Ages for Late-Glacial High-Frequency Hydrological Events at Searles Lake, California. Quaternary Research 49, 11–23. URL: http://www.sciencedirect.com/science/article/pii/S0033589497919499, doi:10.1006/qres.1997.1949.

Lisiecki, L.E., Raymo, M.E., 2005. A Pliocene-Pleistocene stack of 57 globally distributed benthic $\delta 18O$ records. Paleoceanography 20. URL: http://doi.wiley.com/10.1029/2004PA001071, doi:10.1029/2004PA001071.

Lowenstein, T.K., Hein, M.C., Bobst, A.L., Jordan, T.E., Ku, T.L., Luo, S., 2003. An assessment of stratigraphic completeness in climate-sensitive closed-basin lake sediments: Salar de Atacama, Chile. Journal of Sedimentary Petrology 73, 91–104.

Ludwig, K.R., 2003. Mathematical-Statistical Treatment of Data and Errors for 230Th/U Geochronology. Reviews in Mineralogy and Geochemistry 52, 631–656. doi:10.2113/0520631.

Ludwig, K.R., 2012. User's Manual for Isoplot Version 3.75–4.15: A Geochronological Toolkit for Microsoft Excel. Technical Report 5. Berkeley Geochronological Center Special Publication.

Ludwig, K.R., Paces, J.B., 2002. Uranium-series dating of pedogenic silica and carbonate, Crater Flat, Nevada. Geochimica et Cosmochimica Acta 66, 487–506. doi:10.1016/S0016-7037(01)00786-4.

Luo, S., Ku, T.L., 1991. U-series isochron dating: A generalized method employing total-sample dissolution. Geochimica et Cosmochimica Acta 55, 555–564. doi:10.1016/0016-7037(91)90012-T.

Lyle, M., 1983. The brown-green color transition in marine sediments: A marker of the Fe(III)-Fe(II) redox boundary. Limnol. Oceanogr. 28, 1026–1033.

Ma, Z., Wang, Z., Liu, J., Yuan, B., Xiao, J., Zhang, G., 2004. U-series chronology of sediments associated with Lake Quaternary fluctuations, Balikun Lake, northwestern China. Quaternary International 121, 89–98.

Mackay, A.W., Bezrukova, E.V., Boyle, J.F., Holmes, J.A., Panizzo, V.N., Piotrowska, N., Shchetnikov, A., Shilland, E.M., Tarasov, P., White, D., 2013. Multiproxy evidence for abrupt climate change impacts on terrestrial and freshwater ecosystems in the Ol'khon region of Lake Baikal, central Asia. Quaternary International 290-291, 46–56. URL: http://dx.doi.org/10.1016/j.quaint.2012.09.031https://linkinghub.elsevier.com/retrieve/pii/S1040618212032041, doi:10.1016/j.quaint.2012.09.031.

McGee, D., Quade, J., Edwards, R.L., Broecker, W.S., Cheng, H., Reiners, P.W., Evenson, N., 2012. Lacustrine cave carbonates: Novel archives of paleohydrologic change in the Bonneville Basin (Utah, USA). Earth and Planetary Science Letters 351-352, 182–194. URL: http://linkinghub.elsevier.com/retrieve/pii/S0012821X1200386X, doi:10.1016/j.epsl.2012.07.019.

McIntyre, G., Brooks, C., Compston, W., Turek, A., 1966. The statistical assessment of Rb-Sr isochrons. Journal of Geophysical Research 71, 5459–5468.

McLaren, S.J., Rowe, P.J., 1996. The reliability of uranium-series mollusc dates from the western Mediterranean basin. Quaternary Science Reviews 15, 709–717. doi:10.1016/0277-3791(96)00032-7.

Metcalfe, S., Say, A., Black, S., McCulloch, R., O'Hara, S., 2002. Wet conditions during the last glaciation in the Chihuahuan Desert, Alta Babicora Basin, Mexico. Quaternary Research 57, 91–101. doi:10.1006/qres.2001.2292.

Mix, A.C., Harris, S.E., Janecek, T.R., 1995. Estimating lithology from nonintrusive reflectance spectra: Leg 138. Proceedings of the Ocean Drilling Program, Scientific Results 138.

Murphy, R.J., Lenhart, J.J., Honeyman, B.D., 1999. The sorption of thorium (IV) and uranium (VI) to hematite in the presence of natural organic matter. Colloids and Surfaces A: Physicochemical and Engineering Aspects 157, 47–62. URL: http://linkinghub.elsevier.com/retrieve/pii/S0927775799001156, doi:10.1016/S0927-7757(99)00115-6.

Nagao, S., Nakashima, S., 1992. The factors controlling vertical color variations of North Atlantic Madeira Abyssal Plain sediments. Marine Geology 109, 83–94. URL: https://linkinghub.elsevier.com/retrieve/pii/0025322792902224, doi:10.1016/0025-3227(92)90222-4.

Nowaczyk, N.R., Haltia, E.M., Ulbricht, D., Wennrich, V., Sauerbrey, M.A., Rosén, P., Vogel, H., Francke, A., Meyer-Jacob, C., Andreev, A.A., Lozhkin, A.V., 2013. Chronology of Lake El'gygytgyn sediments – A combined magnetostratigraphic, palaeoclimatic and orbital tuning study based on multi-parameter analyses. Climate of the Past 9, 2413–2432. doi:10.5194/cp-9-2413-2013.

Palacios-Fest, M.R., Alin, S.R., Cohen, A.S., Tanner, B., Heuser, H., 2005. Paleolimnological investigations of anthropogenic environmental change in Lake Tanganyika: IV. Lacustrine paleoecology. Journal of Paleolimnology 34, 51–71. doi:10.1007/s10933-005-2397-1.

Peng, T.H., Goddard, J.G., Broecker, W.S., 1978. A Direct Comparison of 14C and 230Th Ages at Searles Lake, California. Quaternary Research 9, 319–329.

Pérez, L., Lorenschat, J., Bugja, R., Brenner, M., Scharf, B., Schwalb, A., 2010. Distribution, diversity and ecology of modern freshwater ostracodes (Crustacea), and hydrochemical characteristics of Lago Petén Itzá, Guatemala. Journal of Limnology 69, 146–159.

Petit, J., Jouzel, J., Raynaud, D., Barkov, N., Barnola, J.M., Basile, I., Bender, M., Chappellaz, J., Davis, M., Delaygue, G., Delmotte, M., Kotlyakov, V., Legrand, M., Lipenkov, V., Lorius, C., Pépin, L., Ritz, C., Saltzman, E., Stievenard, M., 1999. Climate and atmospheric history of the past 420,000 years from the Vostok ice core, Antarctica. Nature 399, 429–436. doi:10.1038/20859.

Phillips, F.M., Zreda, M.G., Ku, T.L., Luo, S., Huang, Q., Elmore, D., Kubik, P.W., Sharma, P., 1993. 230Th/234U and 36Cl dating of evaporite deposits from the western Qaidam Basin, China: Implications for glacial-period dust export from Central Asia. Geological Society of America Bulletin 105, 1606–1616.

Plater, A.J., Ivanovich, M., Dugdale, R.E., 1992. Uranium series disequilibrium in river sediments and waters: the significance of anomalous activity ratios. Applied Geochemistry 7, 101–110. doi:10.1016/0883-2927(92)90029-3.

Porcelli, D., Andersson, P., Wasserburg, G., Ingri, J., Baskaran, M., 1997. The importance of colloids and mires for the transport of uranium isotopes through the Kalix River watershed and Baltic Sea. Geochimica et Cosmochimica Acta 61, 4095–4113. URL: http://linkinghub.elsevier.com/retrieve/pii/S0016703797002354, doi:10.1016/S0016-7037(97)00235-4.

Powell, R., Hergt, J., Woodhead, J., 2002. Improving isochron calculations with robust statistics and the bootstrap. Chemical Geology 185, 191–204. URL: http://linkinghub.elsevier.com/retrieve/pii/S000925410100403X, doi:10.1016/S0009-2541(01)00403-X.

Prokopenko, A.A., Hinnov, L.A., Williams, D.F., Kuzmin, M.I., 2006. Orbital forcing of continental climate during the Pleistocene: a complete astronomically tuned climatic record from Lake Baikal, SE Siberia. Quaternary Science Reviews 25, 3431–3457. doi:10.1016/j.quascirev.2006.10.002.

Przybylowicz, W., Schwarcz, H.P., Latham, A.G., 1991. Dirty calcites 2. Uranium-series dating of artificial calcite-detritus mixtures. Chemical Geology: Isotope Geoscience Section 86, 161–178. doi:10.1016/0168-9622(91)90060-A.

Reeder, R.J., Nugent, M., Lamble, G.M., Tait, C.D., Morris, D.E., 2000. Uranyl Incorporation into Calcite and Aragonite: XAFS and Luminescence Studies. Environmental Science & Technology 34, 638–644. URL: https://pubs.acs.org/doi/10.1021/es990981j, doi:10.1021/es990981j.

Reeder, R.J., Nugent, M., Tait, C.D., Morris, D.E., Heald, S.M., Beck, K.M., Hess, W.P., Lanzirotti, A., 2001. Coprecipitation of Uranium(VI) with Calcite: XAFS, micro-XAS, and luminescence characterization. Geochimica et Cosmochimica Acta 65, 3491–3503. URL: http://linkinghub.elsevier.com/retrieve/pii/S0016703701006470, doi:10.1016/S0016-7037(01)00647-0.

Roberts, H.M., Bryant, C.L., Huws, D.G., Lamb, H.F., 2018. Generating long chronologies for lacustrine sediments using luminescence dating: a 250,000 year record from Lake Tana, Ethiopia. Quaternary Science Reviews 202, 66–77. URL: https://doi.org/10.1016/j.quascirev.2018.10.037, doi:10.1016/j.quascirev.2018.10.037.

Robinson, L.F., Adkins, J.F., Fernandez, D.P., Burnett, D.S., Wang, S.L., Gagnon, A.C., Krakauer, N., 2006. Primary U distribution in scleractinian corals and its implications for U series dating. Geochemistry, Geophysics, Geosystems 7. doi:10.1029/2005GC001138.

Robinson, L.F., Henderson, G.M., Hall, L., Matthews, I., 2004. Climatic Control of Riverine and Seawater Uranium-Isotope Ratios. Science 305, 851–854. URL: http://www.sciencemag.org/cgi/doi/10.1126/science.1099673, doi:10.1126/science.1099673.

Robinson, L.F., Henderson, G.M., Slowey, N.C., 2002. U-Th dating of marine isotope stage 7 in Bahamas slope sediments. Earth and Planetary Science Letters 196, 175–187. doi:10.1016/S0012-821X(01)00610-0.

Rodbell, D.T., Abbott, M.B., the 2011 ICDP Lake Junin Working Group, 2012. Workshop on drilling of Lake Junin, Peru: Potential for development of a continuous tropical climate record. Scientific Drilling 3, 58–60. doi:10.2204/iodp.sd.13.10.2011.

Rowe, P.J., Richards, D.A., Atkinson, T.C., Bottrell, S.H., Cliff, R.A., 1997. Geochemistry and radiometric dating of a Middle Pleistocene peat. Geochimica et Cosmochimica Acta 61, 4201–4211. doi:10.1016/S0016-7037(97)00213-5.

Rudnick, R., Gao, S., 2003. Composition of the Continental Crust, in: Treatise on Geochemistry. Elsevier. volume 3, pp. 1–64. doi:10.1016/B0-08-043751-6/03016-4.

Sarin, M., Krishnaswami, S., Moore, W., et al., 1990. Chemistry of uranium, thorium, and radium isotopes in the ganga-brahmaputra river system: Weathering processes and fluxes to the bay of bengal. Geochimica et Cosmochimica Acta 54, 1387–1396.

Schmeide, K., Pompe, S., Bubner, M., Heise, K.H., Bernhard, G., Nitsche, H., 2000. Uranium(VI) sorption onto phyllite and selected minerals in the presence of humic acid. Radiochimica Acta 88, 723–728. URL: http://www.degruyter.com/view/j/ract.2000.88.issue-9-11/ract.2000.88.9-11.723/ract.2000.88.9-11.723.xml, doi:10.1524/ract.2000.88.9-11.723.

Schnurrenberger, D., Russell, J., Kelts, K., 2003. Classification of lacustrine sediments based on sedimentary components. Journal of Paleolimnology 29, 141–154.

Schoene, B., Condon, D.J., Morgan, L., McLean, N., 2013. Precision and Accuracy in Geochronology. Elements 9, 19–24. doi:10.2113/gselements.9.1.19.

Schwalb, A., Locke, S.M., Dean, W.E., 1995. Ostracode δ^{18}O and δ^{13}C evidence of Holocene environmental changes in the sediments of two Minnesota lakes. Journal of Paleolimnology 14, 281–296. doi:10.1007/BF00682429.

Schwarcz, H.P., Latham, A.G., 1989. Dirty calcites 1. Uranium-series dating of contaminated calcite using leachates alone. Chemical Geology: Isotope Geoscience Section 80, 35–43. doi:`10.1016/0168-9622(89)90046-8`.

Seltzer, G., Rodbell, D., Burns, S., 2000. Isotopic evidence for late Quaternary climatic change in tropical South America. Geology 28, 35. URL: `https://pubs.geoscienceworld.org/geology/article/28/1/35-38/187921`, doi:`10.1130/0091-7613(2000)28<35:IEFLQC>2.0.CO;2`.

Shanahan, T.M., Peck, J.A., McKay, N., Heil, C.W., King, J., Forman, S.L., Hoffmann, D.L., Richards, D.A., Overpeck, J.T., Scholz, C., 2013. Age models for long lacustrine sediment records using multiple dating approaches – An example from Lake Bosumtwi, Ghana. Quaternary Geochronology 15, 47–60. URL: `http://dx.doi.org/10.1016/j.quageo.2012.12.001https://linkinghub.elsevier.com/retrieve/pii/S1871101412001872`, doi:`10.1016/j.quageo.2012.12.001`.

Shen, C.C., Lawrence Edwards, R., Cheng, H., Dorale, J.A., Thomas, R.B., Bradley Moran, S., Weinstein, S.E., Edmonds, H.N., 2002. Uranium and thorium isotopic and concentration measurements by magnetic sector inductively coupled plasma mass spectrometry. Chemical Geology 185, 165–178. doi:`10.1016/S0009-2541(01)00404-1`.

Shen, C.C., Wu, C.C., Cheng, H., Edwards, R.L., Hsieh, Y.T., Gallet, S., Chang, C.C., Li, T.Y., Lam, D.D., Kano, A., Hori, M., Spötl, C., 2012. High-precision and high-resolution carbonate 230Th dating by MC-ICP-MS with SEM protocols. Geochimica et Cosmochimica Acta 99, 71 – 86. URL: `http://www.sciencedirect.com/science/article/pii/S0016703712005248`, doi:`https://doi.org/10.1016/j.gca.2012.09.018`.

Siegel, D.I., Rodbell, D.T., Mark, B., Brigham-Grette, J., Smith, J., 2005. Memorial to geoffrey owen seltzer (1959–2005). Geological Society of America Memorials 34.

Skrivanek, A., Li, J., Dutton, A., 2018. Relative sea-level change during the Last Interglacial as recorded in Bahamian fossil reefs. Quaternary Science Reviews 200, 160–177. URL: `https://linkinghub.elsevier.com/retrieve/pii/S0277379118304384`, doi:`10.1016/j.quascirev.2018.09.033`.

Smith, A.J., Delorme, L.D., 2010. Ostracoda. Ecology and Classification of North American Freshwater Invertebrates , 725–771doi:`10.1016/B978-0-12-374855-3.00019-4`.

Smith, J.A., Finkel, R.C., Farber, D.L., Rodbell, D.T., Seltzer, G.O., 2005a. Moraine preservation and boulder erosion in the tropical Andes: Interpreting old surface exposure ages in glaciated valleys. Journal of Quaternary Science 20, 735–758. doi:`10.1002/jqs.981`.

Smith, J.A., Seltzer, G.O., Farber, D.L., Rodbell, D.T., Finkel, R.C., 2005b. Early local last glacial maximum in the tropical Andes. Science 308, 678–681. doi:`10.1126/science.1107075`.

Stein, M., Goldstein, S.L., 2006. U-Th and radiocarbon chronologies of late Quaternary lacustrine records of the Dead Sea basin: Methods and applications, in: Enzel, Y., Agnon, A., Stein, M. (Eds.), New frontiers in Dead Sea paleoenvironmental research: Geological Society of America Special Paper 401. Geological Society of America. volume 401, pp. 141–154. URL: `https://pubs.geoscienceworld.org/books/book/558/chapter/3802608/`, doi:`10.1130/2006.2401(09)`.

Stirling, C., Lee, D.C., Christensen, J., Halliday, A., 2000. High-precision in situ 238U–234U–230Th isotopic analysis using laser ablation multiple-collector ICPMS. Geochimica et Cosmochimica Acta 64, 3737–3750. URL: `https://linkinghub.elsevier.com/retrieve/pii/S0016703700004579`, doi:`10.1016/S0016-7037(00)00457-9`.

Stockhecke, M., Kwiecien, O., Vigliotti, L., Anselmetti, F.S., Beer, J., Çağatay, M.N., Channell, J.E., Kipfer, R., Lachner, J., Litt, T., Pickarski, N., Sturm, M., 2014. Chronostratigraphy of the 600,000 year old continental record of Lake Van (Turkey). Quaternary Science Reviews 104, 8–17. doi:10.1016/j.quascirev.2014.04.008.

Thurber, D.L., 1962. Anomalous U^{234}/U^{238} in nature. Journal of Geophysical Research 67, 4518–4520.

Tomlinson, C.W., 1916. The origin of red beds: a study of the conditions of origin of the Permo-Carboniferous and Triassic red beds of the western United States. The Journal of Geology 24, 153–179.

Torfstein, A., Goldstein, S.L., Kushnir, Y., Enzel, Y., Haug, G., Stein, M., 2015. Dead Sea drawdown and monsoonal impacts in the Levant during the last interglacial. Earth and Planetary Science Letters 412, 235–244. URL: http://dx.doi.org/10.1016/j.epsl.2014.12.013, doi:10.1016/j.epsl.2014.12.013.

Trachsel, M., Telford, R.J., 2017. All age-depth models are wrong, but are getting better. The Holocene 27, 860–869. URL: http://journals.sagepub.com/doi/10.1177/0959683616675939, doi:10.1177/0959683616675939.

Van Der Wijk, A., El-Daoushy, F., Arends, A.R., Mook, W.G., 1986. Dating peat with U/Th disequilibrium: Some geochemical considerations. Chemical Geology: Isotope Geoscience Section 59, 283–292. doi:10.1016/0168-9622(86)90077-1.

Vermeesch, P., 2018. IsoplotR: A free and open toolbox for geochronology. Geoscience Frontiers 9, 1479–1493. URL: https://doi.org/10.1016/j.gsf.2018.04.001, doi:10.1016/j.gsf.2018.04.001, arXiv:0-387-31073-8.

Wang, J., Fang, X., Appel, E., Zhang, W., 2013. Magnetostratigraphic and radiometric constraints on salt formation in the Qaidam Basin, NE Tibetan Plateau. Quaternary Science Reviews 78, 53–64. URL: http://dx.doi.org/10.1016/j.quascirev.2013.07.017, doi:10.1016/j.quascirev.2013.07.017.

Wang, Y.J., Cheng, H., Edwards, R.L., An, Z.S., Wu, J.Y., Shen, C.C., Dorale, J.A., 2001. A high-resolution absolute-dated late Pleistocene Monsoon record from Hulu Cave, China. Science 294, 2345–2348. doi:10.1126/science.1064618.

Wendt, I., Carl, C., 1991. The statistical distribution of the mean squared weighted deviation. Chemical Geology: Isotope Geoscience section 86, 275–285. URL: https://linkinghub.elsevier.com/retrieve/pii/016896229190010T, doi:10.1016/0168-9622(91)90010-T.

Winograd, I.J., Coplen, T.B., Landwehr, J.M., Riggs, A.C., Ludwig, K.R., Szabo, B.J., Kolesar, P.T., Revesz, K.M., 1992. Continuous 500,000-Year Climate Record From Vein Calcite in Devils-Hole, Nevada. Science 258, 255–260.

Woods, A., Rodbell, D., Abbott, M., Hatfield, R.G., Chen, C.Y., Lehmann, S., McGee, D., Weidhaas, N., Tapia, P.M., Valero-Garcés, B.L., Bush, M., Stoner, J.S., 2019. Abrupt arctic warming repeatedly led to prolonged drought and glacial retreat in the tropical andes during the last glacial cycle. EarthArXiv doi:10.31223/osf.io/7hd3a.

Wright, H.E., 1983. Late-Pleistocene Glaciation and Climate around the Junín Plain, Central Peruvian Highlands. Geografiska Annaler. Series A, Physical Geography 65, 35–43. URL: http://www.jstor.org/stable/520719.

Wrozyna, C., Frenzel, P., Daut, G., Mäusbacher, R., Zhu, L., Schwalb, A., 2012. Holocene Lake-Level Changes of Lake Nam Co, Tibetan Plateau, Deduced from Ostracod Assemblages and $\delta^{18}O$ and $\delta^{13}C$ Signatures of Their Valves. Developments in Quaternary Science 17, 281–295. doi:10.1016/B978-0-444-53636-5.00016-0.

Xuan, C., Channell, J.E., Hodell, D.A., 2016. Quaternary magnetic and oxygen isotope stratigraphy in diatom-rich sediments of the southern Gardar Drift (IODP Site U1304, North Atlantic). Quaternary Science Reviews 142, 74–89.

Yliruokanen, I., 1980. The occurence of uranium in some finnish peat bogs. Kemia-Kemi 7, 213–217.

York, D., 1968. Least squares fitting of a straight line with correlated errors. Earth and Planetary Science Letters 5, 320–324. URL: http://www.sciencedirect.com/science/article/pii/S0012821X68800597, doi:https://doi.org/10.1016/S0012-821X(68)80059-7.

Ziegler, L., Constable, C., Johnson, C., Tauxe, L., 2011. PADM2M: a penalized maximum likelihood model of the 0–2 Ma palaeomagnetic axial dipole moment. Geophysical Journal International 184, 1069–1089.